THE EFFECT OF SURFACE MODIFICATION ON THE CRYSTAL GROWTH OF IRON OXIDES

by

THOMAS F. BARTON

Dissertation submitted to the Faculty of the
Virginia Polytechnic Institute and State University
in partial fulfillment of the requirements for the degree of

DOCTOR OF PHILOSOPHY

in

CHEMISTRY

APPROVED:

John G. Dillard, Chairman

Brian E. Hanson

Joseph S. Merola

Larry T. Taylor

John G. Mason

April, 1990

Blacksburg, Virginia

The Effect of Surface Modification on the Crystal Growth of Iron Oxides

by

Thomas F. Barton
John G. Dillard, Committee Chairman
Department of Chemistry

(ABSTRACT)

The growth of Fe_3O_4 and FeOOH crystals was investigated. Growth modifiers were used to alter the formation of iron oxides from ferrous hydroxide precipitates. Multifunctional carboxylic acids were found to have a strong influence on morphology of FeOOH. Dicarboxylic acids, containing two and seven carbons, changed the characteristics of α-FeOOH. These changes included alteration of the isoelectic point of the particulates and changes in particle size and shape. EDTA was found to alter the phase of FeOOH formation, favoring the synthesis of γ-FeOOH over α-FeOOH at temperatures below 50°C. The effects of multifunctional carboxlic acids were dependent upon the time of addition, and the presence of other growth modifiers. The changes in FeOOH formation were postulated to occur due to interaction between the acid molecules and Green Rust II, a common intermediate in iron oxide growth.

The growth of Fe_3O_4 was found to be sensitive to solution pH, and the form of the iron starting materials. Examination of reaction intermediates by x-ray diffraction showed that other crystalline phases formed prior to the production of Fe_3O_4. Different intermediate phases occurred depending on the amount of hydroxide in the reaction, and differences in Fe^{3+} starting materials. The production of different intermediate phases affected the morphology of Fe_3O_4. Early precipitation of Fe_3O_4 led to small particles, while formation of crystalline $Fe(OH)_2$ led to large crystals. Formation of a mixture of Green Rust II and $Fe(OH)_2$ early in the oxidation process led to formation of multiple nuclei, and produced smaller average particles with a wide particle size distribution. Fe_3O_4 particles prepared from α-FeOOH seed crystals were spherical, while Fe_3O_4 particles prepared from $FeSO_4$ alone were octahedral crystals.

Acknowledgements

The author would like to thank his advisor, Dr. John Dillard for his support, guidance, and friendship during this work. In addition the author wishes to acknowledge and thank the members of his committee: Drs. Brian Hanson, John Mason, Joseph Merola, and Larry Taylor.

The author wishes to acknowledge the financial support of this research by the Virginia Center for Innovative Technology and Magnox, Inc. The assistance of the cast and crew at Magnox was very helpful in carrying out this work.

The author thanks the following departments and people at Virginia Tech who aided in this research : the guys in the Physics Department machine shop who built the high shear stirrer, the glass shop for keeping things fixed, and the electronics shop for use of the darkroom.

Two undergraduate students who aided in data collection during this project were Keith Becker and David Weiss, and their assistance was welcome.

Finally the author would like to thank the members of the surface groups for their support and friendship, especially Frank Cromer for his patience and talents in the fields of electronics and diplomacy. The current and former students of the Chemistry Department provided the best reason for attending Virginia Tech, and eventually the motivation for leaving; they should consider themselves well thanked and appreciated.

Table of Contents

List of Illustrations

List of Tables

Chapter 1 : Introduction

In the field of science, the search for new knowledge can be both the goal and the reward of research. The examination of new concepts, and the study of new phenomena increases the sum total of information available, which in itself is a benefit. In more practical applications, the sum of general knowledge can be used to invent schemes that adapt scientific fundamentals, facts, and concepts into keystones of usable technology. In turn, often new processes or materials can become like the tail wagging the dog, in that success of a technology produces a reason and motivation to re-examine scientific fundamentals, so that the individual technology can continue to improve. The study of the crystal growth of iron oxides is such a case where the usefullness of the materials has led to a resurgence of investigation into the fundamentals of crystal nucleation and growth.

In some ways the increase in use of iron oxides for their magnetic properties has paralleled the development of the computer. Iron oxides were first used for magnetic recording media in the 1940s, and their desirable characteristics led to their use in computer storage tapes and discs. As computers have grown in data capacity and speed, and as sound and video recording have become important, the requirements for storage media have become increasingly more stringent. To a hardware designer, the ideal recording medium would have infinite storage capacity in the smallest possible space with zero time required for data storage and retrieval. The characteristics of magnetic iron oxide crystals are such that compromises must be made in the formulation of real recording products.

A magnetic tape is commonly formed by dispersing magnetic iron oxide crystals in a polymer binder material, which is then coated onto a polymer substrate. Because the process of information storage requires a fixed magnetic axis on the tape, the magnetization of individual oxide crystals must be both anisotropic and orientable. The orientation of the crystals is produced by passing the still liquid iron oxide/binder dispersion under a strong permanent magnet, which aligns all the crystals in a single direction. The magnetic anisotropy requirement

for individual oxide crystals is far more complex a problem, and is where the chemistry of iron oxide formation becomes important.

The magnetic character of an iron oxide such as γ-Fe_2O_3 comes from unpaired 3d electrons of the Fe^{3+} ions. If all the Fe^{3+} ions were in similar sites in a crystal lattice, the unpaired electrons would sometimes be aligned parallel, and other times antiparallel, with the net effect of zero magnetization. In the inverse spinel lattice of γ-Fe_2O_3 there are both tetrahedral sites and octahedral sites, which form two distinct sublattices. If the two lattices were equally occupied by Fe^{3+} ions, the net magnetic moments would cancel, and no magnetism would exist. In γ-Fe_2O_3, however, the octahedral sites are not all occupied, and the presence of octahedral vacancies next to Fe^{3+} ions occupying tetrahedral sites leads to non-zero magnetic moments.

The magnetism of γ-Fe_2O_3 is greatly enhanced by shape anisotropy. The magnetic field in the particle can align along the long axis. This gives stronger magnetic character to the crystals, and allows easy orientability on a recording tape.

γ-Fe_2O_3, which cannot be grown directly as acicular crystals, is commonly produced by conversion of acicular precursor crystals such as FeOOH. The control of morphology of the precursor crystals is important in maintaining the proper magnetic characteristics of the final magnetic iron oxide products.

This dissertation describes work carried out to examine the formation of FeOOH and Fe_3O_4 from Fe^{2+} species in solution. Emphasis was placed on the control of morphology of the oxide crystals by altering the chemistry of the growth environment. Particular attention was directed to the effect of growth modifiers on crystal morphology and phase. Two classes of growth modifiers studied were: metal ions, which could incorporate into the oxide lattice, and multifunctional organic acids which strongly adsorb to iron oxides. Also examined were other key variables in morphology control such as reaction temperature, pH, and oxidation rate. The goal of this research was to understand the fundamental processes that occur during the

nucleation and growth of iron oxides from solution, and to determine how crystalline phase and morphology are controlled by reaction conditions. Having learned more about how crystallization occurs, iron oxide materials with more desirable characteristics could be made.

The nucleation and growth of iron oxides are also important in such fields as geology, corrosion science, and pigment research in addition to applications in magnetic recording. In natural environments, the formation of different iron oxide phases and morphology is complicated by the number of phase transformations, oxidation processes, and possible oxide stoichiometries. By isolating key factors in the laboratory, this dissertation might also aid geologists in determining how mineral formation occurs, or how corrosion of steam pipes proceeds in power plants.

If the role of technology is to provide motivation for re-examination of scientific fundamentals, perhaps the role of scientific research is to tie together dissimilar fields based on those fundamentals. The crossover potential of research can only make it more worthwhile.

Chapter 2 : Literature Review

The written record of use of iron oxides for their magnetic characteristics goes back nearly to the beginning of man's recorded history. Theophrastus wrote in Περι λιθων in 325 B.C. about lodestones, minerals which had an ability to attract iron metal (1). These natural minerals contain Fe_3O_4, one of the two most commonly used magnetic iron oxides today, the other being γ-Fe_2O_3. The dark black color of Fe_3O_4 made it useful as a commercial pigment material (2). The magnetic character of Fe_3O_4 led to its use in magnetic cores (3) and early magnetic recording tapes (4). The same deep color which made Fe_3O_4 appropriate for pigments, combined with the fact that Fe_3O_4 is magnetic allowed this iron oxide to be used in a magnetic image transfer sheet patented by Sutheim and Southcomb (5). This plastic sheet covered with dispersed Fe_3O_4 in wax was the precursor to modern photocopying processes (6).

γ-Fe_2O_3 was also used in magnetic cores in the early 1900s (3). The first use of γ-Fe_2O_3 in a modern type magnetic tape for recording purposes was noted by G. M. Kline in 1945 when he discussed wartime work with plastics in Germany (7). The tape was made by dispersing a slurry of oxide in a polymer solution, and spreading the dispersion over a plastic film. The use of γ-Fe_2O_3 has been widespread for the last four decades in the production of commercial magnetic recording materials, due mostly to the fact that γ-Fe_2O_3 can be produced very cheaply in large quantities (8). The early use of spherical γ-Fe_2O_3, which is easy and cheap to produce, was superceded by the development of acicular γ-Fe_2O_3 which is more complicated to grow, but has better magnetic properties (9).

Within the past fifteen years, the development of cobalt modified γ-Fe_2O_3 materials has taken the efficiency of particulate magnetic recording materials another large step forward (10). Incorporating cobalt(II) at concentrations between 0.2 and 3 wt.% into the bulk of γ-Fe_2O_3 could double or triple the coercivity of the crystals (11). Coercivity is the measure of force required to reverse the polarity of a magnetic crystal, and is an indirect measure of the amount of information which can be stored in a given area on a tape (12). Increasing the coercivity with

the addition of cobalt(II) increased the efficiency of the tapes. A drawback to bulk incorporation of cobalt(II) was the temperature dependence of some of the magnetic characteristics of the product tapes (13). Coercivity was reduced at higher temperatures, and this instability complicated information storage and retrieval. Later work by Umeki, Saitoh, and Imaoka (14) showed that surface coatings of cobalt-containing species also increased the coercivity of γ-Fe_2O_3 crystals, but produced less coercivity temperature dependence than that of bulk incorporation of cobalt into γ-Fe_2O_3. The surface coating of $CoFe_2O_4$-like species is made by coprecipitating Co(II) and Fe(II) hydroxides onto γ-Fe_2O_3, and heating the suspension to reflux for several hours. Surface modified Co-γ-Fe_2O_3 crystals are currently the most widely used high efficiency particulate recording materials. Their position is threatened only by metallic film recording materials (12).

The morphology of iron oxide particles used for magnetic materials is critical for several reasons. In electrostatic imaging processes that use Fe_3O_4 particles, there is both an ideal size and shape for the crystals. While the ideal particle size may vary for each type of imaging system, the optimal Fe_3O_4 diameter ranges from about 0.01 μ to 5 μ. (15). Particles larger or smaller than the optimum value lead to problems in particle dispersion and transfer. The magnetic characteristics of the imaging process dictate that ideal toner particles be spherical rather than cubic or octahedral (16). Particles which contain vertices are less efficient since magnetic and shape anisotropies conflict.

For γ-Fe_2O_3 crystals used in magnetic tapes, the opposite shape relationship holds true. An acicular magnetic oxide particle is preferred over a spherical particle for magnetic tapes. This is due to the anisotropy of magnetization in needlelike crystals. An elongated particle allows proper orientation on a magnetic tape, and produces an easy axis of magnetization. Acicular particles of a single uniform size on the order of one micron in length are considered to be most desirable based on their magnetic properties (17). Uniformity among the crystals reduces the size of the magnetic switching field required for information storage. The absence of

dendrites on the crystals eliminates secondary magnetic axes. The length of the crystals and their length to width aspect ratio define many of the magnetic characteristics of a recording tape manufactured with those crystals. The control of crystal size and shape as well as the method of phase production has been researched extensively since the development of magnetic recording tapes. The primary method for growing acicular γ-Fe_2O_3 in the past twenty years has been the conversion of acicular precursor crystals such as α-FeOOH and γ-FeOOH. These so called Fe_2O_3-H_2O crystals can be grown directly from aqueous iron species as acicular particles. The FeOOH crystals are then dehydrated to α-Fe_2O_3, reduced to Fe_3O_4 with H_2 at 300°C, and reoxidized to γ-Fe_2O_3 with O_2 at 250°C (18). Matsumoto et al. (19) patented a process to produce γ-Fe_2O_3 directly from α-Fe_2O_3. The advantage of this process is that it eliminates the dehydration step found in other processes which can create porosity and nonuniformity in γ-Fe_2O_3 particles. The Matsumoto method produces a magnetic particle which the inventor describes as " well-defined, relatively uniform, single crystalline, with an acicular crystallographic configuration." However, to produce γ-Fe_2O_3 directly from α-Fe_2O_3 requires temperatures near 250°C. The direct coversion is carried out in a sealed vessel capable of withstanding hydrothermal pressures. The expense of the direct conversion has limited the use of the process in the production of low cost γ-Fe_2O_3.

The structural transformations from α-FeOOH and γ-FeOOH to their respective oxides have been studied extensively. Francombe and Rooksby (20) studied the changes in FeOOH unit cell dimensions as a function of temperature and weight loss. The x-ray powder diffraction pattern changed as water was given off during the heating cycle. The needle axis of α-FeOOH and γ-FeOOH was the [001]. The needle axis in γ-Fe_2O_3 was the [110]. Welo and Baudisch (21) monitored the changes from paramagnetic FeOOH to ferromagnetic γ-Fe_2O_3, then to paramagnetic α-Fe_2O_3, as temperature was increased. The increase of magnetism followed closely the sharpening of x-ray diffraction lines.

The dehydration of FeOOH has been recognized as an important process also in geological

transformations (22). Sosman and Posnjak (23) found that γ-FeOOH could be transformed directly into γ-Fe_2O_3 by heating at 180°C. Herroun and Wilson (24) also carried out dehydration experiments on γ-FeOOH and made magnetic susceptibility measurements on the resulting γ-Fe_2O_3. They found that there was a significant difference between the magnetics of γ-Fe_2O_3 formed directly from γ-FeOOH and that formed by the reduction of Fe_3O_4. More recent researchers (9) determined that γ-Fe_2O_3 formed from Fe_3O_4 had better magnetic characteristics for use in magnetic recording media. The crystals made from Fe_3O_4 showed higher uniformity in the crystal direction and magnetic anisotropy. Currently commercial production of γ-Fe_2O_3 from γ-FeOOH is made by transformation first to Fe_3O_4 rather by the direct conversion. Fe_3O_4 is not just found as an intermediate in oxide transformations but occurs naturally.

Fe_3O_4 in its mineral form is found all over the world. In 25 A.D. Pliny (25) wrote about a mineral he called magnes that came from a mountain in what is now Ethiopia. The mineral name magnetite for Fe_3O_4 was first recorded by Haidlinger in 1845 (26). γ-Fe_2O_3 was given the name maghemite around 1900 because it had characteristics of α-Fe_2O_3, called hematite, and magnetite. The first natural deposit of maghemite was not discovered until 1925 (23). Crystallographic information about γ-Fe_2O_3, α-Fe_2O_3, and Fe_3O_4 is listed in Table 2.1.

FeOOH is also a naturally forming mineral with several crystallographic forms. The most common form is α-FeOOH. The natural occurrence of α-FeOOH was first reported by Becher in 1789 (27). The new mineral was given the name Goethite, after the poet Goethe, by Lenz in 1806 (28). The less common form of naturally occurring FeOOH is γ-FeOOH. γ-FeOOH was first reported by Ullmann in 1814 (29), and given the name lepidocrocite. The word lepidocrocite is derived from Greek words for scales and fibers since natural γ-FeOOH crystals are found as fibrous flakes. There are two additional crystallographic forms of FeOOH which are rarely found in nature, β-FeOOH, called akageneite, and δ-FeOOH. The structures of γ-FeOOH and α-FeOOH are shown in Figure 2.1. Crystallographic information about the four forms of FeOOH is listed in Table 2.1.

Table 2.1 Crystallographic Data for Phases of FeOOH

Composition	Mineral Name	Space Group	Dimensions (Å)
α-FeOOH	Goethite	Pbnm	a = 4.587, b = 9.937,c = 3.015
β-FeOOH	Akageneite	I4/m(?)	a = 10.48, c = 3.06
γ-FeOOH	Lepidocrocite	Cmcm	a = 3.87, b = 12.51, c = 3.06
δ-FeOOH		P312(?)hex.	a = 2.941, c = 4.58

Bernal, Dasgupta, and Mackay, Clay Minerals Bull. **1959**, *4*, p 17

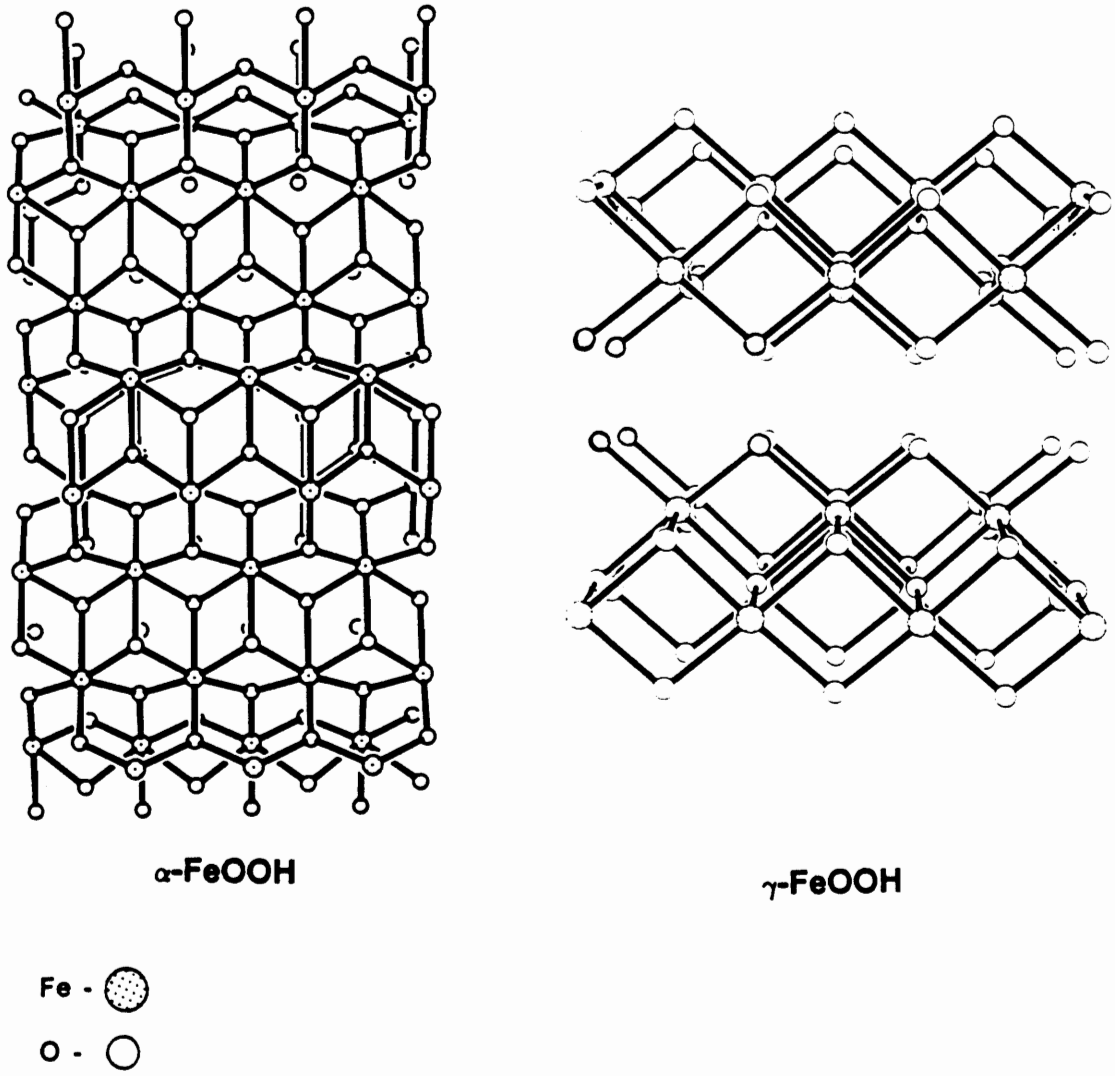

Figure 2.1 Structures of α-FeOOH and γ-FeOOH

All of the crystallographic forms of FeOOH can be grown from Fe^{2+} in aqueous solution. The list of the researchers who have worked on the hydrolysis, oxidation, and formation of iron oxides and hydroxides includes some of most well known chemists in history. Scheele (30) published his findings in 1777 on the reaction of solution Fe species with different proportions of phlogiston, that reactive part of the air now known as oxygen. Mellor's Comprehensive Treatise on Inorganic and Theoretical Chemistry states that both Priestley and Lavoisier worked on the stages of oxidation of iron, Gay Lussac was the first to recognize iron oxides containing both Fe^{3+} and Fe^{2+} in a single crystalline form, and Thomsen and le Chatelier calculated the heats of formation of the series of iron oxides (31). These types of experiments produced a strong foundation for modern research in iron oxide chemistry, but even after several hundred years of study, there is still much to learn about the reactions of iron at the atomic level.

In the past three decades a number of groups have studied fundamentals of the precipitation of iron hydroxides, and subsequent oxidation, nucleation, and growth into FeOOH crystals. Bernal et al. (32) wrote a key paper in 1959 about the structural interrelationships of iron oxides, and discussed the idea of topotaxy. Topotaxy occurs when a phase is transformed into a second phase with the retention of certain crystalline parameters. If a fraction of material is added or taken away from within a crystal lattice, the remaining structure retains a relationship to the initial structure. In this way the phase transformations can be predicted based on the location and extent of atoms removed from or added to the lattice. Bernal used the idea of topotaxy to explain the conversion from $Fe(OH)_2$ to green rusts to FeOOH. Sodium hydroxide was added to a $FeCl_2$ solution to precipitate $Fe(OH)_2$. By bubbling air through the hydroxide suspension, blue-green compounds were formed. X-ray powder diffraction photographs were taken of the 'Green Rusts' and their composition was calculated. In a chloride solution, a green rust compound, named Green Rust I occurred initially. Green Rust I had a composition estimated at $Fe^{2+}_3Fe^{3+}_1(O,OH,Cl)_9$, and had a rhombohedral unit cell. Green Rust I

transformed topotaxically to a second green rust, named Green Rust II. Green Rust II then transformed to γ-FeOOH. Under the same experimental conditions, starting with an $FeSO_4$ solution, only Green Rust II was found during the preparation of α-FeOOH. The composition of Green Rust II was not given, but the x-ray powder photograph indicated a hexagonal unit cell. X-ray powder data for Green Rust I and Green Rust II are listed in Appendix A. By proceeding through two steps, $Fe(OH)_2$ to green rust, then green rust to FeOOH, the conversion was carried out topotaxially. The direct transformation of $Fe(OH)_2$ to FeOOH would not be topotaxial and would require some dissolution-reprecipitation mechanism.

Misawa et al. (33) pursued the intermediates in the formation of FeOOH from perchloric acid solution. The formation of a $Fe(II)_1$-$Fe(III)_3$ complex was found during the oxidation of Fe^{2+} by O_2 This complex appeared to be related to Green Rust I, but was a true complex in solution and not a precipitated hydroxide. The UV-visible and Raman spectra of the iron perchlorate solution were monitored during the oxidation and showed adsorption bands that corresponded to a complex for which the authors suggest a configuration of a central Fe^{2+} ion linked to three Fe^{3+} ions through oxo-bridges. The existence of this intermediate suggested a method for oligomer formation during the nucleation and growth of FeOOH. In a related paper published at the same time, Misawa et al. (34) found a $Fe(II)_1$-$Fe(III)_1$ intermediate complex in the oxidation of Fe(II) sulfate solutions. The difference between this complex and that found for perchloric acid emphasized the effect of anions in solution, even for those anions which are historically considered to be non-reactants in hydrolysis and oxidation chemistry of metals.

In a third paper, Misawa (35) outlined the differences between green rusts and green complexes and the conditions of their formation. The difference between two green rust compounds was in both the anion present and solution pH. Green Rust II was restricted to the oxidation of Fe^{2+} or the conversion of $Fe(OH)_2$. Green Rust I was formed from neutral or slightly alkaline iron chloride solutions. The transformation to FeOOH occurred either by conversion of the two green complexes by way of green rusts, or by solid state conversion of

$Fe(OH)_2$ to green rust to FeOOH. The phase of the FeOOH product depended on the path of conversion, the anions present, and the pH.

The process of nucleation of Fe(III) hydroxides is still under investigation. Hsu studied the stability of Fe(III) hydroxide sols seeded into solutions of $Fe(ClO_4)_3$ (36). By adding $HClO_4$ to the solution, the system became saturated with FeOOH. The resulting particle size distribution of precipitated material indicated that nucleation was dependent upon the Fe(III) hydroxide sol added initially. Nucleation did not occur spontaneously from $Fe(ClO_4)_3$, but only from the hydroxide species. This seeding effect of Fe(III) hydroxide in the nucleation of FeOOH appears to be common in many iron oxide growth reactions. The hydrolysis of Fe(III) nitrate was studied by Van der Woude and de Bruyn (37). Their experiments were carried out at low pH between 1.6 and 2.4, where the hydrolysis-polymerization process is quite slow, and reaction kinetics can be followed. They calculated a critical nucleus size of 16 to 32 iron atoms based on induction time, Fe^{3+} concentration, pH, and ionic strength. While it was likely that this critical nucleus led to the formation of crystalline α-FeOOH at this pH range, their data could not be extrapolated to high hydroxide concentrations. In a similar study, Knight and Silva (38) postulated that $Fe_2(OH)_2^{4+}$ was the precursor to formation of polycations in the growth of nuclei during the hydrolysis of Fe(III) solutions. This conclusion was based on kinetic studies, x-ray powder diffraction, and electron microscopy studies. Work by Dousma and deBruyn (39) divide the hydrolysis process into four parts: hydrolysis to monomers and dimers, reversible rapid growth to small polymers, formation of slow reacting polymers, and precipitation of the solid phase.

Atkinson, Posner, and Quirk (40) carried out experiments on the nucleation and growth of iron oxide crystals from Fe(III) chloride solutions at both high and low pH at 65°C. At pH 1-2 they found that chloride inhibited the nucleation of α-FeOOH and α-Fe_2O_3 and led to the formation of rodlike crystals of β-FeOOH. At pH 12, no inhibition by chloride of α-FeOOH nucleation was found. Also noted was that the conversion of β-FeOOH to α-FeOOH at pH 12

proceeded only with the presence of α-FeOOH seed crystals which was evidence for a mechanism of transformation based on dissolution-reprecipitation.

The phenomenon of dissolution-reprecipitation or crystallization can be very important in the growth of Fe_3O_4. Kiyama (41) studied the formation of Fe_3O_4 from the air oxidation of $Fe(OH)_2$. The growth was carried out between 5°C and 85°C from a gel produced by the reaction of NaOH and $FeSO_4$. The formation of Fe_3O_4 appeared to occur by a recrystallization process between Green Rust II, precipitated $Fe(OH)_2$, and $FeOH^+$ ions in solution. Changing the pH of the solution altered the ratio of Green Rust II and $Fe(OH)_2$, but did not affect the growth of Fe_3O_4 above 70°C.

An investigation was carried out by Sugimoto and Matijevic (42) on the growth of Fe_3O_4 from ferrous hydroxide gels to determine the effects of solution conditions on morphology. They grew Fe_3O_4 from $FeSO_4$ and KOH in the presence of KNO_3 and O_2, and analyzed the Fe_3O_4 formed as an aging process was carried out. Their conclusions were that initial Fe_3O_4 nuclei aggregated into larger particles, and further growth occurred by the particles trapping other smaller aggregates until the volume around the spheres was depleted. As aging time increased the spherical particles densified through a recrystallization process. With insufficient temperature or time of aging, only limited recrystallization took place, and particles were not densified enough to remain intact after drying. The presence of nitrate ion was shown to be an alternate oxidation source in the conversion of $Fe(OH)_2$ to Fe_3O_4.

Kanzaki and Katsura (43) confirmed by Mössbauer spectroscopy, the presence of Green Rust II as an intermediate during the crystal growth of Fe_3O_4 from $Fe(OH)_2$. Tamaura et al. (44) showed that the combination of suspended γ-FeOOH and $FeSO_4$ in solution could be converted to Fe_3O_4 or Green Rust II depending on the experimental conditions. The reversibility of the green rust formation indicated the connection between dissolution and crystallization in the formation of Fe_3O_4. The topotaxial conversion of γ-FeOOH to Fe_3O_4 in an aqueous suspension mimicked the dehydration and reduction by H_2 at 300°C, but the mechanism of transformation

was entirely different.

The hydrolysis, oxidation, and crystal formation of FeOOH and Fe_3O_4 are dependent upon many experimental variables. The many factors which influence the phase and morphology of the iron oxide crystals grown from soluble Fe(II) salts include temperature, pH, oxidation rate, oxidizing agent, pressure, anions in solution, and the presence of certain chemical agents that act as morphology modifiers.

Temperature strongly influences iron oxide phase formation. Biernat and Robins (45) published potential/pH diagrams of the iron/water/sulfur system at 25°C, 100°C, 150°C, 200°C, and 300°C. At 25°C in the pH range between 2 and 12, the stable species in the iron/water/sulfur system were $Fe(OH)_2$, $FeOH^+$, $Fe(OH)_3$, $Fe(OH)_2^+$, FeOOH, $FeOH^{2+}$, Fe_3O_4 and SO_4^{2-}. As temperature was increased to 100°C, the number of stable species between pH 2 and 12 remained the same, but the domain of crystalline species increased. The stable species at 100°C were FeOOH, Fe_3O_4, $FeOH^+$, $Fe(OH)_2^+$, $FeOH^{2+}$, $Fe_2(OH)_2^{4+}$, SO_4^{2-}, and HSO_4^-. As temperature was increased to 200°C and 300°C, Fe(II) species were limited to $FeOH^+$ and $HFeO_2^-$, and the dominant Fe(III) species were Fe_3O_4, Fe_2O_3, $Fe(OH)_2^+$, and $FeOH^{2+}$. The 200°C and 300°C diagrams referred to hydrothermal processes only. Solcova et al. (46) studied the effect of precipitation and aging temperature on the properties of FeOOH. Precipitation temperature had no effect on α-FeOOH properties, but increasing the aging temperature from 313°C to 363°C increased the ratio of α-Fe_2O_3 to α-FeOOH formed from $FeSO_4$.

The influence of pH on the crystallinity of FeOOH is based on the conversion and stability of different hydrolysis products of iron. Baes and Mesmer (47) compiled a text on the hydrolysis of cations. Excluding H_2O ligands, increasing pH changed the predominance of mononuclear species from Fe^{2+}, to $FeOH^+$, to $Fe(OH)_2$ to $Fe(OH)_3^-$ for Fe^{2+}, and Fe^{3+}, to $FeOH^{2+}$, to $Fe(OH)_2^+$, to $Fe(OH)_3$, to $Fe(OH)_4^-$. By increasing the pH, the predominant species shift to iron complexes with multiple OH^- ligands. $Fe(OH)_3$ can additionally convert to FeOOH and H_2O, but this more commonly occurred as a polynuclear reaction rather than as a

mononuclear reaction (48). Knight and Silva (38) stated that an $OH^-:Fe^{2+}$ ratio less than 2 decreased the formation of dimer and trimer complexes based on potentiometric measurements. Fewer polynuclear species led to less precipitation of crystalline material.

The effect of pH on driving the formation of one phase of iron oxide to another is discussed by Lewis and Schwertmann (49). They studied the conversion of ferrihydrite, which is an amorphous Fe(III) hydrous oxide that can be converted to well crystalline α-FeOOH by treatment with hydroxide for several hours. Leskela and Leskela (50) studied the transformation of $FeSO_4$ to α-FeOOH, α-Fe_2O_3 and Fe_3O_4 at a range of pHs from 2 to 13. This study was done primarily to obtain different colored pigments based on three phase mixtures produced at different pH. By varying the pH and temperature, the combination of α-FeOOH, α-Fe_2O_3, and Fe_3O_4 gave colors ranging from light yellow through orange to red to green to black. The wide range of color shows the variability in the ratio of phases produced through modification of just these two factors, pH and temperature.

The effect of pressure on the determination of crystallinity and morphology of iron oxides cannot easily be separated from the effect of temperature, since the majority of published data on high pressure crystal growth has been based on hydrothermal processing above 150°C. In 1925 Bohm (51) discussed the conversion of amorphous iron hydroxides to crystalline α-FeOOH in 2M KOH at 140°C. Above 150°C, hydrothermal methods produce primarily α-Fe_2O_3, γ-Fe_2O_3, and Fe_3O_4, and little α-FeOOH.

The rate of oxidation as well as the source of oxidation can have an effect on the phase and morphology of FeOOH grown at non-hydrothermal temperatures. In 1927 Miyamoto (52,53) published accounts of his experiments on the rate of oxidation of $Fe(OH)_2$ by air. He states that the rate of oxidation of $Fe(OH)_2$ was dependent only on the rate of dissolution of air into the hydroxide suspension. Incorporation of O_2 was immediate and irreversible. At very low oxidation rates, the aging process becomes important in the crystallization and morphology of FeOOH (36,38,54). In these studies the aging period was sometimes measured in days and

weeks. Long slow oxidation times led to higher uniformity in particle size and shape. The particular morphology was dependent on other experimental conditions, but the effect of long aging time was to allow a true chemical equilibrium to occur during crystal growth. Very high oxidation rates can alter the phase of the resulting FeOOH. The fast oxidation of $Fe(OH)_2$ by hydrogen peroxide precipitated δ-FeOOH (55). In the formation of δ-FeOOH, the more rapid the oxidation was carried out, the sharper the lines in the x-ray diffraction pattern, indicating more perfect crystallinity. The role of hydrogen peroxide itself, beyond its effect as an oxidant in the phase determination, was not studied. Other oxidizing agents such as the nitrate ion have been shown to aid in the formation of iron oxides (42).

The presence of anions in solution can affect FeOOH nucleation and growth. In 1876 von Hauer (56) wrote a paper on crystallogenesis. In this journal on geological research he made a statement on the effect of anions as follows: " The presence of a heterogenous sustance in a solution acts in a constant and regular way on the crystallization of the dissolved substance....in no case are these admixtures embodied into the products of crystallization and their mode of action is as yet wrapped in deepest obscurity. " Many researchers have studied the effects of anions on formation of iron oxides, but there remains some obscurity in the role of anions. The sulfate ion has been shown to accelerate the corrosion of metallic iron (57). Sapieszko et al. (58) carried out experiments to determine the thermodynamic quantities for the formation of aqueous ferric hydroxide and sulfate complexes at low pH. $FeSO_4^+$ and $NaSO_4^-$ dominated at pH 1.8. Increasing pH shifted the dominant species to ferric hydroxide complexes.

Strahm et al. (59) carried out a very similar study for ferric chloride complexes. $FeCl^{2+}$ and $FeCl_2^+$ were the dominant species in 1M $HClO_4$. Bohm (51) first reported the formation of β-FeOOH from the slow hydrolysis of a solution of Fe(III) chloride. Murphy, Posner, and Quirk (60) conducted extensive aging studies on ferric chloride solutions. They showed that initial polynuclear clusters formed as spheres 1.5 - 3 nm in diameter from Fe(III) chloride solution.

Further aging led to coalescence of the spheres into rod structures, and the eventual formation of β-FeOOH crystals. The preparation of γ-FeOOH from Fe(II) chloride solution was noted by Hamada and Kuma (61). γ-FeOOH was produced in 100% yield at 25°C between pH 5 and 6.5. Above 30°C at the same pH range nearly 100% α-FeOOH was formed. γ-FeOOH was formed by the conversion of Green Rust 1, which has been shown to contain Cl^- (22). Kiyama et al. (62) found that γ-FeOOH could be made directly from $FeBr_2$ or iron metal without passing through the intermediate Green Rust I. X-ray powder diffraction patterns showed less distinct crystallinity for γ-FeOOH made from metal than for γ-FeOOH formed from $FeCl_2$ via Green Rust I (62). Murphy et al. (63) did a study of FeOOH formed from ferric perchlorate solution, and determined that γ-FeOOH could be grown in 0.1M $Fe(ClO_4)_3$ solution by keeping a OH^-:Fe ratio at 0.5. They postulated that while β-FeOOH and α-FeOOH formed by the coalescence of spherical nuclei, γ-FeOOH formed from polymerization of $FeOH^{2+}$ and $Fe_2(OH)_2^{4+}$.

The effect of phosphate on iron oxide growth has been reported by Liepina and Vaivads (64). They found traces of colloidal γ-FeOOH during the corrosion of steel in the presence of phosphate ion. Hand (65) patented a process for the use of phosphate to stabilize γ-FeOOH grown from $FeCl_2$. The mechanism of phosphate action on FeOOH was not mentioned.

The influence of cation substitution can also affect the crystallinity and morphology of FeOOH. Kuhnel, Roorda, and Steensma (66) reported the inhibition of nucleation of α-FeOOH caused by the presence of silica. At pH 12, precipitates formed from $Fe(OH)_3$ were amorphous after 20 hours in the presence of silica. Silica itself could form stable sols, and appeared to stabilize amorphous Fe(III) hydroxide. Mann, Cornell, and Schwertmann (67) investigated the effect of incorporating aluminum into the α-FeOOH lattice. The presence of aluminum at concentrations of up to 15 mole % decreased the overall length of α-FeOOH crystals, and formed platelets rather than needles at higher aluminum contents. The dissolution of aluminum substituted α-FeOOH was carried out by Schwertmann (66). The formation of pores and pits in the crystals after treatment with HCl, was evidence of multiple domains in the particles,

indicating non-uniform incorporation of aluminum. The imperfect crystallinity was thought to be due to the incorporation of the smaller radius Al^{3+} ion into Fe^{3+} sites which led to crystal defects and lattice strain in α-FeOOH.

Organic compounds have been used to alter iron oxide nucleation and growth. Hamada and Matijevic (69) noted that alcohol added to an aqueous solution of ferric chloride enhanced the Fe(III) hydrolysis and α-FeOOH nucleation at 100°C. Complexation of the iron by alcohol was thought to be the cause of the enhancement of hydrolysis, though no coordination between the alcohol and α-FeOOH was detected. Carboxylic acids have been found to inhibit the crystallization of α-FeOOH and α-Fe_2O_3 from amorphous Fe(III) hydroxide (70). Citrate, tartrate, and malate slowed the crystallization of α-FeOOH, while this inhibition was not noted for acetate and formate. The effect of oxalate seemed to favor α-Fe_2O_3 formation over α-FeOOH below pH 10. Those acids which could coordinate in a bidentate fashion influenced the nucleation of α-FeOOH, while monodentate acids did not. The relative strength of the bidentate coordination may have been the source of the activity. Cornell and Schwertmann (71) found that in the inhibition of the nucleation of ferrihydrite, citrate was more active than tartrate, which in turn was more active than lactate. No correlation was found between the stability of ferric ion/acid complexes and inhibition behavior.

Waite and Morel (72) discovered that citrate ion greatly increased the photoreductive dissolution of γ-FeOOH. The increase in dissolution was speculated to occur by solution phase redox reactions activated by the adsorption of citrate on the γ-FeOOH surface. The ligand-like adsorption of citrate on γ-FeOOH was thought to be enhanced due to the possible multidentate association. The charge transfer bands in the surface adsorbed ions were directly excited by photons during illumination. This excitation led to electron transfer from citrate to iron, and caused dissolution of a citrate-Fe(II) complex.

Van der Woude et al. (73) showed that citrate increased the stability of Fe(III) hydroxide sols. The kinetic stability of the sols at high ionic strength was due to the strong adsorption of citrate

which affected the surface charge of the Fe(III) hydroxide particles. Altering the surface charge prevented aggregation and precipitation of the sol.

The crystallinity and morphology of Fe_3O_4 appears to be less sensitive to experimental conditions than FeOOH. The two most important variables in the nucleation and growth of Fe_3O_4 were pH and temperature. Kiyama (41) ran a series of experiments with pH and temperature variation, and plotted the results as a phase diagram which is reproduced in Figure 2.2. The formation of Fe_3O_4 began at an oxidation temperature of 40°C and a OH^-:Fe^{2+} ratio of 2. As temperature was increased, the OH^-:Fe^{2+} ratio window became increasingly wider, to a range from 1 to above 8 at 70°C. Outside of the pure Fe_3O_4 phase area, the products were mixtures of α-FeOOH, γ-FeOOH, and Fe_3O_4. A great deal of research has been done on the growth and stability of Fe_3O_4 under hydrothermal conditions due to the importance of this area in geological studies and power plant operation. Bohnsack (74) edited a book on the solubility of Fe_3O_4 under a variety of conditions, primarily at high temperatures and pressures. At temperatures below 100°C the crystallization of Fe_3O_4 was primarily a problem with transport of species. At hydrothermal conditions up to 350°C, the solubility of Fe_3O_4 was increased to the point that recrystallization following nucleation and precipitation was possible. Higher density Fe_3O_4 was produced with increased perfection in lattice ordering.

Sapieszko and Matijevic (75) produced well ordered Fe_3O_4 crystals at 250°C by aging ferric salts with triethanolamine (TEA). They used H_2O_2 and N_2H_4 to control the oxidation state of the resulting oxides. They concluded that the use of hydrazine was necessary at 250°C to form Fe_3O_4 with no α-Fe_2O_3 impurity. The chelating agent TEA increased the rate of recrystallization of Fe_3O_4. The use of another chelating agent, EDTA, in the formation of Fe_3O_4 was noted by Jones and Bloom (76). At 300°C, in the presence of EDTA, a thick crystalline film of Fe_3O_4 was produced on the surface of steel pipe. In the absence of EDTA, the film was not as thick, and less regular. The chelating ability of EDTA increased the solubility of Fe^{3+} at 300°C, and increased recrystallization following initial oxide formation.

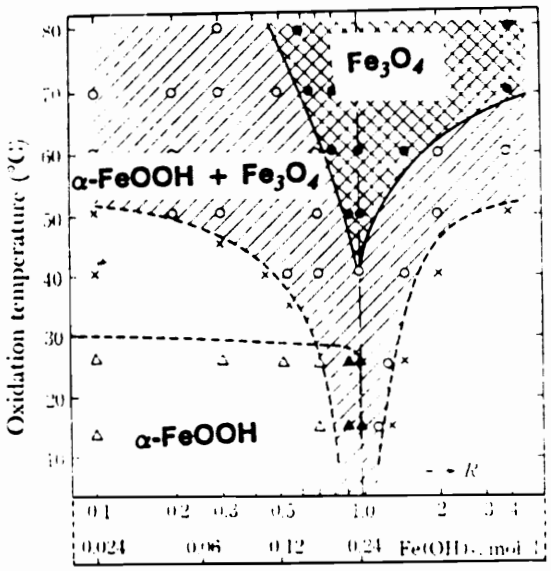

Kiyama, M., Bulletin of the Chemical Society of Japan, Vol. 47(7), p. 1649 (1974)

Figure 2.2 Phase Diagram for Fe_3O_4 + α-FeOOH

The incorporation of cations into Fe_3O_4 is well known. Fe_3O_4 forms a solid solution with other ferrite species such as $MnFe_2O_4$, $CaFe_2O_4$, $ZnFe_2O_4$, $CoFe_2O_4$, and $MgFe_2O_4$ (77). Cd(II), Mg(II), Zn(II), and Fe(II) were incorporated into ferrites by direct reaction with γ-FeOOH above 60°C at pH 8-10. Broadening in the Mössbauer spectrum of the cadmium product indicated non-stoichiometric incorporation of Cd(II) into the ferrite. Takada and Kiyama (78) incorporated Ba(II) into Fe_3O_4. They noted that the size of the ferrite particles increased as the reaction temperature increased, as the rate of formation decreased, and as the concentration of Ba(II) increased.

The incorporation of species into iron oxide can occur during crystallization or by the adsorption and further reaction between adsorbed species and the oxide surface. α-FeOOH has been used as a model surface for adsorption. In 1929 Freundlich and Greensfelder (79) studied the coagulation of α-FeOOH sols resulting from adsorption of Na_2SO_4 from solution. This early work led to theoretical work on the surface charge of suspended particles and their resulting interaction. Other adsorption phenomena, such as the ion exchange properties of α-FeOOH and β-FeOOH were investigated by Paterson and Rahman (80,81). The tubular pores of β-FeOOH were found to adsorb Cl^- ions, but not Na^+ ions from salt solutions. Perchlorate ions were excluded from the pores in β-FeOOH on the basis of their size. Electroneutrality on the oxide was maintained by adsorption of protons into β-FeOOH. α-FeOOH showed amphoteric behavior. Anion adsorption on α-FeOOH was greatest at low pH, and decreased to zero at neutral pH. Cation capacity was greatest at high pH. The ion exchange results pointed to an α-FeOOH protonation/deprotonation mechanism, rather than ion trapping in pores as was found for β-FeOOH.

The adsorption of cations onto α-FeOOH has been studied as a method for wastewater treatment. Goncalves, Sigg, and Stumm (82) carried out electrochemical experiments for the analysis of Pb(II) ions adsorbed on α-FeOOH. From their study they were able to determine

an equilibrium adsorption coefficient for Pb(II) on α-FeOOH. This provided information on the mechanism of adsorption. Further kinetic data was determined for the adsorption of Cd(II) on α-FeOOH by Dzombak and Morel (83). They concluded that the adsorption of Cd(II) followed a surface coordination process involving two different types of sites on α-FeOOH. They also stated that several days were required to reach equilibrium conditions at high Cd(II) concentrations. Farley et al. (84) used radioactive ^{109}Cd to monitor the competitive adsorption of Cd(II) and Cu(II) on α-FeOOH. A surface precipitation model was developed. Theis and West (85) investigated the effect of cyanide complexation on the adsorption of metal ions on α-FeOOH. They concluded that the adsorption of complexes was dependent upon surface - ion electrostatics. Uncomplexed cyanide showed no adsorption on α-FeOOH, but $Fe(CN)_6^{3-}$ and $Ni(CN)_4^{2-}$ showed strong adsorption at low pH.

The adsorption of neutral species on α-FeOOH has been carried out in solution. Zeltner and Anderson (86) determined that adsorption of CO_2 onto α-FeOOH decreased the zero point of charge of the crystals from 9.0 to 8.1. Nitrogen purging for two months removed all traces of adsorbed CO_2. The decrease in adsorbed CO_2 was confirmed by infrared spectroscopy, which showed sharpening in the surface hydroxyl stretching vibration, and the absence of carbonate stretches below 1550 cm^{-1}.

An infrared study was made by Buckland (87) on the adsorption of carboxylic acids on α-FeOOH from carbon tetrachloride solution. Carboxylic acids adsorb on α-FeOOH in a bidentate chelating configuration. A comparison between dicarboxylic acids and single functional carboxylic acids showed that the adsorption of dicarboxylic acids was more effective in the inhibition of corrosion formation on iron (88). The adsorption of hydroxycarboxylic acids on α-FeOOH was studied by Cornell and Schindler (89) using infrared spectroscopy. They concluded that coordination of carboxyl groups to the surface of α-FeOOH occurred through both oxygens of each acid group giving distinctive symmetric and asymmetric stretches in the IR region between 1400 and 2100 cm^{-1}. They also proposed a model of surface adsorption

of organic molecules on α-FeOOH. This model assigned adsorption sites for carboxylic acids based on the location of the functional groups on the organic molecule and the position of Fe atoms on particular crystal faces of α-FeOOH. Experimental measurements of total adsorbed tartrate molecules best fit the theoretical value of sites predicted by the model.

The idea of site specific adsorption of multifunctional carboxylic acids on iron oxides was also suggested for the mechanism of adsorption of iminodiacetic acid on α-Fe_2O_3 (90). Rueda, Grassi, and Blesa (91) carried out adsorption of EDTA on α-FeOOH. They determined that the surface coverage was on the order of 10^{-18} μmole/100 $Å^2$ at pH 5.3. The adsorption of EDTA was determined to cause cathodic reduction of Fe_3O_4 films in NaOH solution above 100°C (92). The oxidation of Fe_3O_4 led to dissolution of Fe(III) complexes from the surface of iron metal. The same oxidation of EDTA was found to occur in the presence of ferric complexes in solution (93).

Techniques of Iron Oxide Characterization

Adsorption of ions, morphology and crystallinity, and hydrolysis and oxidation all require complex analytical characterization. A review of the literature revealed a myriad of analytical techniques that have been used in characterization of FeOOH and Fe_3O_4. In addition to standard chemical titration techniques to determine Fe^{3+}/Fe^{2+} ratios and pH measurement, at least fourteen instrumental methods were found. In order of most surface sensitive to least surface sensitive, they were:

1. X-ray photoelectron spectroscopy (XPS)
2. Secondary ion mass spectroscopy (SIMS)
3. Gas adsorption
4. Electrophoresis
5. Viscometry
6. Electron microscopy (TEM,SEM)
7. Differential scanning calorimetry (DSC)

8. Infrared spectroscopy (IR)
9. Differential pulse polarography (DPP)
10. Mössbauer spectroscopy
11. Thermal gravimetric analysis (TGA)
12. Electron diffraction
13. Neutron diffraction
14. X-ray diffraction (XRD)

This section is not intended to list every researcher who has used each technique, but rather to describe some of the experimental parameters of each type of analysis by a few representative illustrations.

X-ray photoelectron spectroscopy (XPS) was used be Haber et al. (94) to determine the functionality of surface oxygen groups on metal oxides. Oxide and hydroxide peaks were assigned binding energies of 530.0 and 531.4 eV, respectively. The position and shape of the oxygen 2s spectrum were found to be independent of the metallic cation. Oku and Hirokawa (95) used XPS to analyze the surface chemistry of Fe_3O_4. The oxidation states of iron could not be resolved from 2p spectra due to the high overlap of Fe^{2+} and Fe^{3+} photopeaks. No analysis of oxygen spectra was done. SIMS has been used as a technique to probe the surface chemistry of iron oxides. Mitchell, Sproule, and Graham (96) used Xe^+-SIMS to investigate hydroxyl functionalities on the surface of passive iron oxide films. Static SIMS sputter profiles were made at 4 Å/min m/z 72, $^{56}FeO^+$, and 73, $^{57}FeO^+$ and $^{56}FeOH^+$. By ratioing counts at m/z 73 and 72, an estimate of 10% surface hydroxyl groups was made for electropolished iron films.

Micale, Kiernan, and Zettlemoyer (97) characterized the surface of α-FeOOH by water adsorption isotherm measurements before and after hexamethyldisilazane (HMDS) treatment. Water adsorption was carried out as a gravimetric technique to determine the hydrophilicity of α-FeOOH. Ten molecules of water per 100 $Å^2$ of α-FeOOH surface were found to adsorb at

25°C. Vacuum treatment removed all of the adsorbed water indicating that the adsorption was reversible. HMDS treatment reduced the amount of water that adsorbed at 25°C to 5.8 molecules per 100 $Å^2$ of α-FeOOH surface. The silation process deactivated surface hydroxyl groups, and therefore reduced the number sites for water adsorption.

Using a microelectrophoresis apparatus, Matijevic and Scheiner (98) measured the point of zero charge of β-FeOOH crystals grown from ferric chloride sols. The PZC was found to be 7.2 for β-FeOOH, and did not change due to variation in aging time and temperature of the sol. Gasca, Cornejo, and Arambarri (99) used electrophoresis to determine isoelectric points of 8.3 and 7.8 for α-FeOOH and γ-FeOOH, respectively.

The dependence of viscosity on zero point charge was investigated by Heller (100) for a suspension of monodispersed β-FeOOH crystals. The viscosity measurement was carried out by detecting discontinuities in flow light scattering at critical shear rates. While this technique is not the most common or convenient method for viscosity measurement, it was used to point out difficulties in interpretation of Couette type viscometers which are essentially two concentric cylinders. The errors in viscosity of dilute solutions were determined to within $\pm$ 1% with the flow light scattering procedure which was an order of magnitude better than that for the Couette device. These two techniques were significantly more accurate than Cannon type viscometers.

The use of electron microscopy for the study of particle size and morphology is common among many iron oxide researchers. SEM is used to determine shape of non-uniform oxide particles (42). TEM was used by Maeda and Hirono (101) to study dendrite formation in α-FeOOH. The angle between dendrites and the body of the crystals was found to be 120°. Dendrites occurred by twinning at the (020) plane. Cornell, Mann, and Skarnulis (102) carried out high resolution electron microscopy studies of α-FeOOH and β-FeOOH. Micrographs showed planes often contiguous across grain boundaries. Dendrite growth and small regions of local disorder were seen on (100) faces, and were postulated to occur due to precipitation of secondary nuclei such as α-Fe_2O_3.

MacKenzie, Paterson, and Swaffield (103) conducted experiments using differential scanning calorimetry on α-FeOOH to determine the extent of surface hydroxyl groups. The complex shape in the endothermic curve was due to three types of surface hydroxyl groups. No explanation of the difference among the three types of groups was given. An early use of thermal gravimetric analysis was to determine the amount of water in so called 'Fe_2O_3-H_2O' crystals (104). The amount of hydration was used to confirm iron oxygen stoichiometries.

Infrared spectroscopy was used to examine surface hydroxyl groups on α-FeOOH by Rochester and Topham (105). α-FeOOH was exposed to deuterium oxide vapor which exchanged surface hydroxyls to deuteroxyl groups. Based on shifts of bands from deuterium exchange, hydroxyls were assigned to four classes; unperturbed surface hydroxyls, hydrogen bonded surface hydroxyls, adsorbed water molecules, and bulk hydroxyls. These classes may be similar to those three types of hydroxyls discovered using calorimetry by MacKenzie et al. (103). In an infrared spectroscopy study, Tejedor-Tejedor and Anderson (106) carried out attenuated total reflectance *in situ* at the α-FeOOH-water interface. To do this investigation, a cylindrical internal reflectance cell was designed from a ZnSe crystal. They concluded that anions such as NO_3^- and Cl^- adsorbed at the α-FeOOH-water interface, changed the ordering of water molecules at the oxide surface.

Differential pulse polarography was used to examine the effect of surface adsorption of Pb(II) on α-FeOOH on the redox potential of Pb ions (82). This study gave indirect measurement of an adsorption coefficient of metal ions on α-FeOOH, and the pH dependence of cation adsorption.

A paper by Dziobkowski, Wrobleski, and Brown (107) combined infrared and Mössbauer spectroscopies in an examination of ferric complexes with dicarboxylic acids. Infrared confirmed the existence of symmetric and asymmetric streches of carboxyl groups coordinated through both oxygen atoms of the carboxyl in the ferric-dicarboxylate complexes. Mössbauer spectra taken from 15 to 300K indicated that a Fe_3O center might exist in the ferric complexes. This

subcritical nucleus might have implications in the growth of FeOOH from dicarboxylate complexes. Music et al. (108) used Mössbauer spectroscopy to investigate the formation of FeOOH from hydrolysis of ferric salts. They concluded that NO_3^- and SO_4^{2-} did not coordinate with Fe-O polymer species, but Cl^- did coordinate. The formation of $FeSO_4^+$ was found to suppress the polymerization process. This suppression may have been involved with the difference in phase production of FeOOH from $FeCl_2$ and $FeSO_4$. Mössbauer spectroscopy was used by Kanzaki and Katsura (43) to examine the conversion of $Fe(OH)_2$ to Fe_3O_4. Mössbauer spectra suggested that the intermediate Green Rust II had an Fe^{3+}:Fe^{2+} ratio 1:2.

Electron diffraction has been used to confirm the phase of microscopic crystals, and to determine the orientation of axes. Cornell, Mann, and Skarnulis (102) determined that dendrites grow about the [100] axis from needlelike crystals which grow in the [001] direction. Jones and Bloom (76) also used electron diffraction to determine mixed phases in primarily Fe_3O_4 films on steel plate. They determined that crystals grew parallel to the steel surface with no preferred direction.

Christensen, Lehmann, and Wright (109) employed small angle neutron scattering to study the aging of $Fe(OH)_3$. They were able to follow the increase in particle size and α-FeOOH densification as aging time increased. Conversion of α-FeOOH to α-Fe_2O_3 occurred particle by particle with no evidence of dissolution and recrystallization. Christensen, Lehmann, and Convert (110) followed deuterium oxide exchange into γ-FeOOH with neutron powder diffraction. γ-FeOOH crystals with an average crystal length of 200 Å underwent complete deuterium-hydrogen exchange in 6 minutes at 100°C. A crystal structure of the unit cell was developed based on two possible space groups, Cmcm and $Cmc2_1$. The higher symmetry of the $Cmc2_1$ made it a more likely candidate than Cmcm, although the R value of $Cmc2_1$ was lower.

X-ray powder diffraction has been widely used as a technique to determine the crystal phase of iron oxide crystals, and less often to estimate average crystal size. Early work with x-ray powder diffraction was done from a powder photograph (20). Bernal (32) used powder

photographs to determine the structure of Green Rust I and Green Rust II. Knight and Silva (38) used XRD to determine composition in mixed precipitates of γ-FeOOH, β-FeOOH, and α-FeOOH. Atkinson (40) used XRD as a kinetic tool to determine the rate of conversion of β-FeOOH to α-FeOOH and α-Fe_2O_3.

This literature review has shown the extent of research that has been carried out in the investigation of how iron oxide crystals nucleate and grow. There are many experimental variables that affect crystallinity and morphology of the resulting phases. Both cations and anions were shown to adsorb on FeOOH phases. Organic anions, particularly dicarboxylic acids, were postulated to adsorb at sites on the surface of FeOOH crystals defined by chemical characteristics of the adsorbate.

This dissertation concerns the alteration of morphology and phase of FeOOH and Fe_3O_4 due to changes in chemical environment during crystal nucleation and growth. The use of multifunctional carboxylic acids as growth modifiers for FeOOH was investigated. While previous researchers examined the adsorption of dicarboxylic acids on iron oxides, there has been no record of morphology changes in oxide crystals due to presence of dicarboxylic acids. The purpose of the work was to better explain the mechanism of iron oxide nucleation and growth from aqueous hydroxide suspensions through the examination of morphology modification due to alterations in the surface of growing crystals.

Chapter 3 : Experimental

In this chapter, the methods and materials used for the dissertation research are described. This chapter has been divided into three sections; the first section examines a study carried out on the growth of FeOOH, the second section describes an investigation of the nucleation and growth of Fe_3O_4, and the third section includes the techniques and instrumental parameters used for analysis of the materials produced during the FeOOH and Fe_3O_4 studies.

In the FeOOH study, the section is divided into analyses of the effects of different types of potential growth modifiers including metal ions, dicarboxylic acids, EDTA, phosphate, and halide ions on nucleation and growth. Other experimental factors which affected nucleation and growth of FeOOH are included in the analyses of growth modifiers. These additional factors include reaction temperature, time of addition of the potential growth modifiers, and the effect of mixing growth modifiers in a single reaction. Also included in the FeOOH section is an experiment in which crystalline intermediates produced during the formation of FeOOH were sampled and analyzed.

The Fe_3O_4 section is divided according to the type of starting materials used to produce the Fe_3O_4 crystals. These starting materials include $FeSO_4$ used alone, a mixture of α-FeOOH and $FeSO_4$, or a mixture of a soluble Fe^{3+} salt and $FeSO_4$. Other experimental factors which were examined include pH, reaction temperature, oxidation rate, the Fe^{3+}/Fe^{2+} ratio of the starting material, and the effect of metal ions and solubilization agents on the growth of Fe_3O_4.

The third section describes techniques used for analysis of iron oxides including x-ray photoelectron spectroscopy (XPS), scanning and transmission electron microscopy (SEM,TEM), BET surface area analysis, viscometry, x-ray powder diffraction (XRD), microelectrophoresis, and photoacoustic infrared spectroscopy (PAS-IR).

I. FeOOH

All of the reactions carried out to produce FeOOH were done in a single apparatus and used a common preparation scheme. The apparatus consisted of a 1.5 liter stainless steel beaker, a high shear stirrer through which oxygen was flowed by means of a stainless steel tube, and a temperature-controlled water bath, A schematic of the stirrer is shown in Figure 3.1. The effect of the stirrer was to agitate the reaction suspension, and to break the flow of oxygen into tiny bubbles which could be efficiently incorporated into the reaction mixture.

The preparative scheme for the production of FeOOH was as follows: 1.2 liters of deionized water were placed into the stainless steel vessel, and the vessel was placed in the water bath. When the water had reached the desired reaction temperature, 168.5 g of $FeSO_4$-$6H_2O$ (Fisher Reagent Grade) were dissolved in the deionized water. This amount of $FeSO_4$ was calculated to produce a 0.4M solution of Fe^{2+} upon addition of all reagents and water. After complete dissolution of $FeSO_4$ occurred, the potential growth modifier was dissolved in 100 ml of deionized water, added to the Fe^{2+} solution, and the mixture was allowed to equilibrate for ten minutes. A NaOH solution consisting of 32.4 g NaOH (Alfa) in 200 ml of deionized water was then added to the Fe^{2+} solution. This hydroxide concentration was calculated to precipitate all Fe^{2+} as $Fe(OH)_2$. After an additional 5 minutes of equilibration time, oxygen was flowed into the reactor at 0.12 cm^2/sec. This oxygen flow rate was found to complete the total oxidation of Fe^{2+} to Fe^{3+} in five hours. After the 5 hr reaction time was completed, the FeOOH product was filtered, washed three times with deionized water, and dried overnight in a vacuum oven at approximately 10^{-1} torr. Two hundred ml of the unfiltered reaction suspension was kept for viscosity measurement.

A. Metal ions

The effect of incorporating different metal ions into the α-FeOOH reaction was examined using Zn^{2+} and Mg^{2+}, both as sulfate salts (Aldrich Reagent Grade). $ZnSO_4$ was placed into

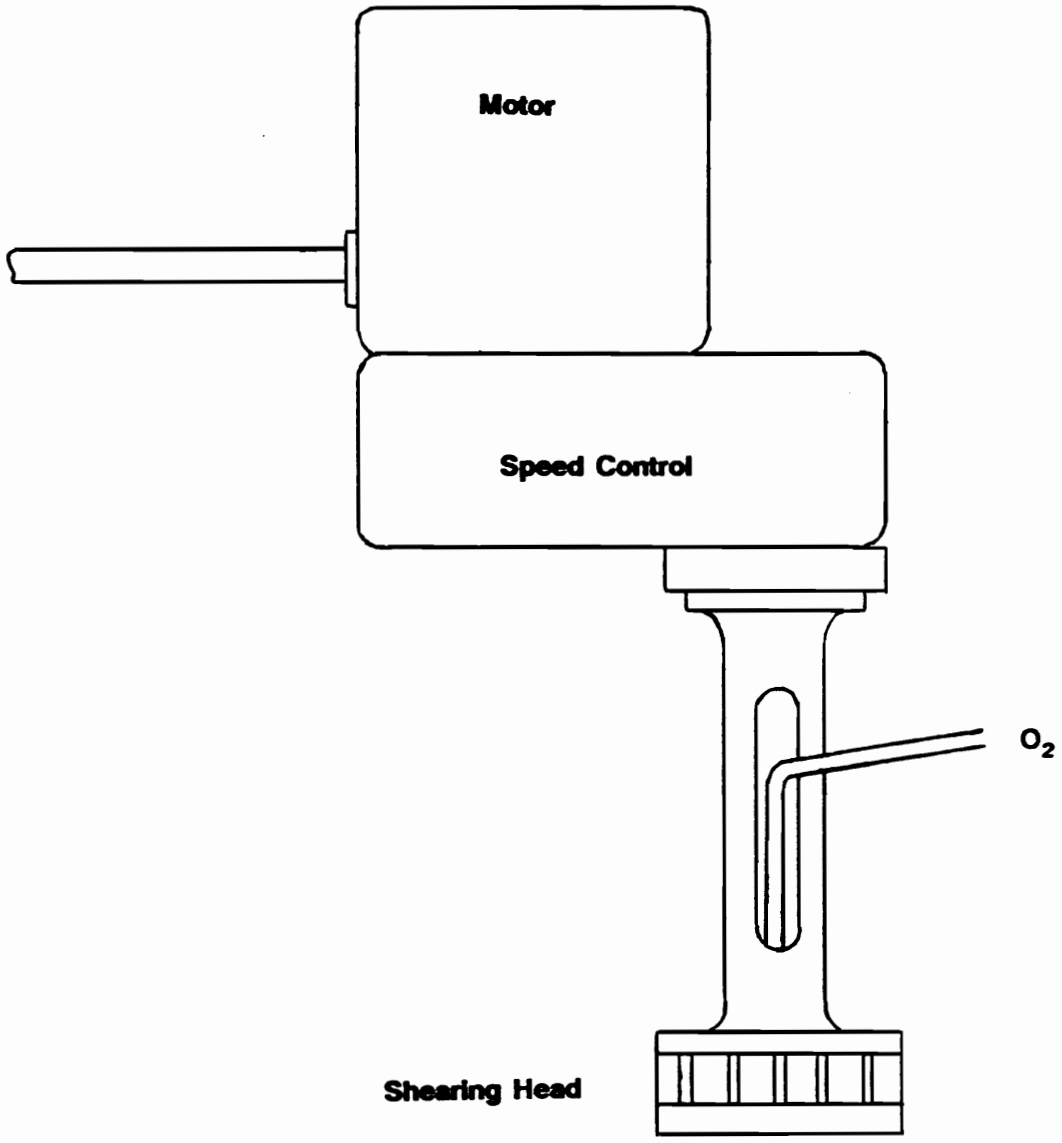

Figure 3.1 The High Shear Stirrer used for FeOOH Growth

the Fe^{2+} solution prior to the onset of oxygen flow in an amount calculated to give a solution concentration of 0.0043M Zn^{2+}. This concentration of Zn^{2+} is equivalent to 3 wt. % of the final FeOOH product if all Zn^{2+} was incorporated into the crystals. Next a series of reactions was carried out containing Mg^{2+} at solution concentrations in a concentration range from 0.0011M to 0.0043M. Then a reaction was run containing 0.0022M Zn^{2+} and 0.0022M Mg^{2+}. To determine what the effect of addition time of a metal ion was on the α-FeOOH product, sufficient $ZnSO_4$ to produce a solution concentration of 0.0088M Zn^{2+} (6 wt. %) was added at four different times during the reaction, at 0, 1, 2, and 3 hours following the start of oxygen flow. The 6 wt. % Zn^{2+} concentration was chosen to allow easier detection by XPS than the 3 wt. % Zn^{2+} used initially.

B. Dicarboxylic Acids

Dicarboxylic acids were chosen as potential modifiers for the nucleation and growth of α-FeOOH. The series of dicarboxylic acids chosen for this study included a range of saturated linear dicarboxylic acids extending from carbonate, which is a one carbon anion with potential bidentate coordination, to pimelic acid, the seven carbon dicarboxylic acid. The names and structures of the series of dicarboxylic acids are listed in Table 3.1.

α-FeOOH growth reactions were performed using two preparative schemes. In the first series of reactions, the dicarboxylic acid was added to yield 0.016M. The second series of reactions contained 0.016M dicarboxylic acid and 0.0044M zinc sulfate to allow comparison of relative effects of two types of additives.

Reactions containing fumaric, maleic, crotonic, and succinic acids were carried out at 0.016M, 0.008M, 0.004M, and 0.002M. These four acids each contain four carbons, but are structurally different (Table 3.1).

All of the previously listed metal ion and dicarboxylic acid reactions were done at 40°C. Two additional reactions were carried out with 0.01M succinic acid and fumaric acid at 50°C.

Table 3.1 Dicarboxylic Acids from FeOOH Study

Carbonate

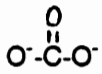

Oxalic Acid

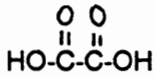

Malonic Acid

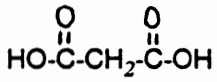

Succinic Acid

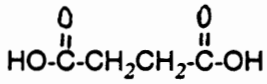

Glutaric Acid

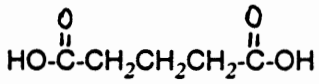

Adipic Acid

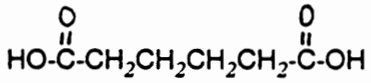

Pimelic Acid

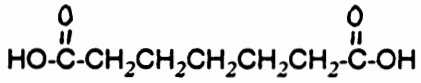

Fumaric Acid

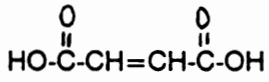

Maleic Acid

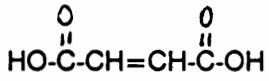

Crotonic Acid

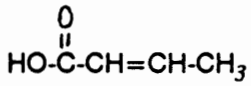

All dicarboxylic acids were Fisher Reagent grade.

Competitive reactions involved adding two dicarboxylic acids at the same time into α-FeOOH growth reactions. The coaddition reactions grouped 0.01M malonic acid with sodium carbonate, oxalic, succinic, or adipic acid, and grouped 0.01M succinic acid with 0.01M sodium carbonate or oxalic acid.

The time of addition study involved adding a dicarboxylic acid into α-FeOOH growth reactions. Malonic acid was added at different times during the oxidation procedure including; 0, 1, 1.5, 2, 2.5, 3, and 4 hours after the start of oxygen flow. Other experiments used succinic acid added at 1.5 and 2.5 hours of reaction time, and oxalic and adipic acid each added at 2.5 hours after oxidation had started.

C. EDTA

Ethylenediaminetetraacetic acid (EDTA) was chosen as a potential growth modifier; the structure of EDTA is shown in Table 3.2. A set of experiments was carried out which examined the relative effects of EDTA concentration and reaction temperature. The concentration of EDTA was varied from 0.0025M to 0.015M in reactions ranging in temperature from 25°C to 50°C, producing a matrix which showed how changes caused by the presence of EDTA were dependent upon reaction temperature.

To see if EDTA would behave similarly in the presence of other known growth modifiers for α-FeOOH, competitive experiments were carried out containing both EDTA and dicarboxylic acids. Reactions contained between 0.01 and 0.015M EDTA along with 0.01M sodium carbonate, or 0.01M malonic, succinic, or adipic acids in the Fe^{2+} solution prior to oxidation. The products of these reactions were examined to see if the effects of EDTA were additive or competitive with the effects of dicarboxylic acids.

A time of addition study, similar to that carried out with the dicarboxylic acids, was done using the addition of sufficient EDTA to yield 0.0125M at various times during a 40°C oxidation reaction. The addition times of EDTA were 0, 60, 80, 100, and 120 minutes following the start of oxygen flow.

Table 3.2 EDTA and Model Compounds

*** Ethylenediaminetetraacetic Acid (EDTA)

$(HO_2CCH_2)_2NCH_2CH_2N(CH_2CO_2H)_2$

* Ethylenediaminediacetic Acid (EDDA)

$(HO_2CCH_2)NHCH_2CH_2NH(CH_2CO_2H)$

** Iminodiacetic Acid

$(HO_2CCH_2)_2NH$

* Ethylenediphosphonic Acid

$(HO)_2OPCH_2CH_2PO(OH)_2$

* Ethylenediaminetetramethylenephosphonic Acid

$[(HO)_2OPCH_2]_2NCH_2CH_2N[CH_2PO(OH)_2]_2$

* Ethylenediaminediorthohydroxyphenylacetic Acid

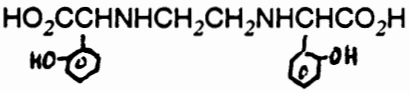

** Butanetetracarboxylic Acid

$HO_2CCH_2CH(CO_2H)CH(CO_2H)CH_2CO_2H$

** Diaminocyclohexanetetraacetic Acid

$(HO_2CCH_2)_2NCHCHN(CH_2CO_2H)$

*** Pyromellitic Acid

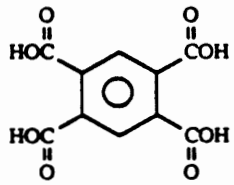

DACHTA

*** Phthalic Acid

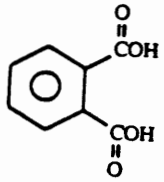

*** Alfa Reagent Grade, ** Sigma Reagent Grade , * Tokyo Kasei Reagent Grade

Two experiments were carried out at 25°C using 0.01M [EDTA-Fe^{III}]$^-$ in place of EDTA. The [EDTA-Fe^{III}]$^-$ was added in solution prior to oxygen addition in the first case, and at 120 minutes following the start of oxidation in the second experiment.

Model compounds were chosen to try to determine the mechanism by which EDTA altered FeOOH nucleation and growth. Table 3.2 list a number of compounds which each share some chemical or structural characteristics with EDTA. These model compounds were each added in place of EDTA to determine if any would induce similar changes in the morphology and crystallinity of FeOOH to that exhibited by EDTA. Model compounds were examined at concentrations ranging from 0.01 to 0.03M, at temperatures from 7°C to 40°C.

D. Phosphate

Using phosphoric acid as a source of phosphate, FeOOH growth reactions were carried out with a phosphate concentration from 0.01M to 0.02M, and in a temperature range from 7°C to 50°C. Model compounds similar in chemistry and structure to phosphate were examined. Those model compounds included $Na_2B_4O_7$, Na_3VO_4, Na_2MoO_4, as well as several substituted phosphonic acids. The structures of these compounds can be found in Table 3.3. The model compounds were added to reactions at the same range of concentration and temperature as used for phosphate experiments.

E. Halides

A study was done to examine the effect of chloride and bromide at concentrations from 0.01M to 0.8M on FeOOH grown from $FeSO_4$. The halide salts were added at the beginning of the oxidation reactions.

F. Adsorption of Acids

Keith Becker, an undergraduate researcher under the direction of the author, carried out an

Table 3.3 Phosphoric Acid and Phosphate Model Compounds

* Phosphoric Acid

$(HO)_3PO$

*** Ethylenediphosphonic Acid

$(HO)_2OPCH_2CH_2PO(OH)_2$

** Fluorophosphoric Acid

$(HO)_2OPF$

** Sodium Tetra Borate

$Na_2B_4O_7$

* Sodium Orthovanadate

Na_3VO_4

* Sodium Molybdate

Na_2MoO_4

* Aldrich Reagent Grade, ** Fisher Reagent Grade, *** Tokyo Kasei Reagent Grade

investigation on the adsorption and desorption of dicarboxylic acids and EDTA on α-FeOOH. Solutions of 0.01M oxalic, succinic, and adipic acids were prepared. Twenty-five ml of each acid solution were added to twenty five ml samples of α-FeOOH product suspension. Each fifty ml solution was then split. The pH was recorded for each suspension containing a dicarboxylic acid. One set of the acid containing suspensions was maintained at its natural pH. The pH of the second set of the acid suspensions was adjusted to 5.2-5.5 with 0.1M NaOH solution. The viscosity of the suspensions at natural pH and pH 5.2-5.5 was measured. Each suspension was allowed to sit for 3 hours, then filtered, washed twice with deionized water, and dried overnight in a vacuum oven at approximately 10^{-4} torr. PAS-IR spectra were taken of the dried samples to determine the extent of adsorption of each dicarboxylic acid onto α-FeOOH.

The adsorption procedure was repeated for 0.01M EDTA. A desorption experiment was also carried out in which α-FeOOH samples grown in the presence of EDTA were placed into solutions adjusted with H_2SO_4 to pH 3.4, 2.4, 2.0, and 1.5. After 2 hours, the suspensions were filtered, washed, and dried. PAS-IR spectra were obtained for the desorption experiment samples.

G. Intermediate Sampling

The search for crystalline intermediates during the formation of FeOOH was carried out by measuring XRD patterns of intermediate samples. During the reaction, 100 ml samples were removed from the reaction suspension at various times during the oxidation. These samples were then centrifuged at high speed for one minute which allowed approximately half of the solution volume to be decanted as a clear solution from the settled suspension. The centrifuged solids were mixed in a 1:1 ratio with a solution of gelatin. The gelatin solution was prepared by mixing a 7 gram package of unflavored gelatin obtained at the supermarket with 50 ml of deionized water saturated with N_2. The gelatin mixture was heated to 60°C to dissolve the gelatin, then cooled to 40°C. The gelatin was mixed with the centrifuged iron hydroxide material, then spread as a film onto aluminum foil. After one minute of setting time, the film was

pressed onto a glass slide, and placed in a desiccator which had been purged with N_2.

Intermediate sampling was carried out for three $FeSO_4$ reactions, and one reaction in which the Fe^{2+} reagent was $FeCl_2$. Of the three $FeSO_4$ reactions, one contained no growth modifier, one reaction contained 0.01M EDTA, and one reaction contained 0.02M phosphoric acid. The $FeCl_2$ reaction contained no growth modifier. Samples were extracted at reaction times of 0, 60, 100, 180, and 300 minutes for reactions run with 300 minute total oxidation times.

II. Fe_3O_4

All of the reactions carried out to produce Fe_3O_4 were done in a single apparatus consisting of a four neck 2 liter round bottom flask with a reflux condenser, a heating mantle, a glass stirring rod with Teflon paddles, and tubes for introduction of N_2 and O_2. A drawing of the apparatus is shown in Figure 3.2.

The procedure for growing Fe_3O_4 was carried out by mixing the Fe^{2+} and Fe^{3+} reagents in 1200 ml of deionized water at concentrations calculated to produce 0.15 moles of Fe_3O_4 per liter. NaOH was added as a 300 ml solution, then the suspension was heated to reaction temperature under N_2, followed by O_2 flow for up to 24 hours. At the end of the reaction time, the Fe_3O_4 was settled with the aid of a strong permanent magnet, washed several times with deionized water, filtered, and dried overnight in a vacuum oven at approximately 10^{-4} torr.

A. $FeSO_4$

Using $FeSO_4$ as the sole source of Fe in the Fe_3O_4 reaction required conversion of two thirds of the initial Fe^{2+} to Fe^{3+} to produce the correct stoichiometric ratio of $Fe^{2+}{}_1Fe^{3+}{}_2O_4$. The optimum oxidation rate was investigated by running experiments in which air or O_2 was flowed at a rate between 0.12 cm^3/sec and 0.60 cm^3/sec into the vessel after reaching reaction temperature. Another approach was to allow room air to diffuse into the reactor over a twenty hour period. This slow diffusion of air occurred naturally due to the open reflux condensor in

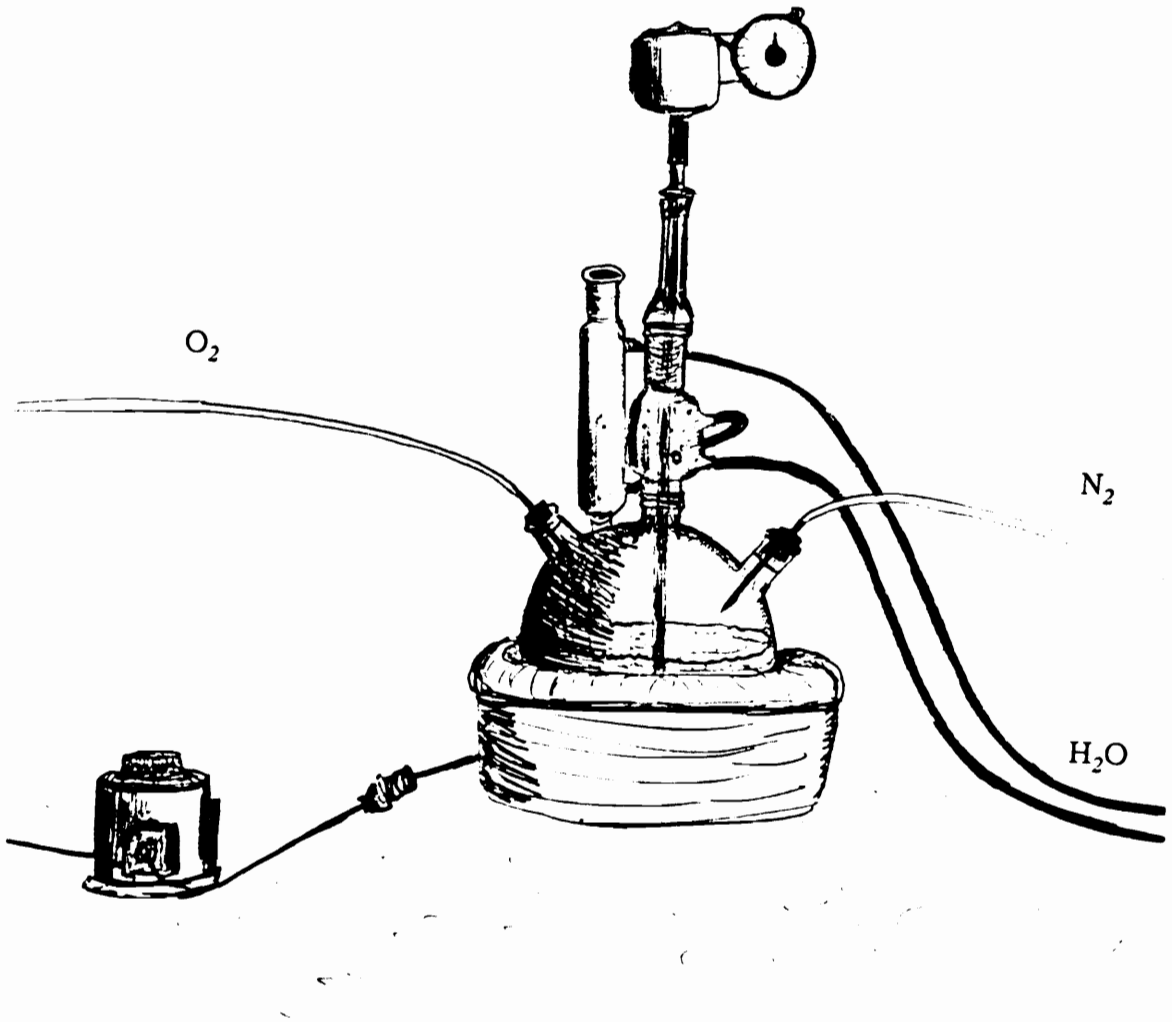

Figure 3.2 Apparatus Used for Fe_3O_4 Production

the apparatus. N_2 flow was maintained over the $Fe(OH)_2$ suspension until the reaction temperature, 90°C was reached 45 minutes following NaOH addition. After N_2 was turned off, air entering the apparatus through the reflux condenser facilitated the oxidation process. The optimum OH^-:Fe ratio of the starting material was studied by adjusting the amount of NaOH from between 1.8 and 4 equivalents per mole of Fe^{2+} in a series of reactions.

In an investigation of the effects of added metal ions on Fe_3O_4 morphology, all reactions were carried out using the following conditions : $FeSO_4$ as the source of Fe^{2+}, 3 equivalents of NaOH per Fe^{2+}, an oxygen flow rate of 0.5 cm^3/g, and 20 hr. total reaction time. The metal ions studied were Zn^{2+}, Mn^{2+}, Cu^{2+}, Ni^{2+}, Mg^{2+}, and Ca^{2+}. All metals were added as sulfates (Aldrich Reagent Grade). The concentration ranges (mole % relative to $FeSO_4$ in the reaction, or relative to Fe^{2+} in the product) examined for the different metal ions are listed in Table 3.4.

Intermediate samples were extracted from two 5 mole % Zn^{2+} reactions. One reaction used 3.5 equivalents of NaOH per equivalent of Fe^{2+}, the other reaction contained 2 equivalents of NaOH per equivalent of Fe^{2+}. Samples were extracted after 60, 180, and 300 minutes following the start of oxygen flow. Samples were suspended in gelatin for XRD measurements as described above.

α-FeOOH + $FeSO_4$

Crystalline α-FeOOH was used as the source of Fe^{3+}. The effect of the starting Fe^{3+}:Fe^{2+} ratio on the morphology of Fe_3O_4 was examined, in addition to other experimental parameters. Using a reaction temperature of 95°C, and a initial stoichiometric Fe^{3+}:Fe^{2+} ratio of 2, the NaOH concentration was varied from 1.8 to 2.6 equivalents of NaOH per Fe^{2+}. Having determined how the stoichiometric addition of Fe^{3+}:Fe^{2+} affected Fe_3O_4 morphology, the Fe^{3+}:Fe^{2+} ratio was reduced to 1:1, keeping a sufficient Fe concentration to produce 0.15 moles per liter.

The 1:1 Fe^{3+}:Fe^{2+} experiments can be divided into two sections, those in which all α-FeOOH and $FeSO_4$ was added at the beginning of the reaction, and those in which Fe reagents were

Table 3.4 Metal Ions Incorporated Into Fe_3O_4

A plus sign in the table indicates that a reaction was carried out at that concentration with that metal ion.

*	**	Zn^{2+}	Mn^{2+}	Ni^{2+}	Mg^{2+}	Ca^{2+}	Cu^{2+}
20%	6.7%	+	+	+			+
10%	3.3%	+	+		+		
5%	1.7%	+	+	+	+	+	+
1%	0.3%	+	+		+		

* Metal ion mole % relative to Fe^{2+} in product

** Metal ion mole % relative to Fe^{2+} in starting $FeSO^4$

Table 3.5 Parameters of Fe_3O_4 Reactions From α-FeOOH and $FeSO_4$

Fe^{3+}:Fe^{2+} ratio = 1:1, all Fe reagents at start

1. 97°C, R = 1, O_2 flow started directly after NaOH addition
2. 97°C, R = 1, N_2 for 1 hour following NaOH addition, air diffusion
3. 97°C, R = 1.1, 30 min N_2 after NaOH addition, air diffusion
4. 97°C, R = 0.9, 40 min N_2 after NaOH addition, air diffusion
5. 97°C, R = 0.9, 50 min N_2 after NaOH addition, air diffusion
6. 97°C, R = 0.8, 70 min N_2 after NaOH addition, air diffusion
7. 97°C, R = 0.9, 180 min N_2 after NaOH addition, air diffusion
8. 97°C, R = 0.9, no N_2 after NaOH addition, air diffusion
9. 97°C, R = 0.9, 90 min N_2 after NaOH addition, O_2
10. 97°C, R = 0.95, 90 min N_2 after NaOH addition, air diffusion
11. 90°C, R = 0.95, 180 min N_2 after NaOH addition, air diffusion
12. 90°C, R = 2, 90 min N_2 after NaOH addition, air diffusion
13. 90°C, R = 1.5, 60 min N_2 after NaOH addition, air diffusion
14. 90°C, R = 1.5, 0.01M Na_2CO_3, 60 min N_2 after NaOH addition, air diffusion
15. 90°C, R = 1.5, 60 min N_2 after NaOH addition, air diffusion, 20 liter reactor

R = OH^- : Fe^{2+} ratio

added at different times during the reaction. In the reactions with all Fe species added at the start, two reaction temperatures were examined, 90°C, and 97°C. The oxygen flow rate ranged from 0.12 cm^3/sec to 0.01 cm^3/sec, the latter value estimated for the diffusion of room air into the vessel. The OH^-:Fe^{2+} ratio was varied from 1.8 to 4. Table 3.5 lists all reaction parameters of experiments with initial addition of Fe reagents.

Those reactions in which Fe reagents were added at different times during the oxidation were termed seed and growth reactions. During the initial seed stage of the reaction, nearly stoichiometric amounts of Fe^{3+} and Fe^{2+} were used, giving a Fe^{3+}:Fe^{2+} initial ratio of 1.9:1. After producing Fe_3O_4 crystals, additional Fe^{2+} was added in the growth step, giving a final Fe^{3+}:Fe^{2+} ratio of 1:1. The experimental parameters examined in the seed and growth reactions included temperature, oxidation rate, and hydroxide concentration. The parameters are listed in Table 3.6.

Intermediate samples were extracted for a reaction containing a equal molar proportions of α-FeOOH and $FeSO_4$, and 2.1 equivalents of NaOH per equivalent of Fe^{2+}. Samples were extracted after NaOH addition, after the reaction mixture reached 90°C, and after 2 hours of oxidation had occurred.

C. Fe^{3+} + $FeSO_4$

The production of Fe_3O_4 from soluble Fe^{3+} salts was carried out by putting $FeSO_4$ and Fe^{3+} salt into solution under N_2 flow, adding NaOH, and then heating to 90°C overnight. The Fe^{3+}:Fe^{2+} ratio was investigated in a range from 0.5 to 2. The amount of NaOH added was calculated as three equivalents for every equivalent of Fe^{3+}, and two equivalents of NaOH for every equivalent of Fe^{2+}. From this calculated value of NaOH, different experiments were run using a range of NaOH from 10% less than the equivalent value, to 30% more than the equivalent value. For those experiments using an Fe^{3+}:Fe^{2+} ratio less than 2, oxidation was carried out using slow diffusion of room air. Most experiments involving soluble Fe^{3+} salts were

Table 3.6 Parameters of Fe_3O_4 Reactions From α-FeOOH and $FeSO_4$

Fe^{3+}: Fe^{2+} ratio = 1:1, Seed and Growth

1. R = 1, 1/2 Fe^{2+} after 60 min seed age, O_2 after NaOH addition
2. R = 1, 1/2 Fe^{2+} after 60 min seed age, O_2 60 min after NaOH addition
3. R = 1, 1/2 Fe^{2+} after 90 min seed age, air diffusion
4. R = 1.5, 1/2 Fe^{2+} after 120 min seed age, air diffusion
5. R = 1.5 seed, R = 1.5 growth, 1/2 Fe^{2+} after 180 min seed age, air diffusion
6. R = 1.5 seed, R = 1.75 grwoth, 1/2 Fe^{2+} after 360 min seed age, air diffusion
7. R = 0.95 seed, R = 1.5 growth, 1/2 Fe^{2+} after 360 min seed age, air diffusion
8. R = 0.9 seed, R = 1.5 growth, 1/2 Fe^{2+} after 360 min seed age, air diffusion
9. R = 0.9 seed, R = 1.25 growth, 1/2 Fe^{2+} after 240 min seed age, air diffusion
10. R = 0.9 seed, R = 1 growth, 1/2 Fe^{2+} after 300 min seed age, air diffusion
11. R = 0.9 seed, R = 0.95 growth, 1/2 Fe^{2+} after 300 min seed age, air diffusion

All reactions carried out at 90°C

R = OH^- : Fe^{2+} ratio

carried out using $Fe_2(SO_4)_3$. Several experiments used $Fe(NO_3)_3$ with Fe^{3+}:Fe^{2+} ratios at 0.3, 0.5, and 1. Two experiments used $FeCl_3$ with Fe^{3+}:Fe^{2+} ratios of 1 or 2.

Intermediate samples were extracted from a reaction containing equal molar amounts of $Fe_2(SO_4)_3$ and $FeSO_4$ and a stoichiometric amount of NaOH. Samples were extracted after NaOH addition, after the mixture reached 90°C, and after 120 minutes of oxidation.

III. Instrumental Techniques

A number of instrumental techniques were used to characterize FeOOH and Fe_3O_4 prepared under a number of experimental conditions. These techniques include x-ray photoelectron spectroscopy (XPS), scanning and transmission electron microscopy (SEM, TEM), BET surface area analysis, viscometry, x-ray powder diffraction (XRD), microelectrophoresis, and photoacoustic infrared spectroscopy (PAS-IR). The sample preparation and instrument parameters will be explained here for each technique.

A. X-ray Photoelectron Spectroscopy

XPS was used to search for surface adsorption of metals and dicarboxylic acids on FeOOH as well as a method for analyzing for contamination of the oxide surfaces by chloride, sodium or sulfate. Surface analysis by XPS is accomplished by bombarding a specimen with monoenergetic x-rays, and energy analyzing the emitted photoelectrons. The spectrum produced is a plot of the number of emitted electrons versus their binding energy. Each element has a unique photoelectron spectrum whose peak positions correspond to electron energy levels within the element. Since the mean free path of the emitted electrons is very small, only electrons from the top few atomic layers lying near the surface of the specimen are detected. The emitted electrons have a kinetic energy which is given as:

$$KE = h\nu - BE - \alpha s$$

where:

KE = the kinetic energy of the electrons

$h\nu$ = energy of x-ray source

BE = binding energy of the atomic orbital of emission

αs = spectrometer work function

The XPS instrument used for this work was a PHI 5300 ESCA system with a hemispherical analyzer. Both a magnesium anode producing 1253.6 eV x-rays and an aluminum anode producing 1486.6 eV x-rays were used for analysis. The spectrometer was calibrated to the silver $3d_{5/2}$ peak with a binding energy of 368.3 eV (111). Some samples required cleaning with a rastered argon ion sputter gun at 25μA. Samples for XPS analysis were prepared on double stick tape. Quantitative elemental analysis was done by dividing peak areas by elemental sensitivity factors and calculating atomic percentages. Elemental analysis was averaged for two measurements of each sample.

B. Scanning Electron Microscopy and Transmission Electron Microscopy

Electron microscopy was used to examine average crystal size, size distribution, and crystalline morphology of iron oxides grown in this work. In SEM a rastered electron beam between 10 and 30 kV impinges on the specimen causing secondary electrons to be emitted. These electrons are detected and displayed on a cathode ray tube. A TEM uses a high intensity focused electron beam at 100 kV which passes through an ultrathin sample, and displays an image of primary transmitted electrons on a phosphoring screen. The principles of TEM make it possible to do very high resolution microscopy at magnifications up to 200,000X magnification. The characteristics of the two techniques make SEM more useful for determining the shape of crystals, and TEM more accurate in particle size determination.

SEM was carried out on a ISI SX40 scanning electron microscope. Samples were prepared as ethanol dispersions on aluminum mounts. TEM was carried out on a Philips EM-420T STEM

instrument. Samples for TEM were prepared by ultrasonic treatment for 5 minutes of ethanol or water dispersions. The dispersions were evaporated onto formvar coated 400 mesh copper grids. SEM photomicrographs were taken up to 20,000X magnification, while TEM photos were taken up to 51,000X magnification.

C. BET Surface Area Analysis

Surface area analysis gives a value for the area per unit weight of a specimen. The surface area can give information about the overall average size of particles if the shape of the particles is known. The area data is derived by adsorption of gaseous nitrogen molecules onto a specimen cooled to liquid nitrogen temperature, approximately 77K. Manipulating the nitrogen gas pressure gives information concerning the volume of nitrogen adsorbed on the specimen, and knowing the area per molecule of nitrogen, and the weight of the specimen, the surface area per gram is found. Surface area analysis was carried out using a Micromeritics Accusorb 2100E. Powder samples were heated to 100°C for one hour under vacuum to remove adsorbed water. Calculations were made using the Micromeritics T-plot program. The error in surface areas was approximately ± 10% based on two repetitions carried out on duplicate samples.

D. Viscometry

Viscometry measures the viscosity of solutions and suspensions. The viscosity of a suspension is an indication of interparticle forces of the individual particles in the suspension. A simple method for viscosity measurement involves a capillary tube with a bulb above and below the capillary. The time for a given volume of suspension above the capillary to pass, due to gravity, through the capillary to the lower bulb, is directly related to the viscosity of the suspension. The viscosity of final suspensions from the growth of FeOOH were measured using a Cannon-Fenske Routine Viscometer with three different nominal capillary sizes, listed as 75, 200, and 300. The choice of capillary size was based on the viscosity range measured. The

measurements were made at 25°C, and the viscometers were calibrated with deionized water, which has a viscosity of 1 centipoise at 25°C (112). The error in viscosity values was determined to be ± 15% based on five repetitions of duplicate samples.

E. X-ray Powder Diffraction

XRD is a technique which uses the diffraction of x-rays by the crystal lattice of small particles as a phase identification method. An x-ray beam is passed through a powder sample in which the crystals are assumed to be arranged randomly. The x-ray beam is swung through a range of angles relative to the powder sample, and the x-ray reflections are measured. According to the Bragg diffraction law, the angle at which a reflection occurs is related to the spacing between the crystal planes in the lattice by the following relationship:

$$n\lambda = 2d\sin\Theta$$

where: n = multiple of the wavelength

λ = wavelength of the x-ray

d = planar spacing

Θ = angle of diffraction

The number, position, and relative intensity of the planar reflections is indicative of the phase of the crystals in the sample. The relative amounts of γ-FeOOH and α-FeOOH in some samples were estimated by ratioing the peak areas of the strongest reflections from the two patterns in the respective XRD spectra. XRD spectra were measured at 30kV and 15mA using a Picker Nuclear Model 3668A x-ray diffractometer with a copper x-ray tube and a graphite monochrometer. Samples were prepared as pressed powders attached by doublestick tape into a recessed pocket in a glass slide. XRD intensity and d spacing values for standard iron oxide materials are listed in Appendix A.

F. Microelectrophoresis

Microelectrophoresis measures the average surface charge on small particles. An electrical potential is placed across a cell filled with a very dilute aqueous suspension of particles. The movement of the particles toward the positive or negative pole of the cell is indicative of the charge of the particles. When a particle has a surface potential that matches the potential of the water around it, no adsorption or desorption occurs, because the system is at equilibrium. If the surface potential of the particle is different from the pH of the solution, adsorption of protons or hydroxyl groups from solution will occur until equilibrium is reestablished. After adsorption of protons or hydroxyl groups, there is a net charge on the surface of the particles that is attracted toward a charged pole of the electrophoresis cell. The higher the surface charge, the stronger the attraction towards the pole, and the faster the particles will move. By sweeping the pH of the solution, and monitoring the speed and direction of the particles' movement, the point is determined where the particles are at rest; that point is called the isoelectric point. A Rank Brothers Particle Microelectrophoresis Apparatus, Mark II was used for these measurements. A constant ionic strength solution was maintained with $NaClO_4$. Measurements were carrried out at 25°C, using a cell voltage of 30V. A flat cell with a 0.76 mm depth was used, and the electrode distance was 107.9 mm. Plots of mobility versus solution pH were used to locate the isoelectric point.

G. Photoacoustic Infrared Spectroscopy

Infrared spectroscopy is a method which examines the vibrational spectra of compounds. Information about coordination and bonding within molecules can be derived from IR data. Photoacoustic IR is a technique which uses a specialized detector to obtain the IR signal (113). The sample is placed into a sealed cell. The IR radiation passes through a window in the cell and shines onto the sample. The optical radiation is converted into heat within the sample which then thermally deexcites and emits an acoustic wave into the gas medium in the cell.

This acoustic wave is picked up by a microphone detector and is Fourier transformed into an IR spectrum. The advantage of PAS-IR over more common methods is the high signal strength and small amount of sample preparation required for solids.

IR spectra were obtained using a Nicolet DXB FTIR using a MTEC Model 100 photoacoustic cell. The bench was run at 4 cm^{-1} resolution at the lowest scan rate setting. The photoacoustic cell was purged with helium for maximum signal since helium has very efficient thermal transmittance. Sample spectra were ratioed to a carbon black backgound spectrum.

Chapter 4: Results and Discussion

This chapter describes observations during experimentation and analysis of iron oxide products, and presents a discussion of these results in terms of iron oxide nucleation and growth. Initial experiments were chosen to investigate the relative importance of different reaction variables. Later experiments such as adsorption studies, intermediate sampling, and use of model compounds, were designed to probe the mechanisms of iron oxide nucleation and growth, and to discover how changes in the chemical environment altered these basic processes. The results presented for the FeOOH study describe how the findings from one reaction led to further experiments, and how data from different analyses were correlated. Next the results of the Fe_3O_4 study are examined, where the effects of additives and changes in product characteristics due to different starting materials are examined.

I. FeOOH

A. Metal Ion Effects

α-FeOOH crystals grown under standard conditions at 40°C with no additives had a surface area of 60 ± 4 m^2/g and a final suspension viscosity of 65 ± 10 cp. The addition of $ZnSO_4$ to give a concentration of 0.0043M Zn^{2+} produced α-FeOOH with a surface area of 75 m^2/g, and a viscosity of 162 cp. The presence of Zn^{2+} yielded smaller α-FeOOH crystals, and the final suspension was more viscous. Because $ZnSO_4$ and Na_2CO_3 are common additives in α-FeOOH production in industry, many of the initial reactions in the FeOOH study contained one or both of these additives, even when the effect of another variable was being investigated. Carrying out a reaction with 0.016M Na_2CO_3 produced α-FeOOH with a surface area of 90 m^2/g and a viscosity of 220 cp. With 0.016M Na_2CO_3 and 0.0043M Zn^{2+}, α-FeOOH was produced with a surface area of 93 m^2/g and a viscosity of 310 cp. The latter surface area is not significantly larger than that found for Na_2CO_3 alone. Compared to a suspension of α-FeOOH

with no Na_2CO_3 or $ZnSO_4$ (65 cp), the increase in suspension viscosity for the reaction containing Na_2CO_3 and Zn^{2+} was approximately equal to the sum of the increases due to the individual additives; increasing 100 cp for 0.0043M Zn^{2+}, and 160 cp for 0.016M CO_3^{2-}. XPS spectra of the crystals from the reaction containing 0.0043M Zn^{2+} showed Zn^{2+} near the level of detection of 0.1 atomic %.

Reactions in which the effect of magnesium was investigated were also carried out in 0.016M Na_2CO_3. In some reactions, Zn^{2+} was also present so that the relative effects of the two metal ions might be investigated. The surface area and viscosity measurements for reactions containing Mg^{2+} are listed in Table 4.1. The effect of Mg^{2+} was not significant when together with Na_2CO_3 or with both Zn^{2+} and Na_2CO_3. The presence of Mg^{2+} at up to 0.0043M did not change the surface area or viscosity outside the range of values found in the absence of Mg^{2+}. XPS spectra showed no evidence of incorporation or adsorption of Mg^{2+} onto α-FeOOH at levels above the limit of detection; 0.1 atomic %.

In time of addition reactions, Zn^{2+}, calculated to give a solution concentration of 0.0088M, was added at different times; 0, 1, 2, and 3 hours following the start of oxygen flow. XPS spectra showed approximately 0.3 atomic % Zn^{2+} at the surface of α-FeOOH regardless of the time of addition. The surface area of the product and viscosity of the final suspension were independent of the time of addition. This indicated that either adsorption of Zn^{2+} occurred throughout the reaction, or that the adsorption occurred after the last addition of Zn^{2+} at two hours of reaction time, and was thus present at the surface of the products following completion of the oxidation. Zn^{2+} did not need to be present at the beginning of the reaction in order to act as a modifier for α-FeOOH growth. No zinc oxide or hydroxide phase was detected by XRD in the product. The lower limit of detection of XRD prevented the detection of any crystalline phase at less than 5 volume %. Of the two metal ions investigated, Mg^{2+} had no measurable effect on the morphology of α-FeOOH, and Zn^{2+} changed both the size of α-FeOOH crystals and the suspension viscosity. There was not sufficient data to determine the mechanism of

Table 4.1 Surface Areas and Viscosities - α-FeOOH with Mg^{2+}

Additives	Suspension Viscosity	Surface Area
0.0043M Mg^{2+}	205 cp ± 15%	87 m^2/g ± 10%
0.0022M Mg^{2+}	215 cp	86 m^2/g
0.0011M Mg^{2+}	220 cp	90 m^2/g
0.0022M Mg^{2+} + 0.0022M Zn^{2+}	313 cp	93 m^2/g
0.0043M Zn^{2+}	310 cp	93 m^2/g
no metal additive	220 cp	90 m^2/g

All reactions contained 0.016M Na_2CO_3

α-FeOOH morphology changes due to the presence of zinc ions. Adsorption of Zn^{2+} on the surface of growing iron oxide crystals may alter lattice free energy of the growing crystal due to substitution of zinc atoms in iron sites. The low level of zinc substitution may prevent detection of lattice changes by XRD.

B. Dicarboxylic Acids

α-FeOOH grown in the presence of 0.016M acetic acid and 0.0043M Zn^{2+} had a surface area of 78 m^2/g and a suspension viscosity of 154 cp. These values are essentially the same for α-FeOOH prepared with Zn^{2+} alone. If one assumes that strongly adsorbed carboxylic acids are potential growth modifiers, the lack of effect by the presence of acetic acid was not surprising, since monocarboxylic acids adsorb only weakly to α-FeOOH (88). The effects of a series of linear dicarboxylic acids, containing two to seven carbons, were investigated in the growth of α-FeOOH. These acids are strongly adsorbed on α-FeOOH (89).

PAS-IR spectra were obtained for α-FeOOH products grown in the presence of the series of dicarboxylic acids with and without Zn^{2+}. Figures 4.1 and 4.2 present IR spectra between 1700 cm^{-1} and 1300 cm^{-1} showing stretching vibrations corresponding to symmetric and asymmetric stretches of carboxyl groups coordinated to iron through both oxygens of the acid groups. These stretching vibrations indicate that dicarboxylic acids are adsorbed on or incorporated into α-FeOOH crystals during nucleation and growth. This finding is in contrast to α-FeOOH grown in the presence of acetic acid which showed no evidence of acetic acid in the IR spectrum. It has been speculated by others (89) that the two acid groups on the dicarboxylic acids act as bidentate ligands bridging two iron atoms on the crystal surface. The presence of two coordinating groups and the ability to act as a bridging ligand presents an explanation for the differences found for dicarboxylic and monocarboxylic acid adsorption behavior.

The surface area values for α-FeOOH produced from the series of dicarboxylic acids with

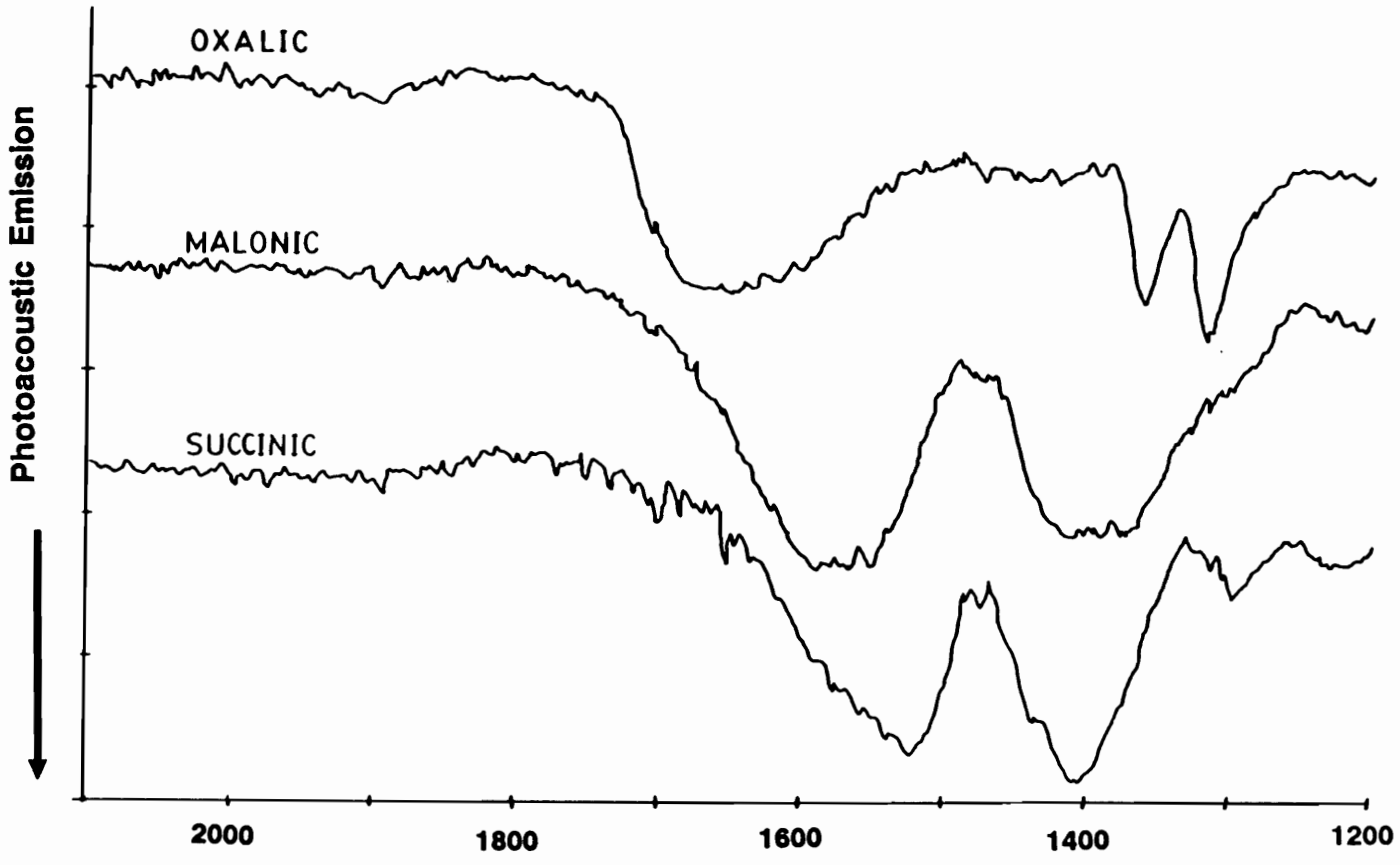

Spectra for α-FeOOH subtracted

Symmetric carboxyl stretch - 1300 to 1450 cm^{-1}
Asymmetric carboxyl stretch - 1500 to 1700 cm^{-1}

Figure 4.1 PAS-IR Spectra for Dicarboxylic Acid Products

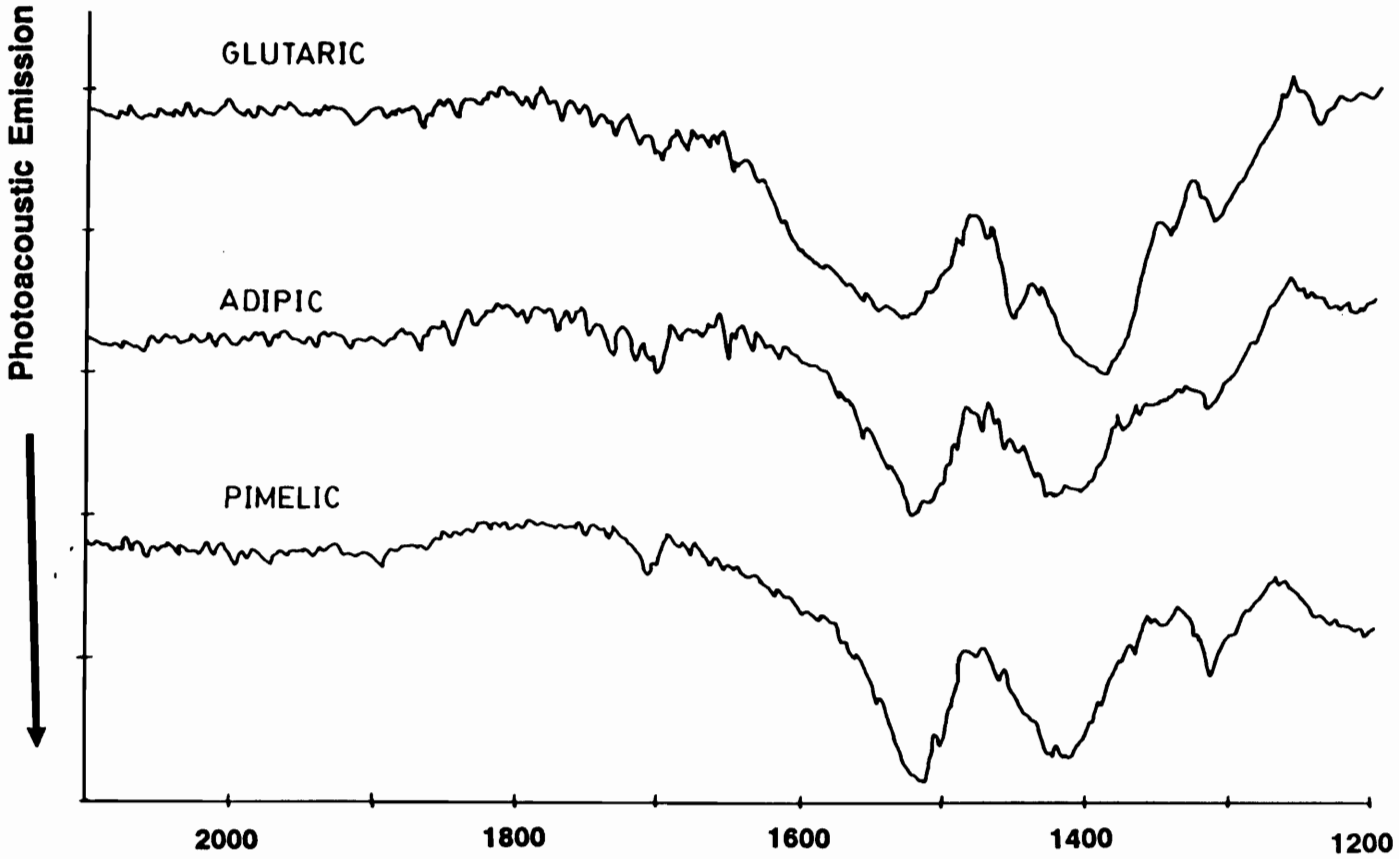

Spectra for α-FeOOH subtracted

Symmetric carboxyl stretch - 1300 to 1450 cm^{-1}
Asymmetric carboxyl stretch - 1500 to 1700 cm^{-1}

Figure 4.2 PAS-IR Spectra for Dicarboxylic Acid Products

and without Zn^{2+} are shown in Figure 4.3. In the absence of Zn^{2+}, 0.016M oxalic and malonic acids did not significantly alter the surface area; 60 m^2/g for α-FeOOH grown without acid. Succinic and glutaric acid lead to a 40% increase in surface area, while adipic and pimelic acid increased the surface area by approximately 15%. For reactions containing 0.0043M Zn^{2+} and dicarboxylic acids, the trend in the surface area values was the same as that found for the acids alone, but shifted 25% higher. The effect on surface area for dicarboxylic acids and Zn^{2+} was additive, in that each type of growth modifier produced individual changes in α-FeOOH, regardless of the presence of the other.

The viscosity values for α-FeOOH grown with dicarboxylic acids with and without Zn^{2+} are shown in Figures 4.4 and 4.5. In the absence of Zn^{2+}, dicarboxylic acids decreased the α-FeOOH suspension viscosity significantly. A 0.016M oxalic acid concentration decreased the viscosity to 33 cp; malonic, succinic and glutaric acids decreased the viscosity to below 3.5 cp; and adipic and pimelic acids reduced the viscosity to below 20 cp. The addition of Zn^{2+} and oxalic acid produced a suspension viscosity of 130 cp. Oxalic acid alone reduced the α-FeOOH suspension viscosity from 60 to 30 cp, or a decrease of 30 cp, while Zn^{2+} increased the viscosity by 100 cp. If the two effects are combined, adding 100 cp from Zn^{2+}, then subtracting 30 cp due to oxalic acid, the result would be 130 cp, which is the value measured. The viscosities for the rest of the series of dicarboxylic acids in the presence of Zn^{2+} were different than for oxalic acid. There was no significant difference between the viscosity with and without Zn^{2+} for dicarboxylic acids other than oxalic.

Microelectrophoresis was carried out on α-FeOOH samples prepared in the reaction with dicarboxylic acid and Zn^{2+} to determine how the surface charge on the crystals was changed due to adsorption of dicarboxylic acids and zinc. The isoelectric point results shown in Table 4.2 correlated with the viscosity values. There was a direct relationship between isoelectric point and viscosity for the samples containing dicarboxylic acids. α-FeOOH prepared in malonic acid, the dicarboxylic acid which gave the lowest viscosity, had the highest isoelectric point,

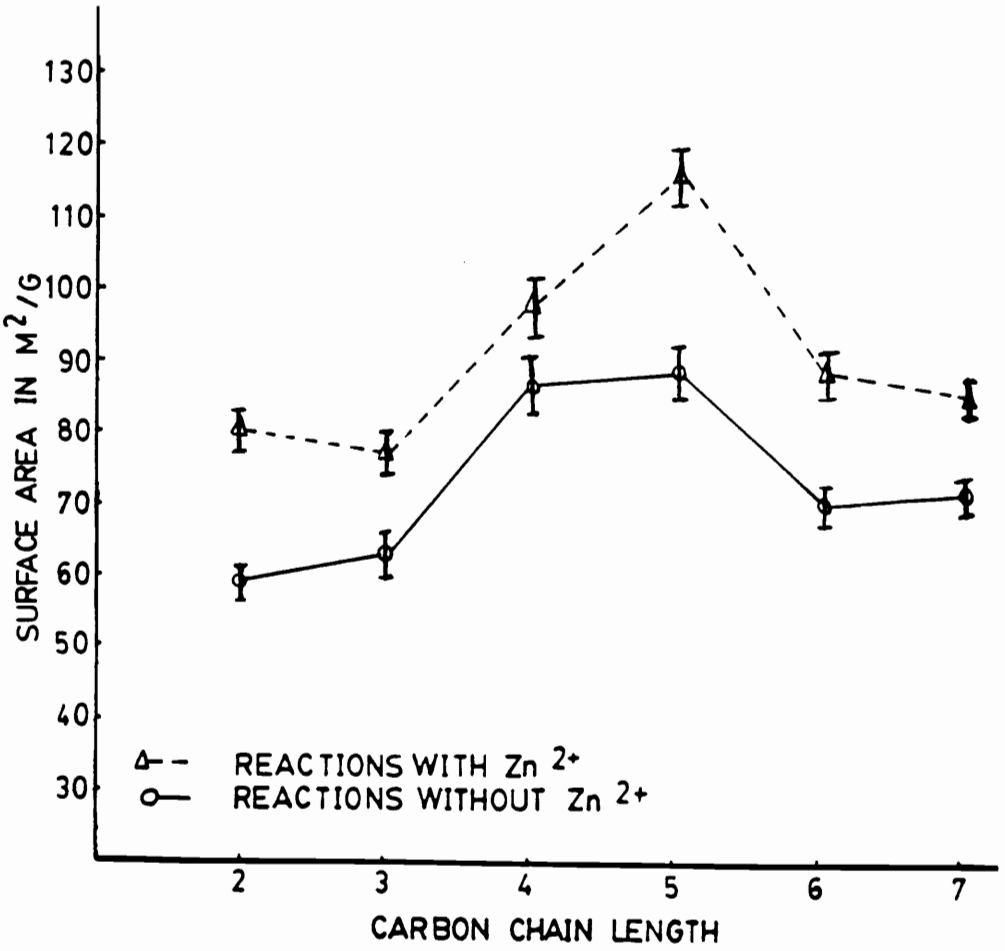

2 carbons - oxalic acid
3 carbons - malonic acid
4 carbons - succinic acid
5 carbons - glutaric acid
6 carbons - adipic acid
7 carbons - pimelic acid

Dicarboxylic acids - 0.016M
Zn^{2+} - 0.0043M

Figure 4.3 Surface Areas of α-FeOOH with Dicarboxylic Acids

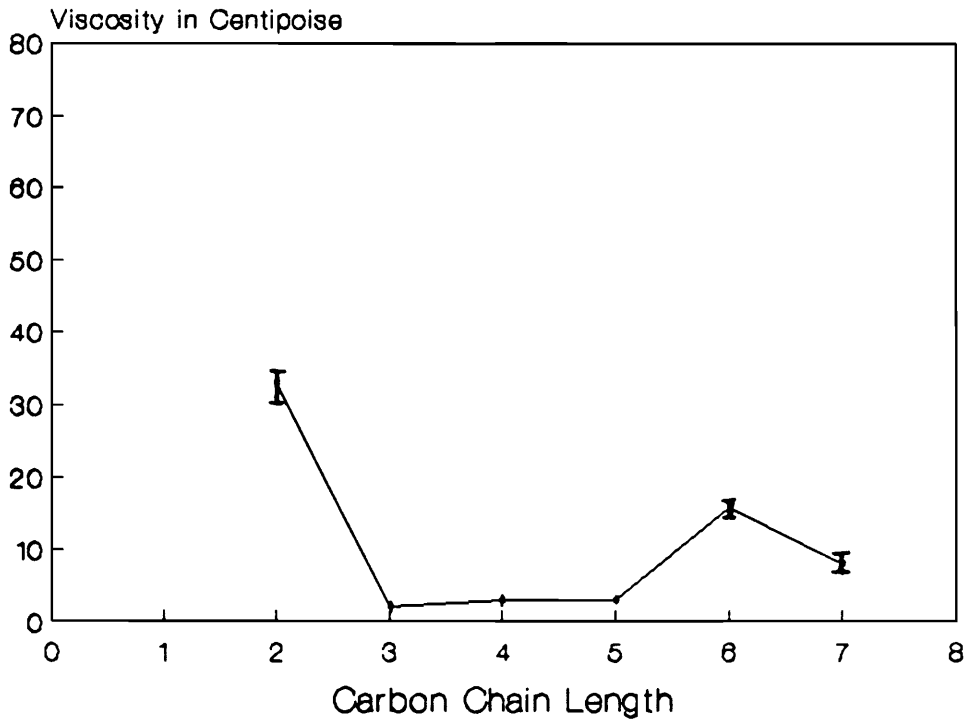

2 carbons - oxalic acid
3 carbons - malonic acid
4 carbons - succinic acid
5 carbons - glutaric acid
6 carbons - adipic acid
7 carbons - pimelic acid

Dicarboxylic acids - 0.016M

Figure 4.4 Suspension Viscosity - Dicarboxylic Acids with no Zn^{2+}

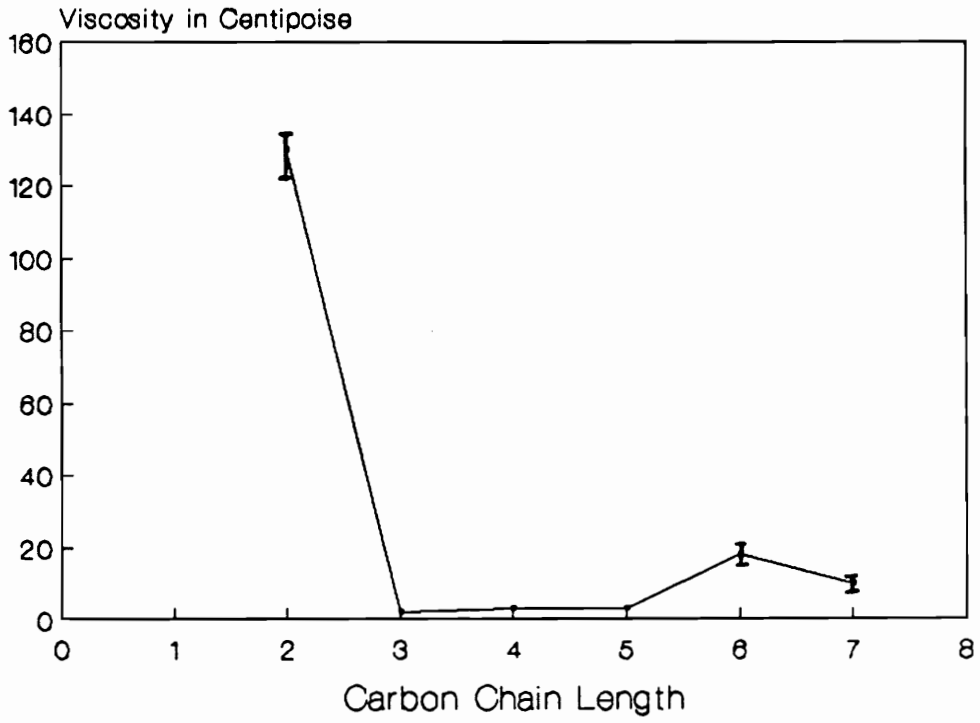

2 carbons - oxalic acid
3 carbons - malonic acid
4 carbons - succinic acid
5 carbons - glutaric acid
6 carbons - adipic acid
7 carbons - pimelic acid

Dicarboxylic acids - 0.016M
Zn^{2+} - 0.0043M

Figure 4.5 Suspension Viscosity - Dicarboxylic Acids with Zn^{2+}

Table 4.2 Isoelectric Point Results for Dicarboxylic Acid Products

Dicarboxylic Acid	Isoelectric Point	Suspension Viscosity
no acid or Zn^{2+}	5.6 ± 0.03	60 cp ± 10%
oxalic acid + 0.0043M Zn^{2+}	4.4 ± 0.04	130 cp
malonic acid + 0.0043M Zn^{2+}	7.0 ± 0.12	3.8 cp
succinic acid + 0.0043M Zn^{2+}	6.7 ± 0.02	4.2 cp
adipic acid + 0.0043M Zn^{2+}	5.9 ± 0.08	16 cp

7.0 ± 0.12. α-FeOOH produced in oxalic acid had the highest viscosity and the lowest isoelectric point of 4.4 ± 0.04. The acids with intermediate viscosities followed the same pattern. A greater isoelectric point was associated with lower viscosity. It appears that the change in charge on the α-FeOOH particles caused by the adsorption of dicarboxylic acids led to coagulation and precipitation of the suspension, which was measured as a decrease in viscosity. The adsorption of dicarboxylic acids can alter the surface charge of α-FeOOH crystals in several ways. The adsorption of the organic molecules covers sites on the oxide surface which can change the surface character of the oxide. The longer chain dicarboxylic acids have a significant non-polar portion that could change the character of the α-FeOOH surface from a hydrophilic polar surface to a hydrophobic nonpolar surface. Additionally, the acid groups might protonate at a different pH than the oxide surface in the absence of dicarboxylic acid. Both of these effects can change the isoelectric point of α-FeOOH containing dicarboxylic acids. It is also possible, but unlikely, that longer dicarboxylic acids could act as bridges between two separate oxide crystals leading to coagulation, in a manner similar to the action of some surfactants.

There were significant morphological changes in α-FeOOH crystals grown with dicarboxylic acids. Analysis of TEM micrographs, shown in Figure 4.6, allowed the dicarboxylic acid products to be divided into three catagories based on the size and shape of the crystals. The crystals grown with oxalic, adipic, and pimelic acids, the two, six, and seven carbon dicarboxylic acids, were approximately 550 nm in length, with length to width aspect ratios of approximately 30:1. These crystals were most similar to α-FeOOH grown with no dicarboxylic acid. Crystals from the reactions containing succinic or glutaric acid, the four and five carbon dicarboxylic acids, were approximately 325 nm long with aspect ratios about 20:1. Malonic acid, the three carbon dicarboxylic acid produced crystals 160 nm long with an aspect ratio of 8:1.

It is postulated that the changes in α-FeOOH crystal morphology occurred due to interactions between the acid molecules in solution and the forming α-FeOOH crystals. Cornell and

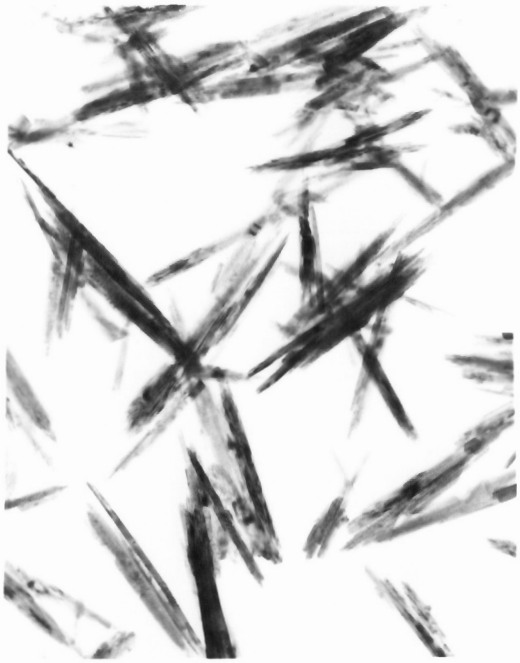

a) No Dicarboxylic Acid

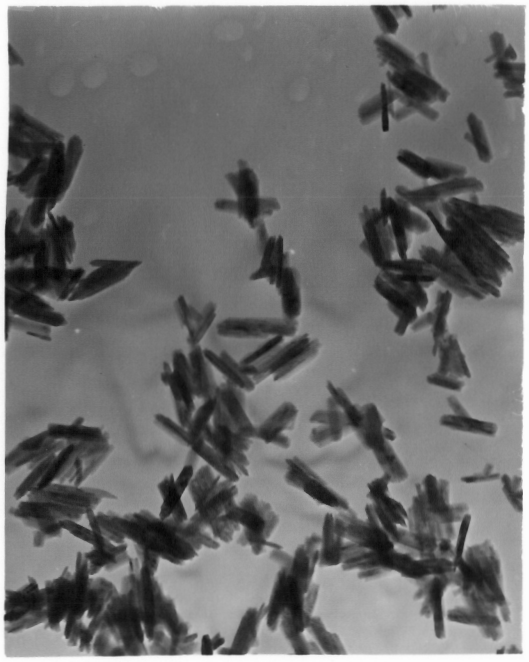

b) Malonic Acid

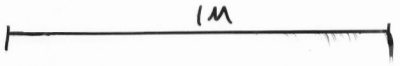

51,000X A11

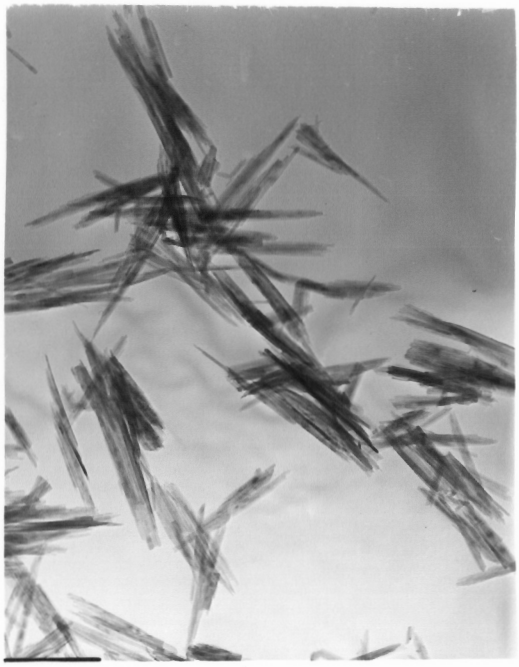

c) Succinic Acid

d) Adipic Acid

Figure 4.6 TEM Micrographs of α-FeOOH Containing Dicarboxylic Acids

Schwertmann (71), who worked with organic anions as growth modifiers, discussed the apparent inhibition by some anions on the conversion of ferrihydrite to hematite and goethite. Organic molecules could affect crystallization processes in three ways. Adsorption of species onto ferrihydrite could prevent the nucleation of goethite, complexation of iron in solution could inhibit crystal growth, or the size and shape of the organic molecules were such that a template effect could occur as the iron species were held in a fixed geometry. Any of these mechanisms could have contributed to changes in morphology of α-FeOOH caused by dicarboxylic acids. The evidence from experiments described later will help to distinguish among possible mechanisms of morphology change.

In addition to the saturated four carbon linear dicarboxylic acid, succinic acid, three other four carbon acids were investigated for effects on α-FeOOH crystallization. Those acids were fumaric and maleic acids, the trans and cis versions of the 2-butenedioic acids respectively, and crotonic acid, the 2-butenoic acid. α-FeOOH preparations were carried out at acid concentrations between 0.004 and 0.016M. The reactions also contained $ZnSO_4$ at 0.0043M. The PAS-IR spectra in Figure 4.7 show that the three dicarboxylic acids were adsorbed on α-FeOOH, while crotonic acid did not. The single acid group on crotonic acid, like the single acid group of acetic acid, did not provide sufficient interaction with the surface of the oxide crystal to cause the crotonic molecules to adsorb. Viscosity and surface area results are listed in Table 4.3 for the products of reactions using the four acids. The suspension viscosity was not significantly affected by crotonic acid. This finding provides further evidence that the single functional carboxylic acid did not adsorb on α-FeOOH crystals. For concentrations of crotonic acid, 0.008M and 0.016M, the surface area was 87 m^2/g. Much more significant changes in the surface area were found for succinic, maleic, and fumaric acids, and these changes occurred at concentrations as low as 0.004M. The double bond in maleic and fumaric acids prevents rotation of the molecule about the central axis. The adsorption occurred for both the trans and cis version of the dicarboxylic acid. In maleic acid, the two carboxyl groups are

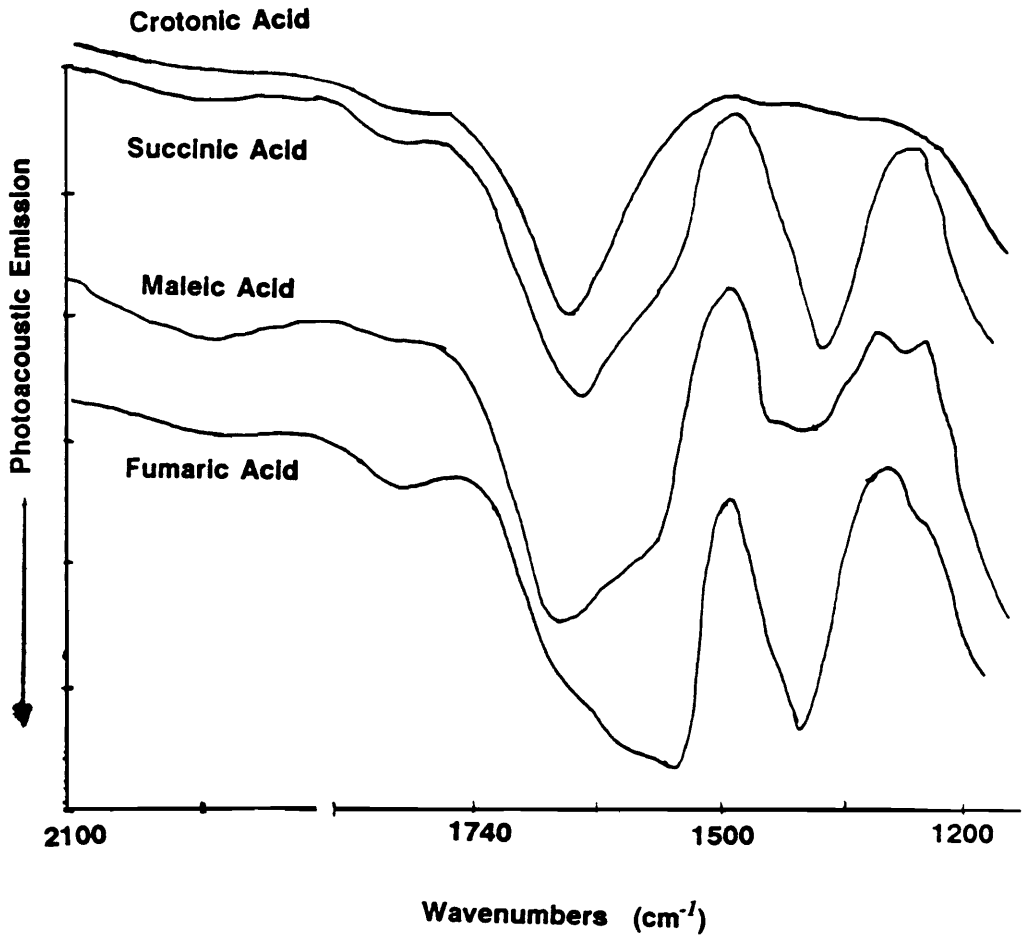

Symmetric carboxyl stretch - 1400 to 1450 cm^{-1}
Asymmetric carboxyl stretch - 1550 to 1600 cm^{-1}
Free water - 1650 cm^{-1}

Figure 4.7 PAS-IR Spectra for α-FeOOH - 4 Carbon Acid Series

Table 4.3 Suspension Viscosities and Surface Areas - 4 Carbon Acid Series

Acid	Conc.	Suspension Viscosity (cp)	Surface Area (m^2/g)
Fumaric	0.016M	1.8 ± 15%	115 ± 10%
	0.008M	12	90
	0.006M	93	91
	0.004M	160	77
Maleic	0.016M	1.6	129
	0.008M	11	110
	0.006M	65	116
	0.004M	162	102
Succinic	0.016M	6	101
	0.008M	56	98
	0.006M	106	97
	0.004M	130	101
Crotonic	0.016M	186	88
	0.008M	199	86
	0.006M	138	78
	0.004M	144	76

All reactions contained 0.0043M Zn^{2+}

Fe Concentration = 0.4M

forced very close together, and limit the manner in which both acid groups can coordinate. Both acid groups are close enough to allow bidentate coordination to a single iron atom. In the trans form, fumaric acid, the groups are forced away from each other in a manner that makes it unlikely that both groups could coordinate to the same iron atom. In succinic acid, rotation about the central axis would allow coordination of the acid groups to either one or two iron atoms. The trend in surface area values versus dicarboxylic acid concentration shows that maleic acid produces the greatest increase in surface area at the lowest concentration. The location of two carboxylic acid groups very close together may have some influence on the ability of a dicarboxylic acid to act as a growth modifier for α-FeOOH. Malonic acid, the three carbon dicarboxylic acid causes the largest change in particle size of α-FeOOH. (See Figure 4.6) Increasing the size and flexibility of the dicarboxylic acid chain is likely to cause the acid groups to remain farther apart. Larger dicarboxylic acids are less effective as growth modifiers. The limited flexibility of oxalic acid, the two carbon dicarboxylic acid, may restrict the manner of adsorption of the molecule, and prevent alteration of α-FeOOH morphology.

At 0.004M the dicarboxylic acids did not significantly affect the suspension viscosity compared to the value for a suspension containing 0.0043M Zn^{2+} alone. Increasing acid concentration decreased the suspension viscosity. Suspensions containing 0.016M fumaric or maleic acid had viscosities approaching 1 cp, the viscosity of water. The higher concentrations of fumaric, maleic, and succinic acids more strongly influenced the surface charge on the α-FeOOH crystals, which led to the effect on viscosity.

Two reactions were run at 50°C, one with 0.016M fumaric acid and 0.0043M Zn^{2+}, and the second with 0.016M succinic acid with no Zn^{2+}, to see if the higher temperature would produce larger α-FeOOH crystals. The product of the 50°C fumaric acid reaction had a surface area of 71 m^2/g and the succinic acid product had a surface area of 65 m^2/g. These surface areas are 30 to 40% lower than the surface areas for α-FeOOH prepared at 40°C. This surface area decrease indicates that the increase in temperature increased the size of the resulting crystals.

In these cases, it is not believed that the higher temperature diminished the effect of the growth modifiers, but rather that the better growth kinetics acted independently of the acitivity of the dicarboxylic acids. Increasing the reaction temperature, in the absence of additives, increases particle size, if that the growth reaction is carried out within the appropriate area of the phase diagram (45).

Having determined that the effects of dicarboxylic acids could be separated into three catagories in terms of the morphology of α-FeOOH, malonic acid producing 150 nm crystals, succinic and glutaric acids producing 325 nm crystals, and oxalic, adipic and pimelic acids producing 550 nm crsytals, experiments were carried out where two dicarboxylic acids were added to the reaction to see if they would act in an additive or competitive manner. PAS-IR spectra of α-FeOOH grown in the reactions containing two dicarboxylic acids were examined. (Figures 4.8-4.11) Using spectral subtraction techniques, it was determined that carbon-oxygen peaks occur for both dicarboxylic acids. The dicarboxylic acid peaks are not shifted with respect to their positions in the spectra of α-FeOOH prepared using only one dicarboxylic acid. Thus the adsorption of one dicarboxylic acid did not appear to affect the coordination of a second dicarboxylic acid. The area of the IR peaks due to both dicarboxylic acids is similar on the samples from the competitive additions, and the peak areas are also similar to the area of IR peaks found when a single acid was adsorbed. Therefore there was no evidence for competition for adsorption sites at these acid concentrations. At higher concentrations of dicarboxylic acids, however, there may be some point when the two acids begin to compete for surface sites. This possible effect was not investigated.

The viscosities of the suspensions from the competitive reactions are listed in Table 4.4. Any combination of malonic acid with another dicarboxylic acid or carbonate gave the same viscosity value as the suspension containing malonic acid alone. The viscosity of suspensions containing succinic acid and carbonate or oxalic acid were equal to the values for suspensions containing succinic acid alone. The viscosity was not an average of the values found for suspensions

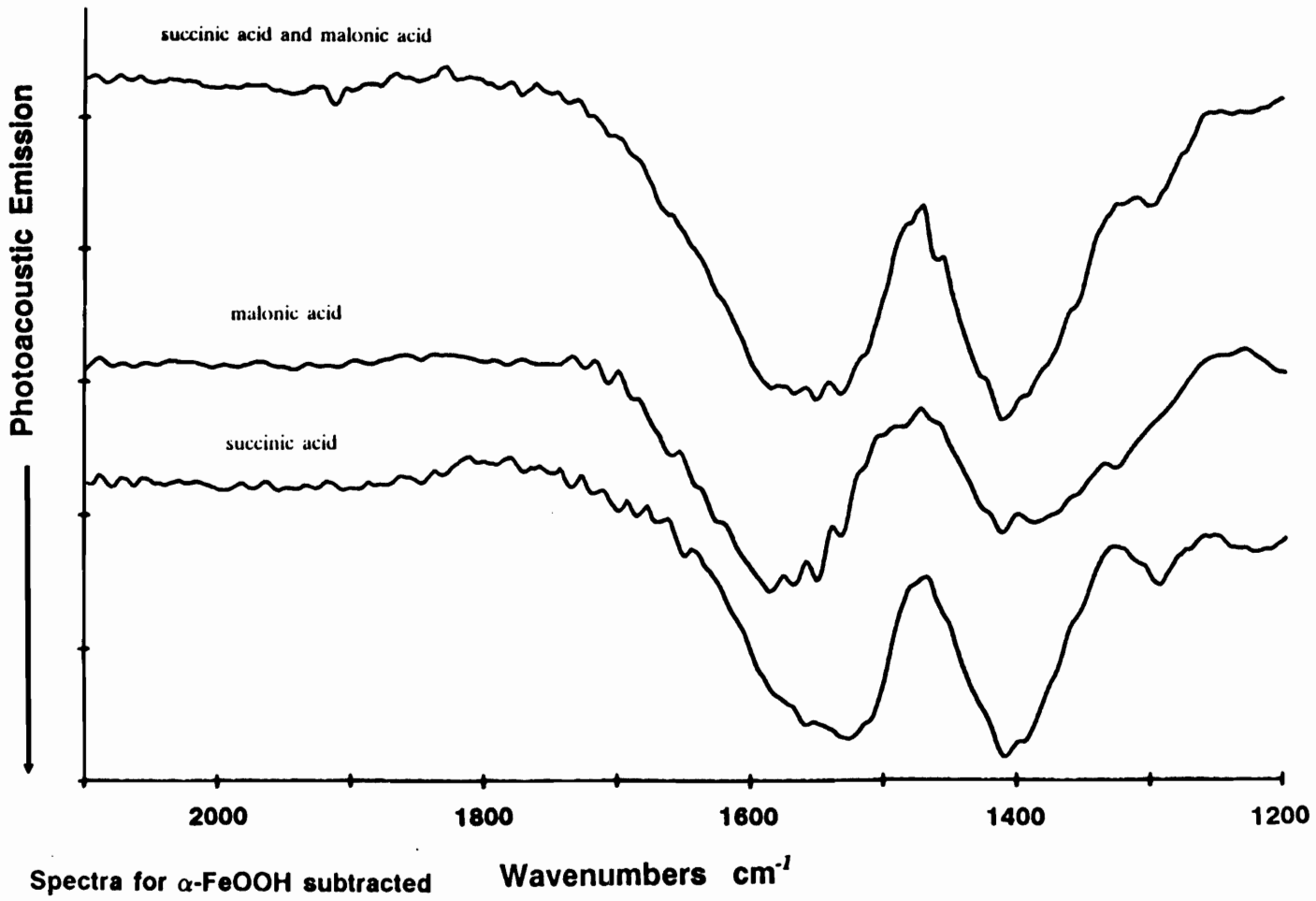

Spectra for α-FeOOH subtracted

Symmetric carboxyl stretch - 1300 to 1450 cm^{-1}
Asymmetric carboxyl stretch - 1500 to 1700 cm^{-1}

Figure 4.8 PAS-IR Spectra for Competitive Addition - Succinic + Malonic Acids

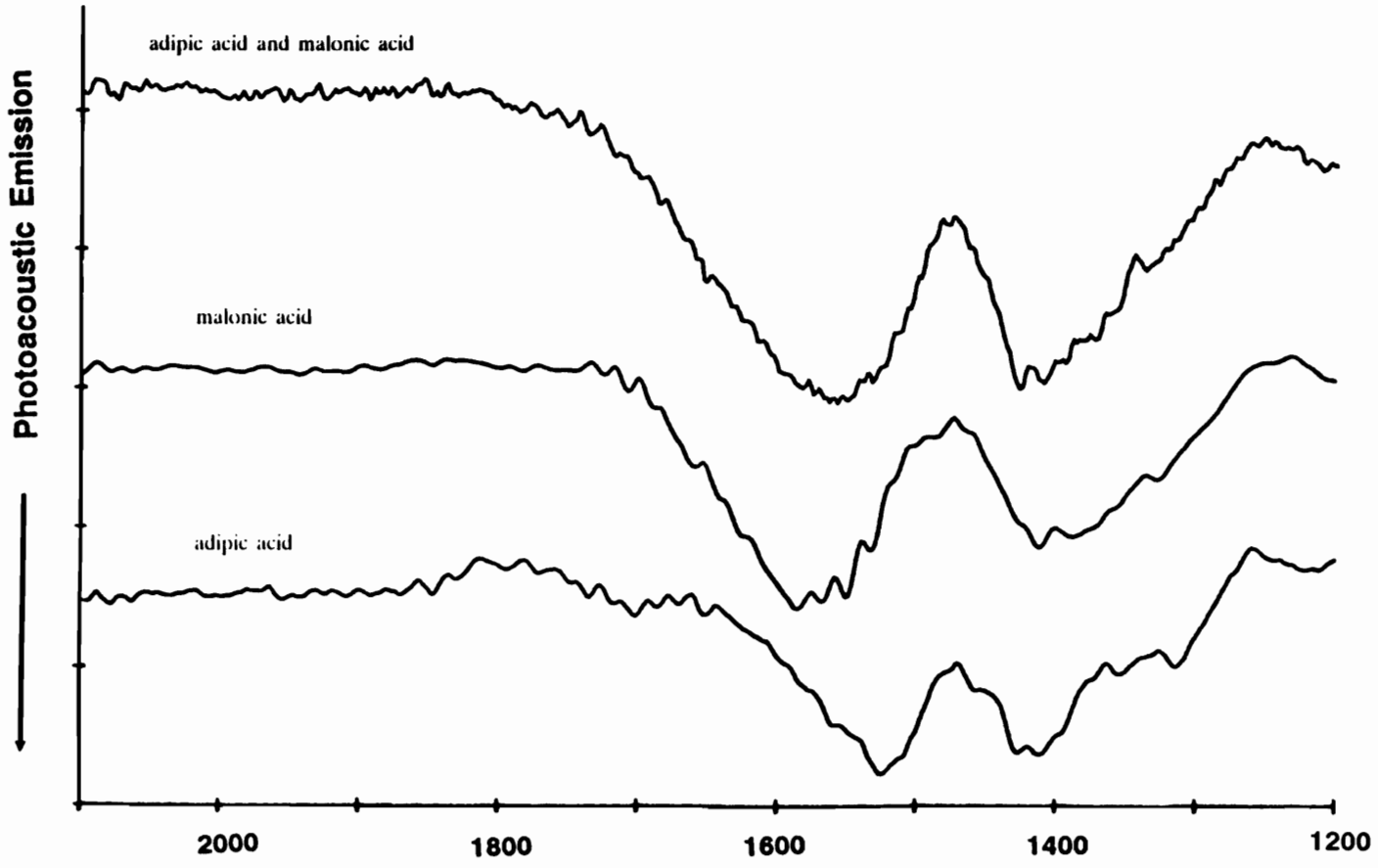

Figure 4.9 PAS-IR Spectra for Competitive Addition - Malonic Acid + Adipic Acid

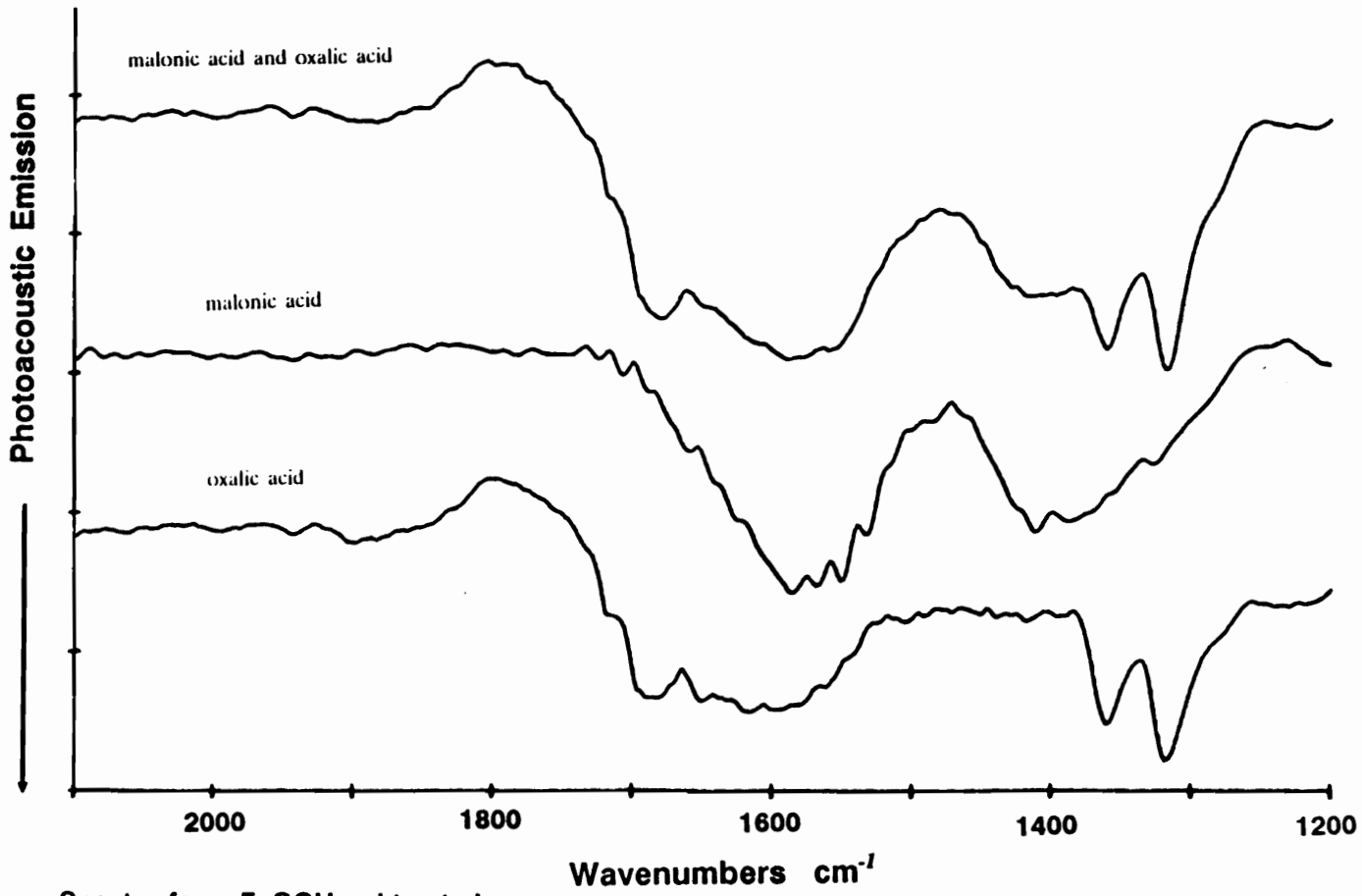

Spectra for α-FeOOH subtracted

Symmetric carboxyl stretch - 1300 to 1450 cm^{-1}
Asymmetric carboxyl stretch - 1500 to 1700 cm^{-1}

Figure 4.10 PAS-IR Spectra for Competitive Addition - Malonic Acid + Oxalic Acid

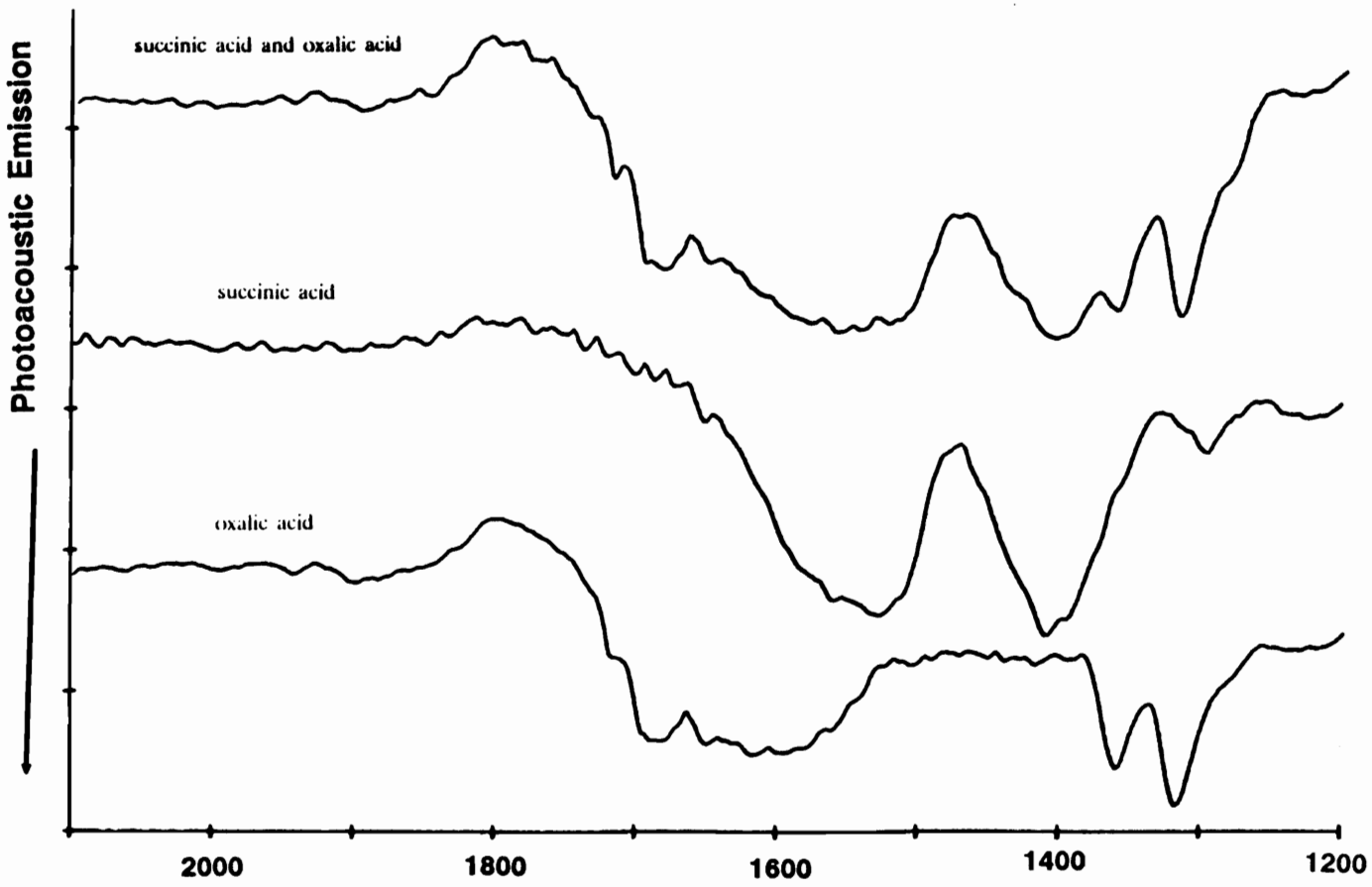

Spectra for α-FeOOH subtracted

Symmetric carboxyl stretch - 1300 to 1450 cm^{-1}
Asymmetric carboxyl stretch - 1500 to 1700 cm^{-1}

Figure 4.11 PAS-IR Spectra for Competitive Addition - Succinic + Oxalic Acid

Table 4.4 Suspension Viscosity - Competitive Addition of Dicarboxylic Acids

Dicarboxylic acids	Suspension Viscosity (cp)
Malonic acid	1.7 ± 15%
Succinic acid	3.4
Oxalic acid	30
Adipic acid	16
Sodium Carbonate	220
Malonic acid and oxalic acid	1.7
Malonic acid and succinic acid	1.5
Malonic acid and adipic acid	1.6
Malonic acid and sodium carbonate	1.9
Succinic acid and sodium carbonate	6.1
Succinic acid and oxalic acid	4.0

no Zn^{2+} was used in the competitive addition reactions

containing the individual dicarboxylic acids, nor was the decrease in viscosity a sum of the decreases due to both acids. One acid may have behaved as a buffer in maintaining the surface charge of the particles, and in that way, controlled the viscosity of the suspension.

TEM photomicrographs in Figure 4.12 show that α-FeOOH crystals grown with malonic acid in combination with carbonate or any other dicarboxylic acid have physical characteristics that are similar to α-FeOOH crystals grown with malonic acid alone. The particles are approximately 160 nm in length with an aspect ratio of about 8:1. The morphology of α-FeOOH grown with succinic acid and carbonate or oxalic acid is similar to α-FeOOH crystals grown with succinic acid alone. The crystals are approximately 300 nm long with an aspect ratio of about 20:1. That the characteristics normally found in α-FeOOH grown with malonic acid alone occurred even in the presence of a second dicarboxylic acid indicates that malonic acid was a 'more effective' growth modifier than carbonate or the other dicarboxylic acids. Succinic acid was less effective than malonic acid as a growth modifier, but was more effective than carbonate or oxalic acid. Among these dicarboxylic acids, growth modification was a competitive effect, even if adsorption on α-FeOOH crystals was not competitive. Malonic caused the greatest alteration of α-FeOOH as far as crystal size, and was also found to influence the morphology of α-FeOOH in a more dominant manner than other dicarboxylic acids. The size of the malonic molecule with two closely spaced carboxylic acid groups is similar to maleic acid, which caused the largest change in α-FeOOH of the four carbon dicarboxylic acids. The position of the acids groups in both molecules may be a key to their growth modification behavior. The exact mechanism of the dicarboxylic acids' effects on the morphology of α-FeOOH is discussed later in this and the following chapters.

The growth modification found for the combination of Zn^{2+} and dicarboxylic acids was additive. The dicarboxylic acids produced a change in α-FeOOH morphology that was independent of Zn^{2+}, but Zn^{2+} also produced a morphology change. The difference between competitive activity found among dicarboxylic acids and additive activity found for Zn^{2+} and

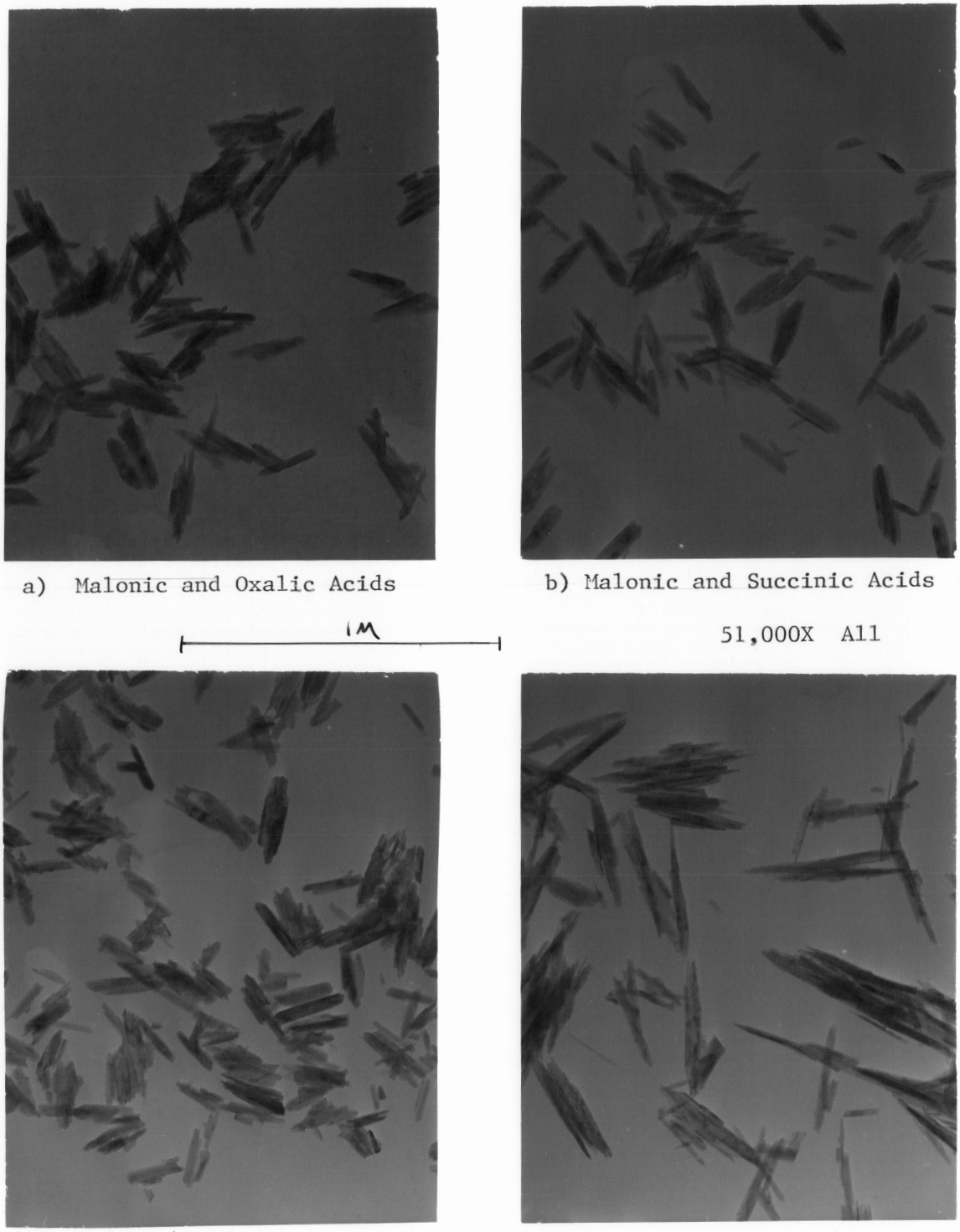

a) Malonic and Oxalic Acids

b) Malonic and Succinic Acids

c) Malonic and Adipic Acids

d) Succinic and Oxalic Acids

Figure 4.12 TEM Micrographs of Competitive Reactions with Dicarboxylic Acids

dicarboxylic acids, could be due to several possible effects. Zinc ions may induce a different mechanism of morphology alteration, or adsorption sites necessary to change the morphology of α-FeOOH are not the same for metal ions and organic molecules. Potentially, zinc can be incorporated into α-FeOOH lattice sites, a mechanism not available to dicarboxylic acids. A mechanism of growth morphology due to Zn^{2+} in Fe^{3+} lattice sites would explain why the effect of Zn^{2+} and dicarboxylic acids are additive rather than competitive. This mechanism assumes that zinc incorporation would not affect the morphological changes due to dicarboxylic acids.

In the variable time of addition study, several dicarboxylic acids were added to the reaction suspension at different times during the oxidation. PAS-IR spectra confirm that oxalic, succinic, and adipic acids, added 150 minutes after the beginning of oxidation, were adsorbed on α-FeOOH crystals. (Figure 4.13) In Figure 4.14, spectra are shown for the products of reactions in which malonic acid was added between 60 minutes and 240 minutes after the start of oxidation in a 300 minute reaction. The peaks corresponding to the symmetric and asymmetric carbon-oxygen stretching vibrations were approximately the same intensity for the 0, 60, 90, 120, and 150 minute additions. The intensity of the IR peaks was less for the 180 and 240 minute addition products. The intensity of the IR peaks can be used as a rough estimate of the amount of malonic acid adsorbed on α-FeOOH. No true quantitation of adsorbed dicarboxlic acid was carried out. The IR peaks of the 180 and 240 minute products indicate that less malonic acid was adsorbed at the later addition times, either due to insufficient time to adsorb, or to unavailability of adsorption sites. Figure 4.15 shows the influence of time of addition of malonic acid on the viscosity of the final suspension. Earlier addition of malonic acid exhibited a greater reduction in suspension viscosity than when malonic acid was added at the later stages of oxidation. The reduction in the amount of acid adsorbed in the late additions, as indicated by the IR data, had less effect on the suspension viscosity.

A series of TEM photomicrographs are shown in Figure 4.16 of α-FeOOH from the variable time of addition reactions with malonic acid. The micrographs indicate that malonic acid added

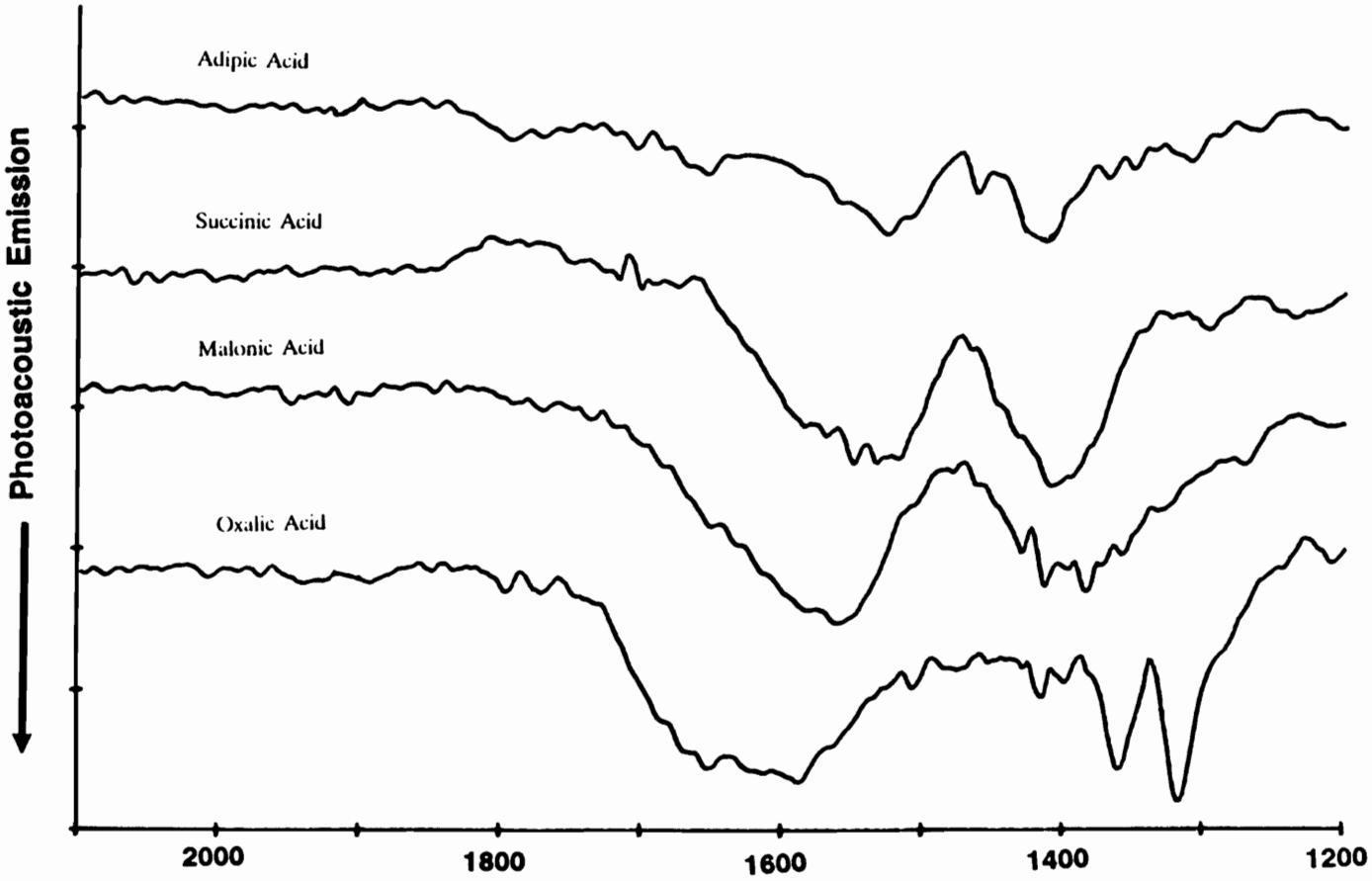

Spectra for α-FeOOH subtracted

Symmetric carboxyl stretch - 1300 to 1450 cm^{-1}
Asymmetric carboxyl stretch - 1500 to 1700 cm^{-1}

Figure 4.13 PAS-IR Spectra for Time of Addition Products - 2.5 hrs

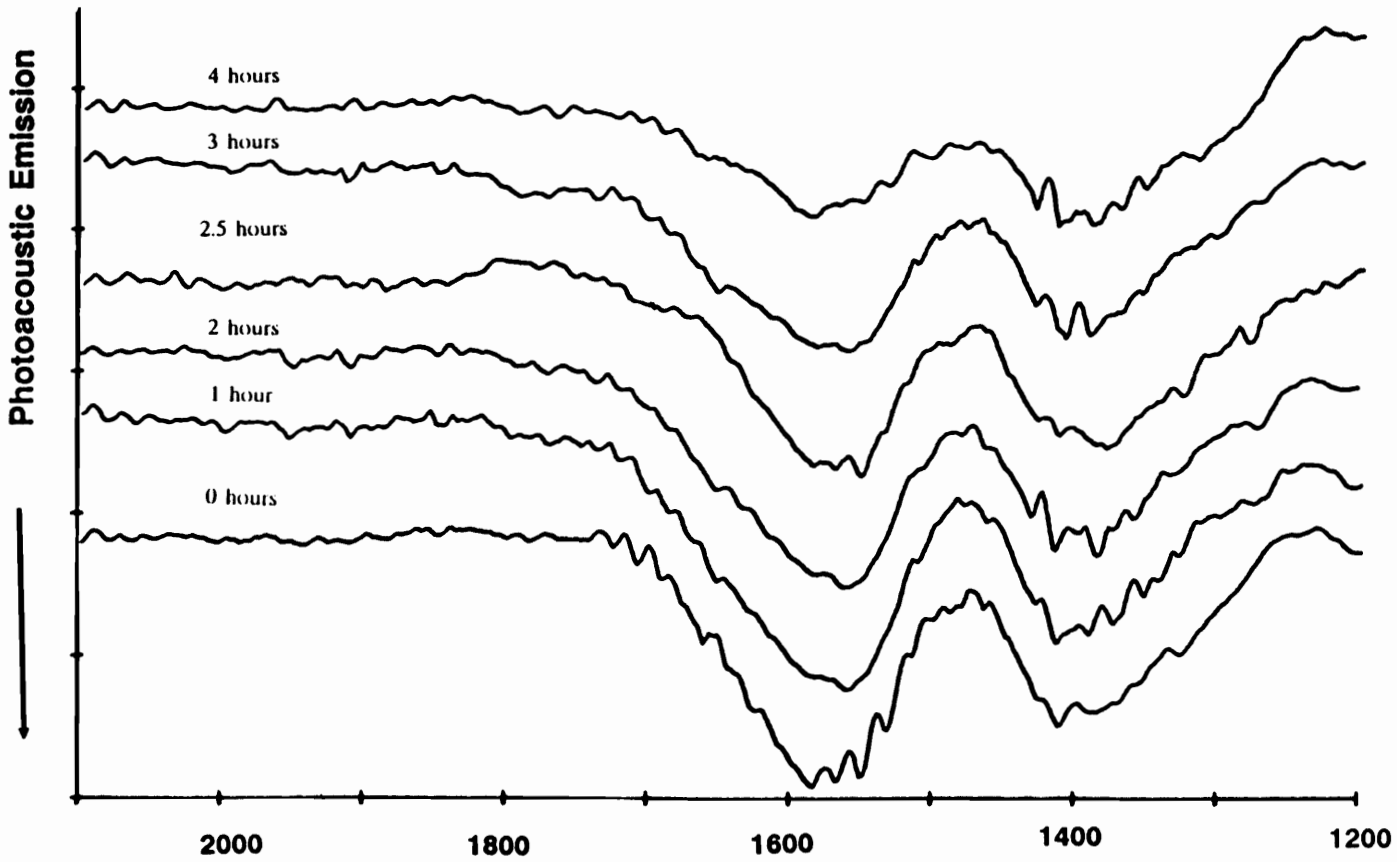

Spectra for α-FeOOH subtracted

Symmetric carboxyl stretch - 1300 to 1450 cm^{-1}
Asymmetric carboxyl stretch - 1500 to 1700 cm^{-1}

Figure 4.14 PAS-IR Spectra for Time of Addition - Malonic Acid

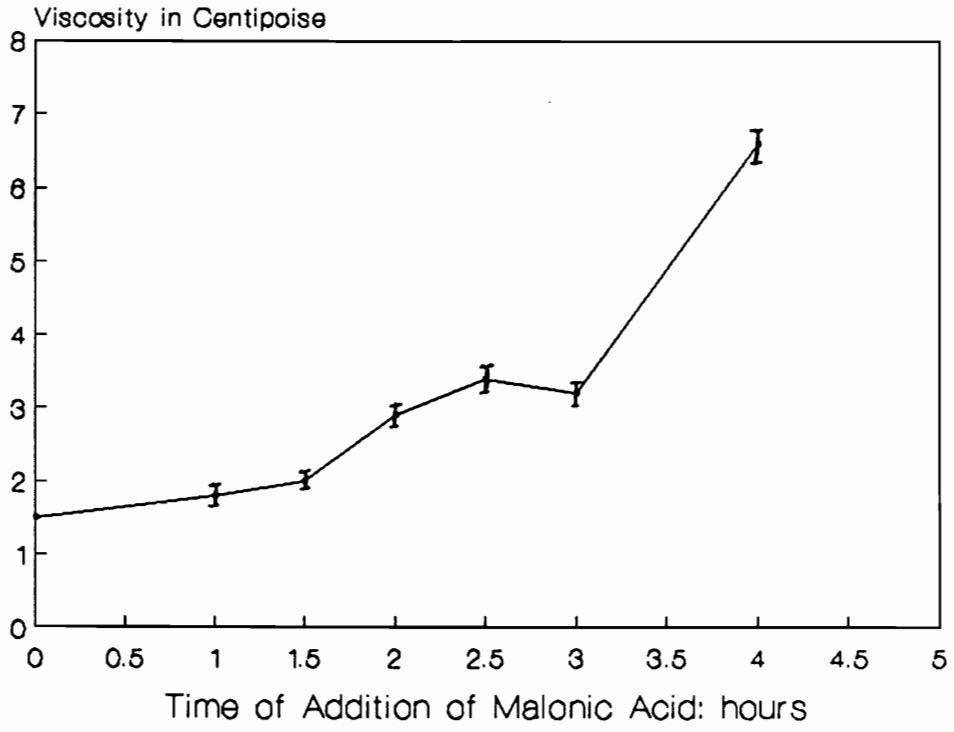

Figure 4.15 Final Suspension Viscosity - Malonic Acid at Various Reaction Times

a) 1 hour

b) 2 hours

1 M

51,000X A11

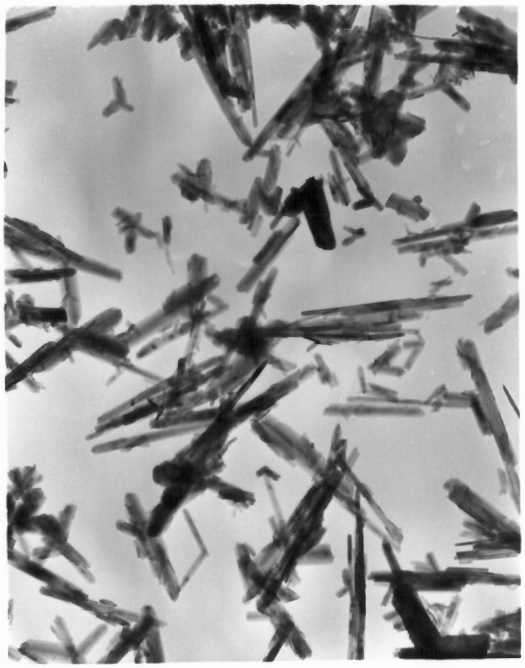

c) 3 hours

d) 4 hours

Figure 4.16 TEM Micrographs of Time of Addition Products - Malonic Acid

between 0 and 120 minutes after the start of oxidation gave small crystals of low aspect ratio but high uniformity. The products from 150, 180 and 240 minute addition time reactions are far less uniform in size and shape. There is a correlation between the suspension viscosity and the amount of malonic acid adsorbed on α-FeOOH crystals (determined by IR), and the extent of malonic acid's effect on morphology. This effect could be due to the amount of time available to affect α-FeOOH growth, or the availability of adsorption sites which facilitate the alteration of growth behavior.

The time of addition study with malonic acid did not give direct evidence of when the dicarboxylic acid affected the growth of α-FeOOH. The study showed that dicarboxylic acids did not need to be present at the start of the reaction to influence crystal formation. The best estimate from the TEM photos is that somewhere approximately halfway through the oxidation, there is a cut-off time after which addition of dicarboxylic acid has a smaller effect on crystal growth.

C. EDTA

EDTA was chosen as a potential growth modifier based on the results that dicarboxylic acids changed the morphology of α-FeOOH. The strong coordination behavior between EDTA and iron species made it likely that EDTA might behave like dicarboxylic acids. The first reaction with 0.01M EDTA at 40°C produced a bright orange reaction suspension when total oxidation of Fe^{2+} to Fe^{3+} had been completed. XRD spectra of the dried crystals determined that the product was 95% γ-FeOOH and 5% α-FeOOH. The XRD patterns for pure γ-FeOOH and α-FeOOH are shown in Figure 4.17. Increasing the concentration of EDTA to 0.0125M EDTA produced 100% γ-FeOOH at 40°C. Photomicrographs of γ-FeOOH and α-FeOOH are shown in Figure 4.18. PAS-IR spectra of α-FeOOH and γ-FeOOH with no additives are shown in Figure 4.19. The many differences between the two phases found in the TEM photomicrographs, IR spectra, and XRD were all used to confirm the presence of γ-FeOOH, and

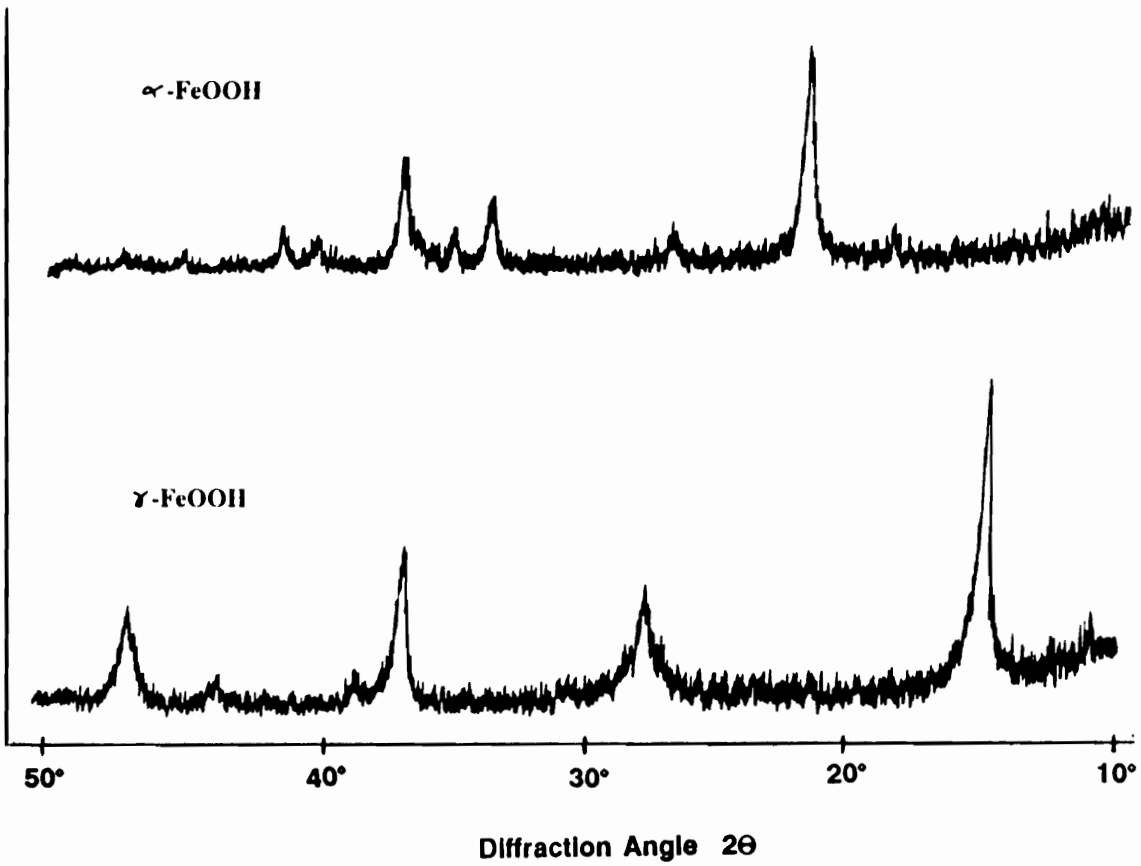

γ-FeOOH - 14, 27, 37, 44, 47°

α-FeOOH - 21, 34, 35, 37, 39, 41°

Figure 4.17 XRD patterns for γ-FeOOH and α-FeOOH

a) α-FeOOH

1 M 51,000X

b) γ-FeOOH

Figure 4.18 TEM Micrographs of α-FeOOH and γ-FeOOH Samples

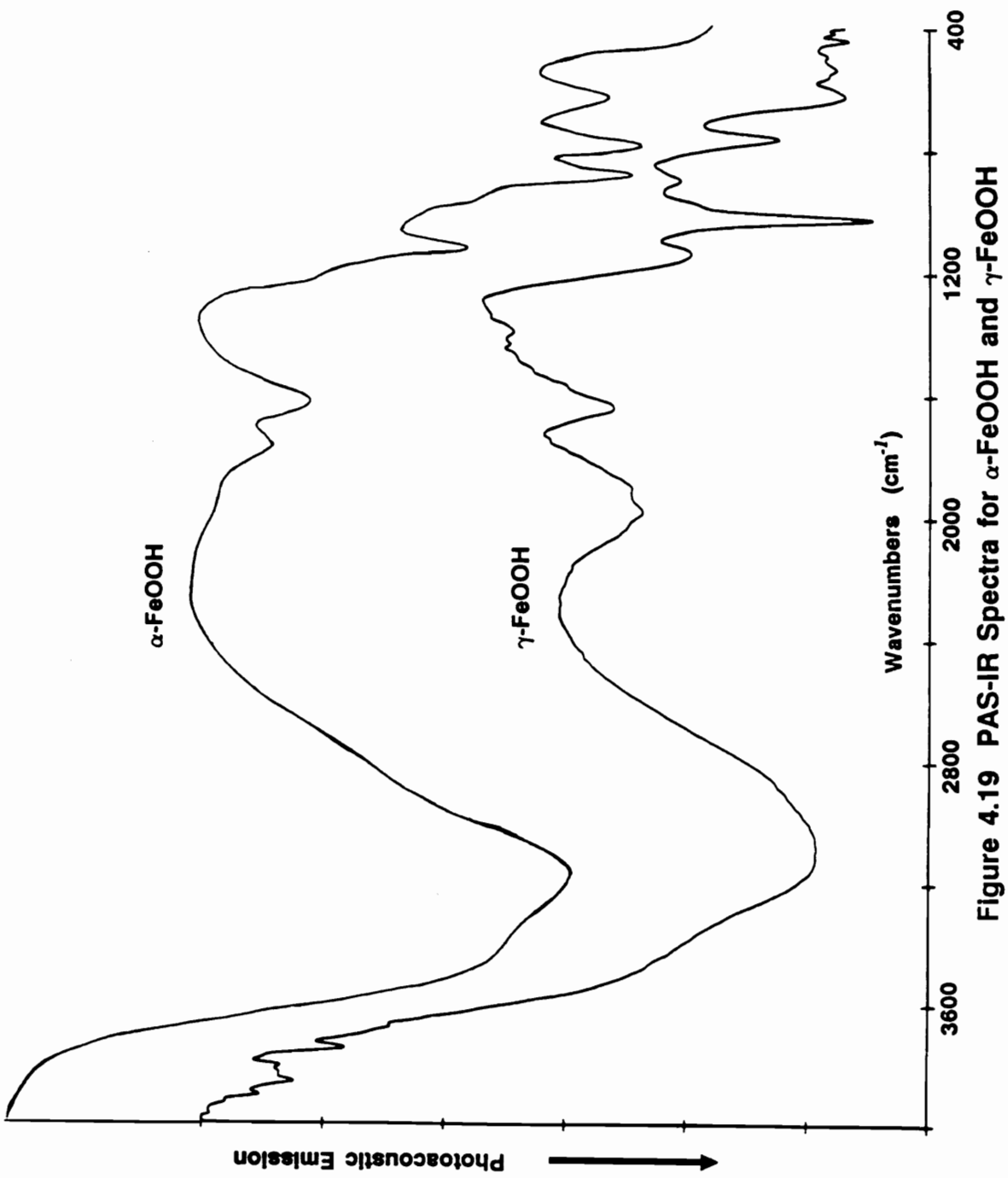

Figure 4.19 PAS-IR Spectra for α-FeOOH and γ-FeOOH

to determine the amount of each FeOOH phase in the reaction products.

In an attempt to grow larger crystals of γ-FeOOH, a reaction containing 0.0125M EDTA was carried out at 50°C. The product of this reaction was 5% γ-FeOOH and 95% α-FeOOH. A graph in Figure 4.20 shows the results of a matrix of experiments carried out at temperatures from 30°C to 50°C at concentrations between 0 and 0.015M EDTA. At 30°C, only 0.0075M EDTA was required to produce 100% γ-FeOOH. Addition of less EDTA than necessary to produce 100% γ-FeOOH gave mixed phase products. The mixed phase product contained γ-FeOOH and α-FeOOH. No other crystalline iron oxide phases were detected. The increased temperature inhibited the production of γ-FeOOH with respect to α-FeOOH. This result is due either to the lower thermodynamic stability of γ-FeOOH relative to α-FeOOH, or to changes in the kinetics of crystal nucleation to favor α-FeOOH at higher temperature. The mechanism by which EDTA induced the production of γ-FeOOH at lower temperatures could be similar to the effects in morphology caused by dicarboxylic acids. EDTA could act as a template during nucleation, or adsorb to intermediates to alter the conversion to FeOOH. The ability of EDTA to act as a solubilizing agent might also have preferentially dissolved α-FeOOH allowing γ-FeOOH to grow.

Competitive reactions were carried out to examine the relative effects of EDTA and dicarboxylic acids on FeOOH growth. EDTA and dicarboxylic acids were added together at the start of FeOOH growth reactions. Table 4.5 lists the percent of γ-FeOOH and α-FeOOH, determined by XRD, in the competitive addition reaction products. At 40°C 0.01M EDTA alone produced 95% γ-FeOOH. The reaction containing 0.01M EDTA and 0.01M succinic acid produced 75% γ-FeOOH and 25% α-FeOOH. The reaction with 0.015M EDTA and 0.01M succinic acid gave 85% γ-FeOOH and 15% α-FeOOH. Similar results were found for adipic and malonic acid, but not for sodium carbonate. When a dicarboxylic acid was present, some α-FeOOH was produced, even at EDTA concentrations which would have produced 100% γ-FeOOH in the absence of the dicarboxylic acid. The dicarboxylic acids acted as nucleating

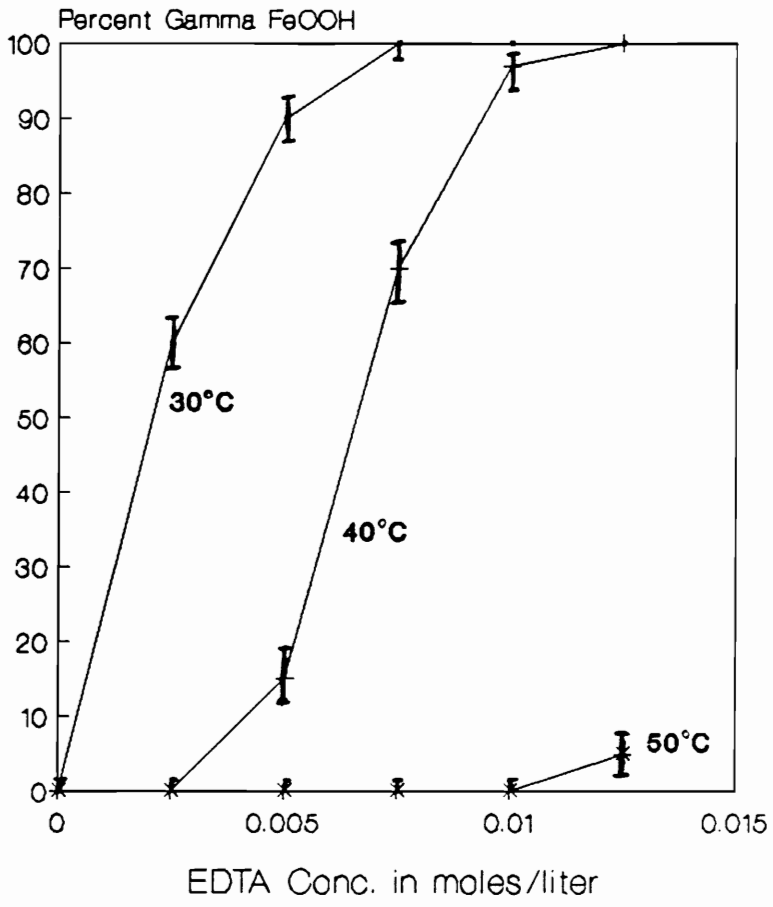

Figure 4.20 Temperature Dependence of γ-FeOOH Growth

Table 4.5 Percent γ-FeOOH Produced with EDTA and Dicarboxylic Acids

Additives	Percent γ-FeOOH
0.01M EDTA	95 ± 5
0.0125M EDTA	100
0.01M EDTA and 0.01M succinic acid	75
0.015M EDTA and 0.01M succinic acid	85
0.01M EDTA and 0.01M malonic acid	65
0.0125M EDTA and 0.01M Na_2CO_3	100

All reactions were carried out at 40°C, and contained no Zn^{2+}

The balance of product in each case was α-FeOOH

agents for α-FeOOH in addition to changing the morphology of α-FeOOH. These results demonstrate that EDTA and the dicarboxylic acids did not act on the same FeOOH crystals, but acted independently in the reaction suspension to form different phases of FeOOH. The independence of the action of EDTA and dicarboxylic acids suggests that the effect of preferential dissolution of α-FeOOH by EDTA is unlikely as the mechanism for γ-FeOOH production. A preferential nucleation mechanism is much more consistent with the crystallization data.

EDTA was placed into reactions at different times to determine when EDTA induced the formation of γ-FeOOH. Addition of 0.0125M EDTA to the reaction mixture before 80 minutes produced nearly 100% γ-FeOOH, as shown in the XRD pattern in Figure 4.21. A small peak near the 100% peak for α-FeOOH may indicate a small fraction of that phase at a concentration near the lower detection limit of XRD. Addition of 0.0125M EDTA after 100 minutes produced essentially 100% α-FeOOH. TEM photomicrographs of the 80 and 100 minute addition products are shown in Figure 4.22. The shape and size of the crystals in the micrographs were similar to the sample crystals of α-FeOOH and γ-FeOOH. PAS-IR spectra of products from the 80 and 100 minute addition of EDTA are shown in Figure 4.23. In the spectrum of the 80 minute EDTA addition product, there are no peaks which are not assigned to γ-FeOOH. If EDTA was adsorbed to γ-FeOOH crystals the concentration was too low to be detected by IR. In the 100 minute EDTA addition product, which was confirmed by XRD and TEM as α-FeOOH, the carboxyl symmetric and asymmetric stretching vibrations are found between 1700 cm^{-1} and 1400 cm^{-1}. These carboxyl peaks indicate that EDTA was coordinated to α-FeOOH crystals through both carboxylic acid oxygens in a manner identical to the coordination of dicarboxylic acids to α-FeOOH. The fact that EDTA adsorbed or coordinated to α-FeOOH, but was not in the IR spectrum of γ-FeOOH may have some bearing on the mechanism of FeOOH growth modification by EDTA. This time dependent behavior of EDTA between the 80 and 100 minute additions indicated that the influence of EDTA might be as a nucleating agent for γ-FeOOH,

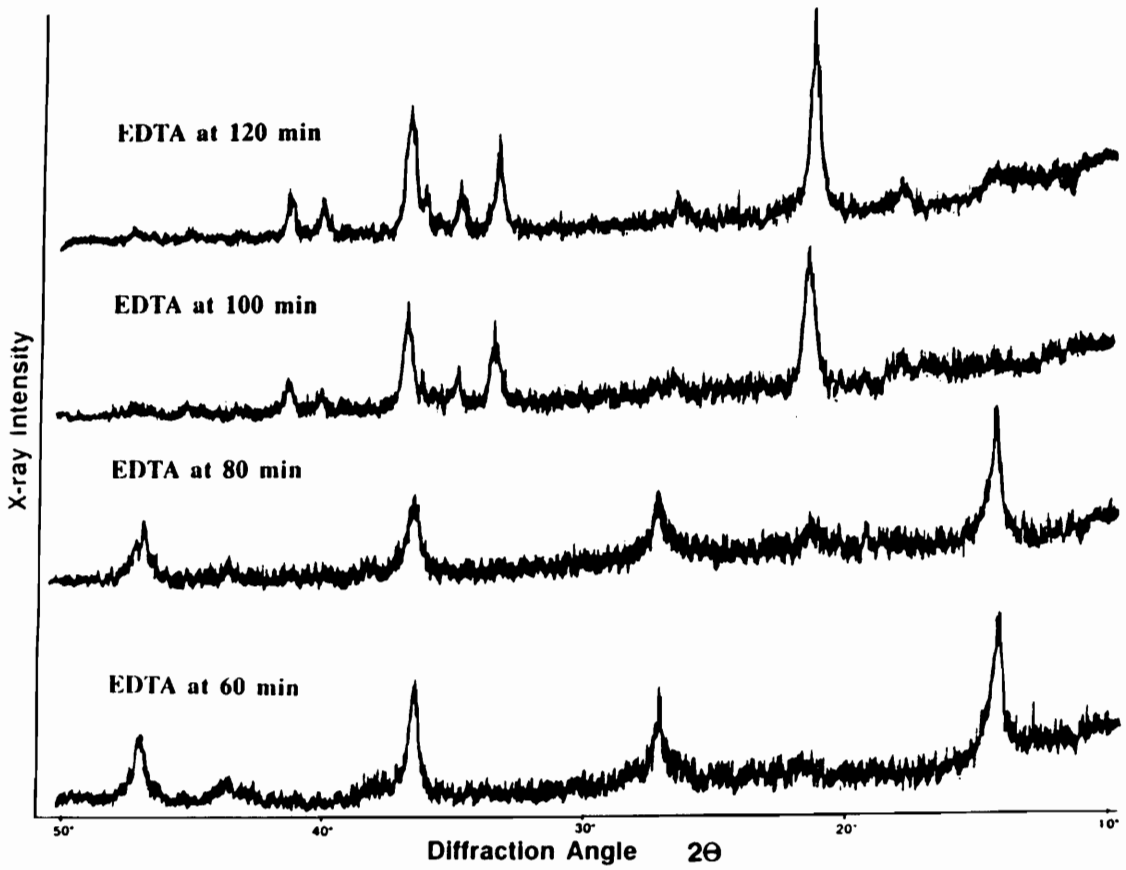

γ-FeOOH - 14, 27, 37, 44, 47°

α-FeOOH - 21, 34, 35, 37, 39, 41°

Figure 4.21 XRD patterns for Time of Addition EDTA Products

a) EDTA at 80 minutes - γ-FeOOH

1 μ 51,000X

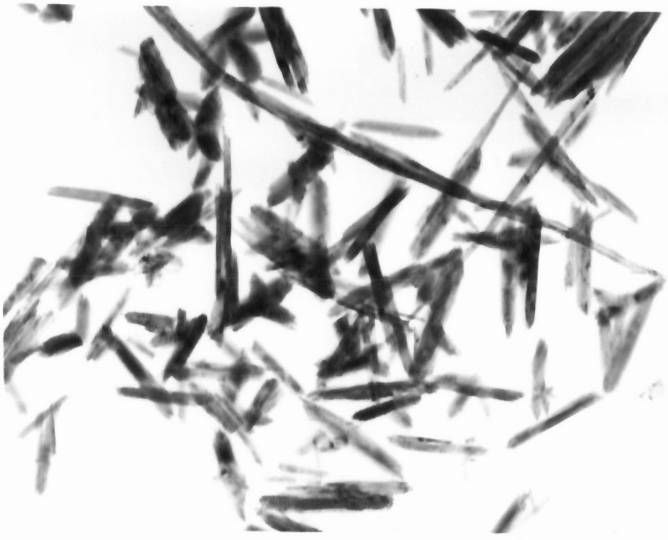

b) EDTA at 100 minutes - α-FeOOH

Figure 4.22 TEM Micrographs of Time of Addition Products - EDTA

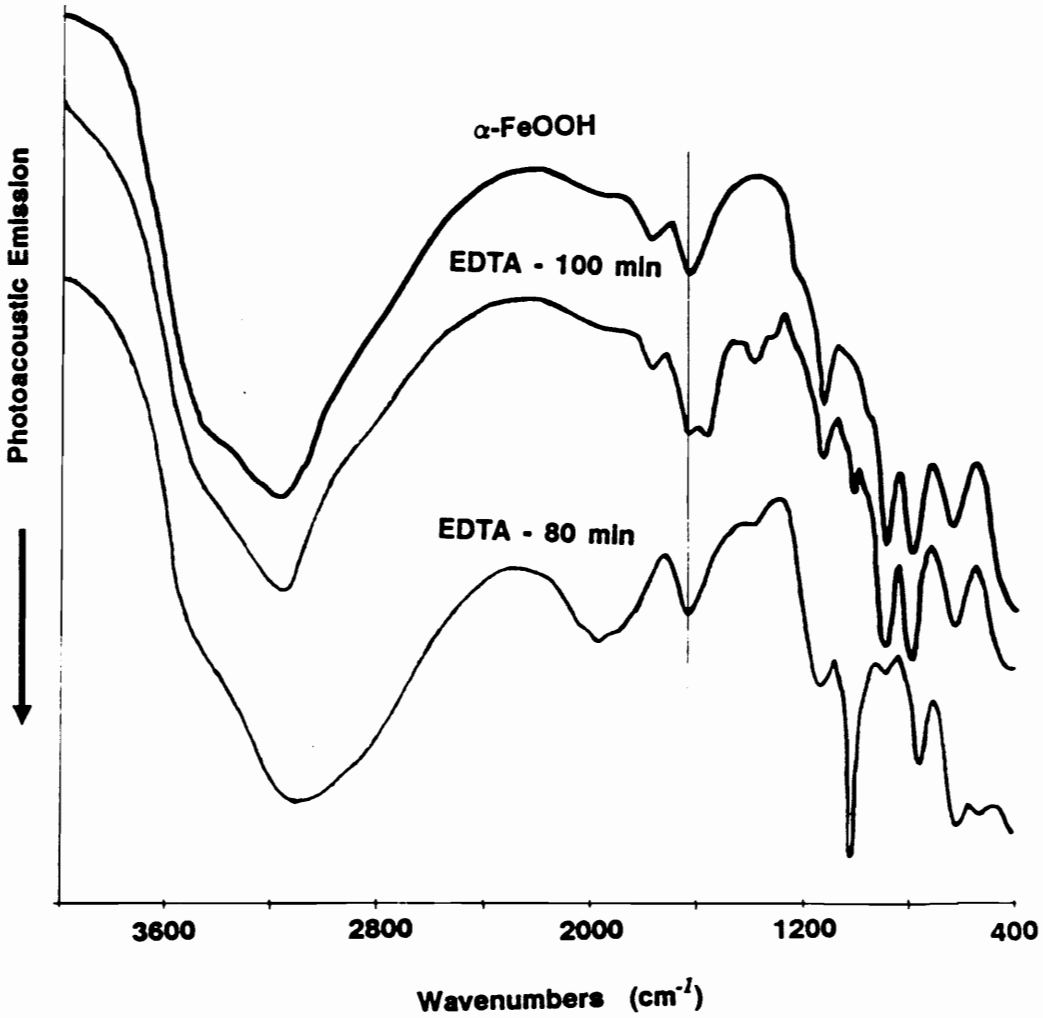

Symmetric carboxyl stretch - 1300 to 1450 cm^{-1}
Asymmetric carboxyl stretch - 1500 to 1700 cm^{-1}

Figure 4.23 PAS-IR Spectra - EDTA Time of Addition Experiments

acting on a species that existed in the suspension before 100 minutes of oxidation. The time of addition study using malonic acid showed that malonic acid acted before two hours of reaction time. The addition time of EDTA in which the product switched from γ-FeOOH to α-FeOOH was also close to the two hour mark. The variability in total reaction time over a number of experiments was as much as $\pm$ 30 minutes, due to difficulties in maintaining constant oxygen flow during the changes in viscosity and stirring rate. Within this variation in total reaction time, the critical times of addition of malonic acid and EDTA may be the same. At some time less than two hours of oxidation, malonic acid and EDTA act to change the phase of FeOOH. After that critical time, the effect of these additives on FeOOH morphology is minimal, although both EDTA and malonic acid adsorb on α-FeOOH when added after two hours. It is difficult at this point to separate the effects of these multifunctional carboxylic acid additives as growth modifiers from their behavior as simple adsorbates. While it is possible to postulate that adsorption of the acids can lead to changes in subsequent FeOOH crystal growth, it appears that under some circumstances adsorption occurs with no growth modification, and under other circumstances growth modification occurs with no adsorption.

Two experiments were carried out at 25°C in which 0.01M [EDTA-Fe^{III}]$^-$ was added to reactions at 0 and 120 minutes after oxygen flow was started. When [EDTA-Fe^{III}]$^-$ was added at the beginning of the reaction, the product was 100% γ-FeOOH. When [EDTA-Fe^{III}]$^-$ was added at 120 minutes, the product was approximately 40% γ-FeOOH, and 60% α-FeOOH. (Figure 4.24) When EDTA was added after 100 minutes, the product was 100% α-FeOOH. [EDTA-Fe^{III}]$^-$ forms γ-FeOOH at a point in the reaction when EDTA alone would not. This indicates that EDTA-Fe^{2+} coordination is not necessary to nucleate γ-FeOOH, and that [EDTA-Fe^{III}]$^-$promotes γ-FeOOH growth. The PAS-IR spectrum of γ-FeOOH grown with [EDTA-Fe^{III}]$^-$ is identical to the spectrum of γ-FeOOH grown with EDTA, and showed no evidence of any EDTA in the product. (Figure 4.25)

A number of compounds were chosen to try to duplicate the effect of EDTA to produce

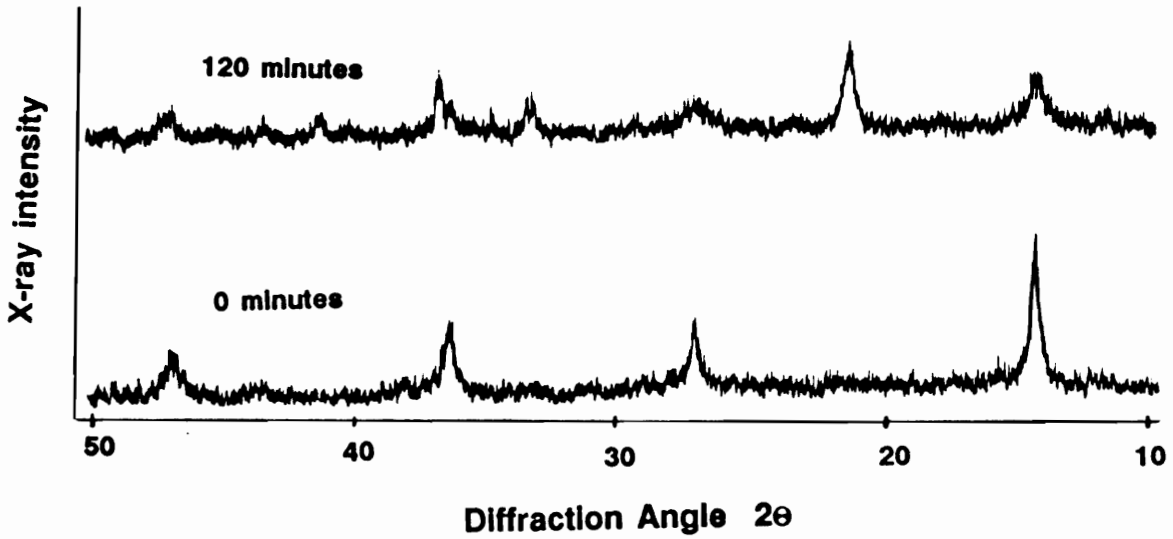

α-FeOOH - 21, 34, 35, 37, 39, 41°

γ-FeOOH - 14, 27, 37, 44, 47°

Figure 4.24 XRD Patterns - Time of Addition of [EDTA-Fe^{III}]$^-$

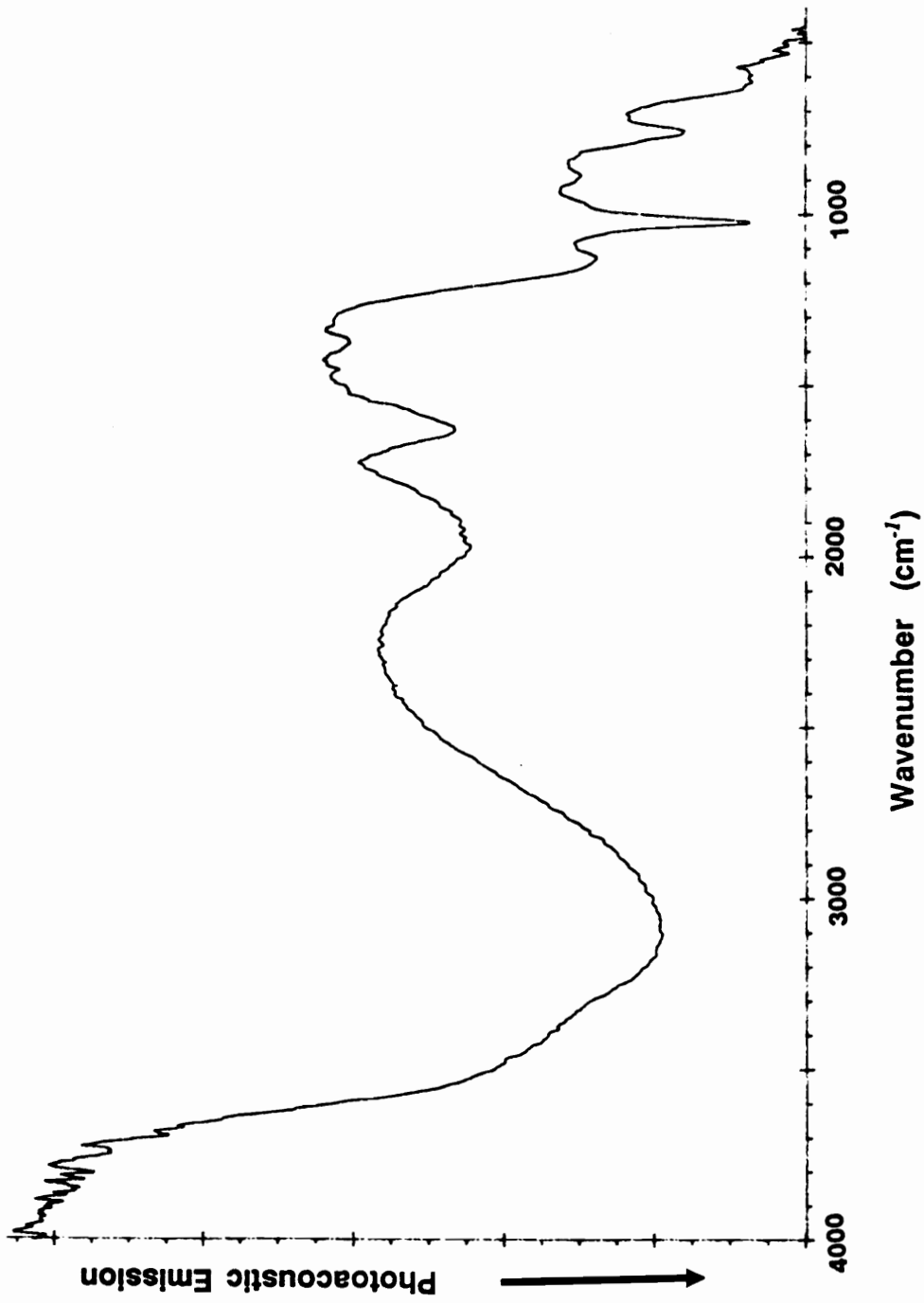

Figure 4.25 PAS-IR Spectrum for γ-FeOOH from $FeSO_4$ + $[EDTA\text{-}Fe^{III}]^-$

γ-FeOOH. These compounds contained some of the same chemical or structural characteristics of EDTA. Iminodiacetic acid (IDA) is similar to either end of EDTA, and was chosen as a model compound to see if the presence of an amine group situated between two carboxyl groups could induce the formation of γ-FeOOH.

Iminodiacetic Acid $(HO_2CCH_2)_2NH$

IDA is similar in size to glutaric acid, the five carbon dicarboxylic acid. The XRD pattern for products produced in 0.0125M and 0.25M IDA showed α-FeOOH as the single crystalline phase. Infrared spectra of the IDA reaction products showed symmetric and asymmetric carbon-oxygen streching vibrations that confirmed the adsorption of IDA on α-FeOOH. A suspension viscosity of 5.1 cp for 0.0125M IDA reaction was in the same range as 2.8 cp measured for the 0.016M glutaric acid suspension. A surface area measurement of 80 m^2/g for the product from the 0.0125M IDA reaction was also comparable to the area measured for the product of the 0.016M glutaric acid reaction. Thus IDA acts more like its dicarboxylic analogue than EDTA. The structure of IDA with an amine group situated between two acetic acids groups is not sufficient by itself to induce the production of γ-FeOOH from $FeSO_4$. The action of EDTA on FeOOH phase production is not just the sum of the action of two halves of its structure.

The second model compound, pyromellitic acid (PMA), was selected because it contains four carboxylic acids groups held at a fixed distance by the rigid ring.

Pyromellitic Acid

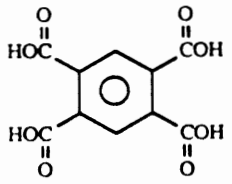

If the distance between the acids groups was similar to those of EDTA in solution, they might act as a template to nucleate γ-FeOOH. The product of the 0.0125M PMA reaction was 100% α-FeOOH, and IR confirmed that this acid was also incorporated into the α-FeOOH crystals. Either the distance between the four acid groups in PMA was not the same as EDTA, or four

acids groups alone are not sufficient to induce γ-FeOOH formation. The viscosity of the α-FeOOH suspension containing PMA was 2.1 cp. The surface area of the α-FeOOH product was 111 m^2/g. PMA has carboxylic acid groups situated in a structure similar to those in maleic acid. Maleic acid at 0.016M produced α-FeOOH with a surface area of 129 m^2/g, and a suspension viscosity of 1.6 cp. PMA produces α-FeOOH like its dicarboxylic analogue, rather than like EDTA.

Ethylenediamine $H_2NCH_2CH_2NH_2$

Ethylenediamine produced only α-FeOOH and did not change any of the characteristics of the oxide crystals. Ethylenediamine did not appear in the IR spectrum of the α-FeOOH crystals. The coordination behavior of ethylenediamine with α-FeOOH was not strong enough to affect the growth process.

Ethylenediaminediacetic Acid $(HO_2CCH_2)NHCH_2CH_2NH(CH_2CO_2H)$

Ethylenediaminediacetic acid (EDDA) contains two carboxylic acid groups, one attached to each of the two nitrogen atoms in the molecule. EDDA was chosen as a model compound to examine if the key characteristic for γ-FeOOH production was the presence of two amine groups and two carboxylic acid groups held at a certain separation distance by a carbon chain. The product of the EDDA reactions was primarily α-FeOOH. Small peaks in the XRD patterns of some EDDA reaction products may be attributed to small amounts of γ-FeOOH, but the results were not reproducible, and may have been due to contamination by EDTA in the EDDA reagent. It is sufficient to say that at temperatures and concentrations of acid studied, EDDA does not induce nucleation of γ-FeOOH. The amine group with a single acetic acid at each end of the molecule either does not coordinate in the same way as EDTA does, or the second carboxlic acid at each end of EDTA plays a part in FeOOH phase formation.

Ethylenediaminetetramethylenephosphonic Acid

$[(HO)_2POCH_2]_2NCH_2CH_2N[CH_2OP(OH)_2]_2$

Ethylenediaminetetramethylenephosphonic acid (EDTMPA) is similar in structure to EDTA, but

contains phosphonic acid groups rather than carboxylic acid groups. The product of the EDTMPA reactions was primarily tiny amorphous particles of iron oxide with a small number of α-FeOOH crystals. EDTMPA and ethylenediphosphonic acid (EDPA) are discussed in more detail in the phosphate addition section.

Butanetetracarboxylic Acid $HO_2CCH_2CH(CO_2H)CH(CO_2H)CH_2CO_2H$

Butanetetracarboxylic acid, another compound with four carboxylic acid groups, produced very small α-FeOOH crystals. It did affect the morphology of α-FeOOH by increasing the surface area to 360 m^2/g, but showed no evidence of altering FeOOH phase production. No other carboxylic acid compound has been found that produces such a large effect on α-FeOOH particle size.

Ethylenediaminediorthohydroxyphenylacetic Acid $HO_2CCHNHCH_2CH_2NHCHCO_2H$ (HO- and -OH on the phenyl rings)

EDDHPA, a substituted version of EDDA, had no effect on the physical or chemical properties of α-FeOOH. It was thought that the extra hydroxyl group on the phenyl substituent might increase the strength of coordination of EDDHPA to FeOOH. IR confirmed adsorption of EDDHPA to α-FeOOH, but that adsorption did not affect the growth of α-FeOOH.

Diaminocyclohexanetetraacetic Acid $(HO_2CH_2)_2NCHCHN(CH_2CO_2H)_2$

The last model compound investigated was Diaminocyclohexanetetraacetic acid (DACHTA). DACHTA is very similar in structure to EDTA, and can be described as EDTA with the carbons of the ethyl midsection formed into part of a cyclohexane ring. The additional four carbons in cyclohexane have the effect of stiffening the molecule, and eliminating rotation about the carbon-carbon central bond. The acetic acid groups of this molecule are directed to the same side of the DACHTA molecule by the cyclohexane ring. The product of a reaction carried out in 0.01M DACHTA at 25°C was 100% γ-FeOOH. Limiting the flexability of the EDTA-type

molecule did not reduce its ability to induce the production of γ-FeOOH. DACHTA is the only compound other than EDTA that produced 100% crystalline γ-FeOOH. PAS-IR of γ-FeOOH made with DACHTA shows no evidence of carbon-oxygen stretching vibrations due to the adsorption of DACHTA on the crystals. (Figure 4.26)

Several reactions were carried out with DACHTA at 40°C to examine whether the temperature/concentration behavior was the same for EDTA and DACHTA. Figure 4.27 shows a comparison of the concentration dependence on γ-FeOOH production using EDTA and DACHTA at 40°C. At 0.0025M and 0.005M, DACHTA produced more γ-FeOOH than was found in reactions containing the same concentration of EDTA. However, at concentrations of 0.0075M and above, EDTA produced more γ-FeOOH than DACHTA. An insufficient number of reactions was carried out at each concentration to determine the statistical significance in the amount of γ-FeOOH produced. Based on the experiments that were carried out, DACHTA seemed to be slightly more efficient at lower concentrations at producing γ-FeOOH. The cyclohexane backbone forces the four acetic acid groups of DACHTA closer together. This arrangement of the potential coordinating groups may be more conducive to the formation of γ-FeOOH.

D. Phosphate

Phosphate is known to affect oxide crystal growth (64), and was chosen as a potential modifier for FeOOH growth. The color of the final suspension from the reaction containing 0.02M phosphate at 40°C was a very dark brown. The XRD pattern of the dried product showed small broad peaks corresponding to γ-FeOOH. The surface area of the material was 295 m^2/g. TEM micrographs (Figure 4.28) of the phosphate product showed that the material was a mixture of tiny amorphous particles mixed with a small number of long fibrous γ-FeOOH crystals. Since a lower concentration of EDTA was required to produce γ-FeOOH at lower temperatures, experiments were carried out with phosphate at temperatures less than 40°C. Reactions carried out at 7°C, 24°C, and 30°C gave materials with surface areas and

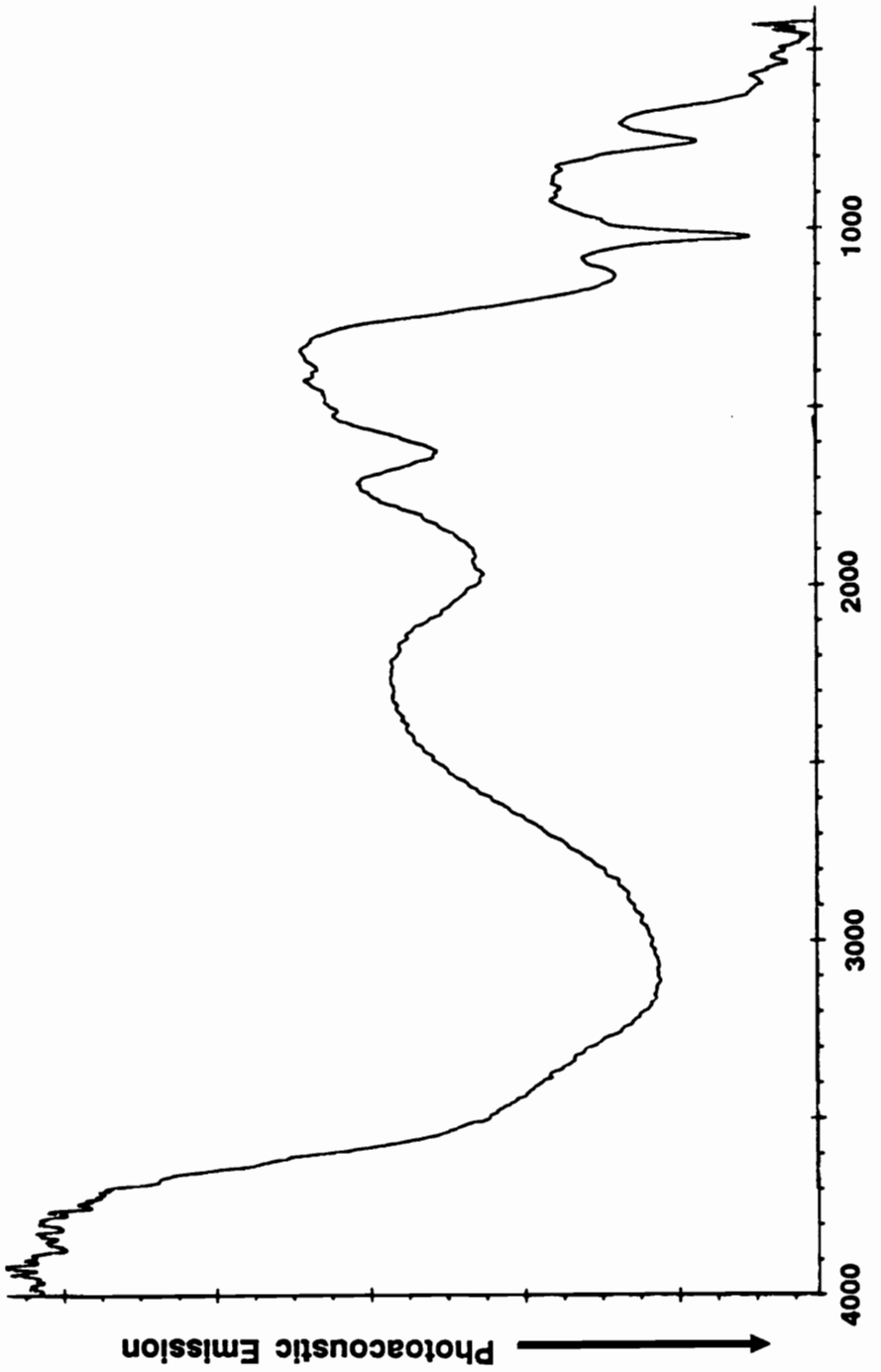

Figure 4.26 PAS-IR Spectrum γ-FeOOH from $FeSO_4$ + DACHTA

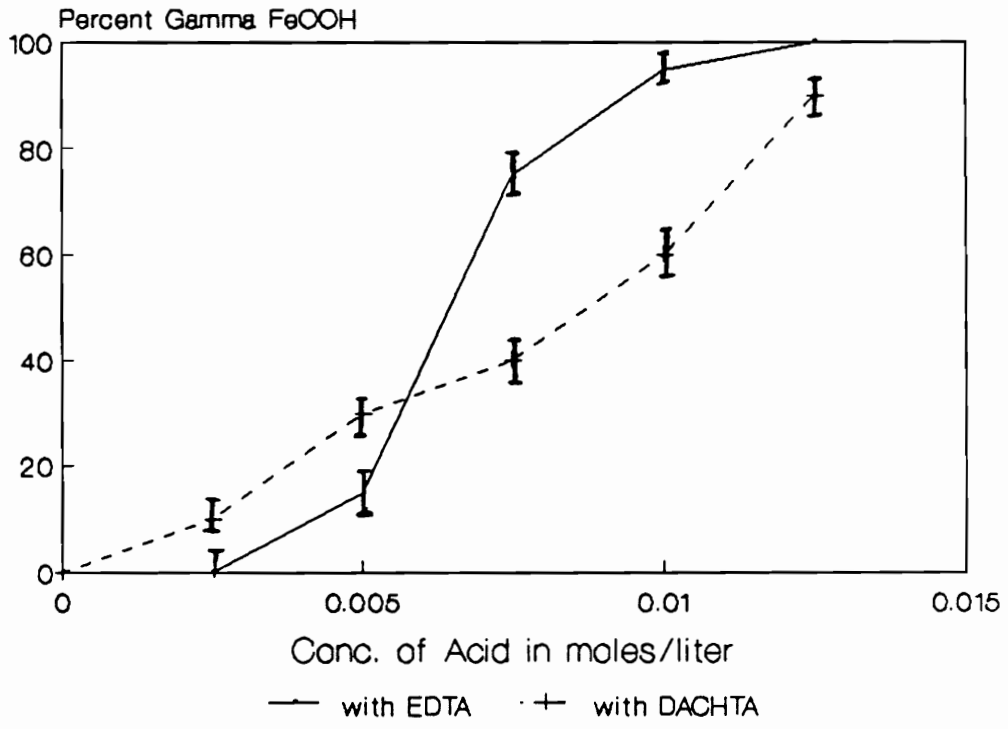

Figure 4.27 Concentration Dependence of EDTA and DACHTA at 40°C

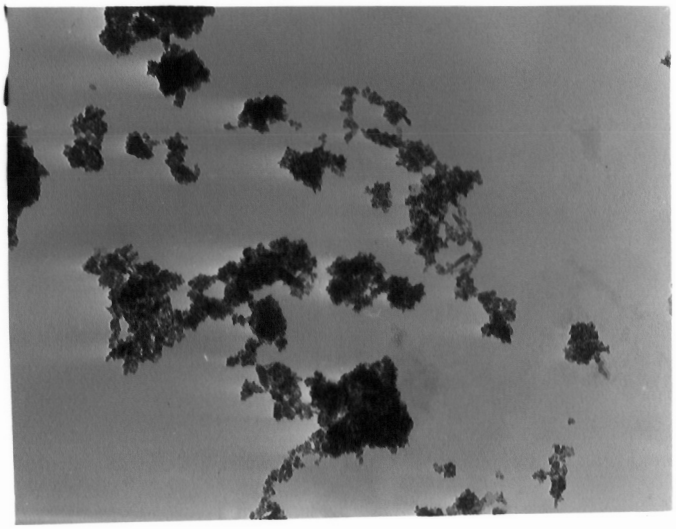

a) Amorphous Material

1 μ

51,000X

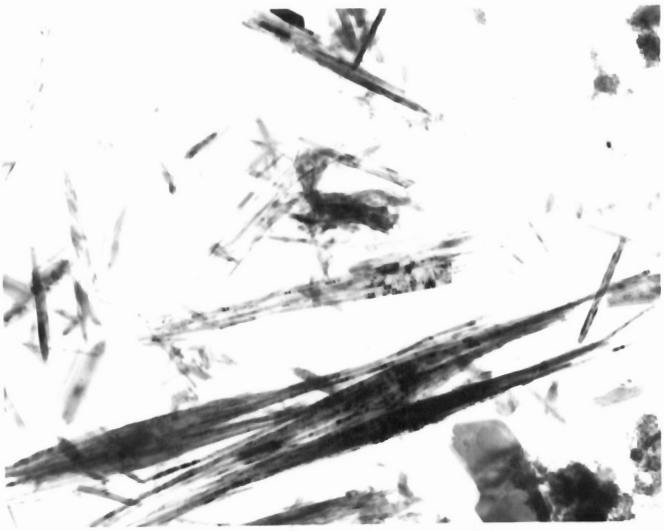

b) Crystalline γ-FeOOH

Figure 4.28 TEM Micrographs of Phosphate Reaction Products

composition similar to the product of the 40°C phosphate reaction. The reaction carried out at 50°C also produced a mixture of amorphous material and some isolated crystals, but the crystals were determined by XRD to be α-FeOOH. The temperature dependence of γ-FeOOH formation with phosphate was similar to γ-FeOOH formation with EDTA. At 50°C, only a small amount of γ-FeOOH was produced at high concentrations of EDTA or phosphate. The similar temperature dependence indicates that both the phosphate reaction and the EDTA reaction may have a common intermediate, and the instability of the intermediate at 50°C leads to less γ-FeOOH formation.

The concentration dependence of phosphate at 40°C is shown in Figure 4.29. At concentrations below 0.02M, a mixture of γ-FeOOH and α-FeOOH is produced. The concentration range of phosphate used to grow γ-FeOOH is similar to the concentration range for EDTA at 40°C. This result can be taken as additional evidence supporting some similarity in the mechanism of phase determination for the two growth modifiers.

Of the six model compounds for phosphate investigated, three were oxides having multiple protonation capability, and three were substituted phosphonic acids. A reaction in 0.02M sodium borate produced 100% α-FeOOH with a surface area of 80 m^2/g, a value somewhat smaller than for a reaction without borate. No boron was detected in the product by XPS, nor was the viscosity of the suspension affected. Sodium orthovanadate produced green crystals. XRD of the green crystals detected only α-FeOOH. XPS showed no vanadium in the product. The origin of the green color was not determined. The viscosity of the orthovanadate suspension was 4.1 cp which indicates that the surface charge was changed relative to α-FeOOH without vanadate. The change in color and the viscosity difference indicate that a small amount of vanadate, less than 0.01 atomic %, may have been on the surface of the α-FeOOH crystals. The concentration was too low to be detected by XPS.

The third oxide model compound, Na_2MoO_4, used at 0.02M, produced tiny crystals of α-FeOOH with a surface area of 300 m^2/g. The influence of MoO_4^{2-} on α-FeOOH crystal growth

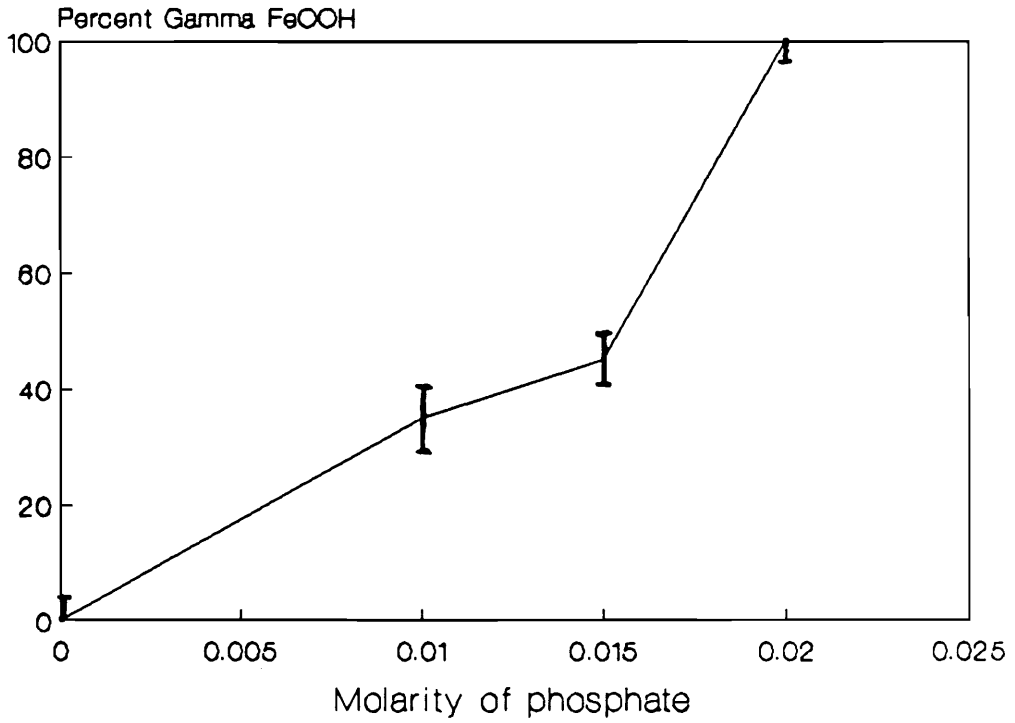

Figure 4.29 Temperature Dependence of γ-FeOOH Growth - Phosphate

may have been primarily as an oxidizing agent rather than as an adsorbate.

The three substituted phosphonic acids behaved similarly to phosphate in that the product of FeOOH growth reactions was a mixture of tiny amorphous particles and some oxide crystals. The oxide crystals produced in the presence of the substituted phosphonic acids were always α-FeOOH. No formation of γ-FeOOH was detected at any temperature or concentration of growth modifier.

E. Halides

The oxidation of ferrous chloride or ferrous bromide forms γ-FeOOH (32). With the hypothesis that the addition of NaCl to ferrous sulfate solutions might also produce γ-FeOOH, a series of reactions containing NaCl and NaBr was carried out. Reactions in concentrations of NaCl up to 0.4M produced only α-FeOOH with a surface area of 60 m^2/g. The surface area was equal to that for α-FeOOH grown in the absence of NaCl. At 0.8M NaCl, a very small peak in the XRD pattern shown in Figure 4.30 may be due to a small amount of γ-FeOOH in the product. The viscosity of the suspension was reduced from 60 cp to 46 cp. Sodium bromide at up to 0.3M produced only α-FeOOH with no effect on the surface area. XPS results shown in Table 4.6 indicate small amounts of halide ions adsorbed on the α-FeOOH surface, but an increase in NaCl solution concentration of almost two orders of magnitude only doubled the surface concentration of chloride ion. No bromide ion was detected by XPS in any NaBr reaction product.

The oxidation of ferrous sulfate solution in the presence of chloride did not produce the same phase of FeOOH as the oxidation of ferrous chloride. Sulfate is regarded as a nonreagent in most reactions. However, counterions such as chloride and sulfate do act to modify FeOOH nucleation and growth processes.

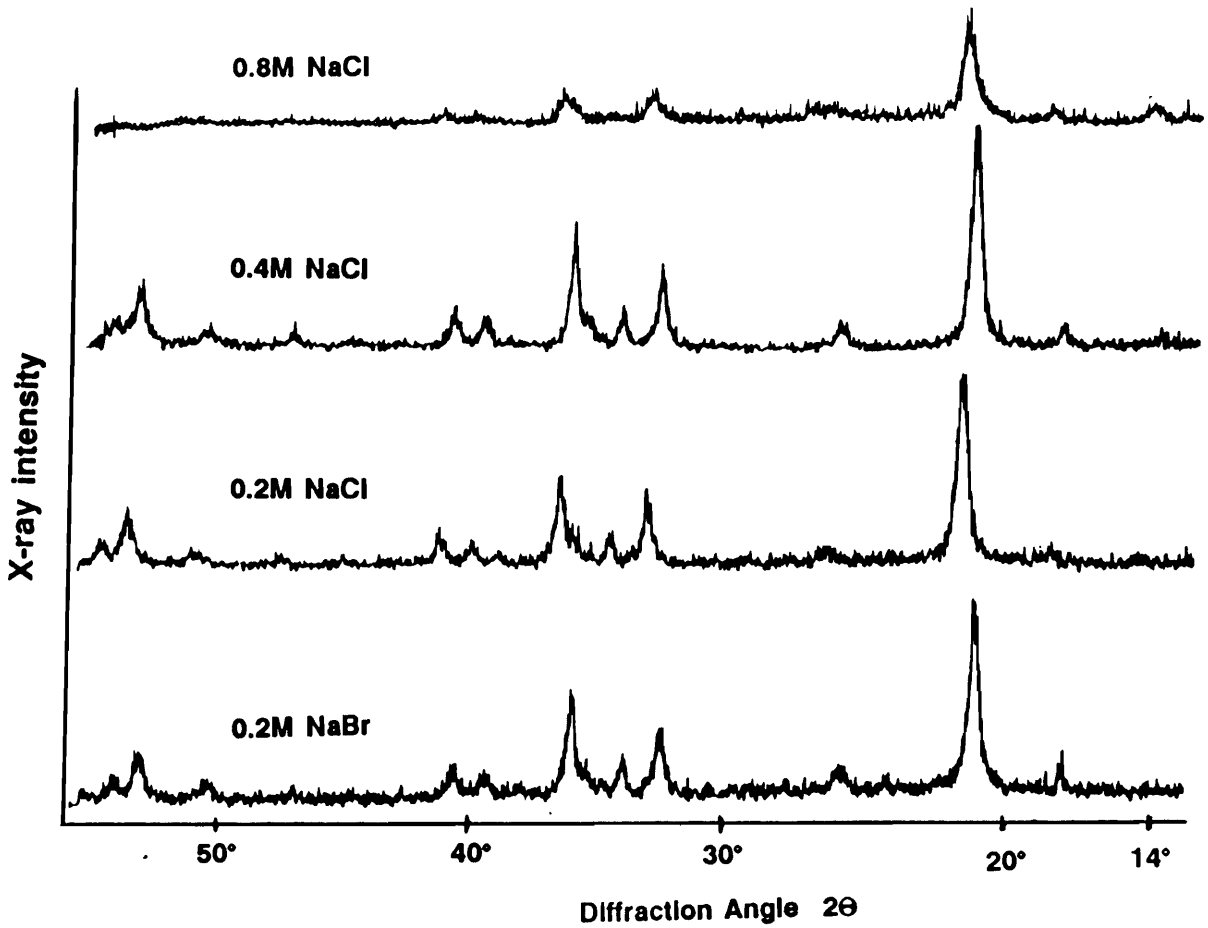

γ-FeOOH - 14, 27, 37, 44, 47°

α-FeOOH - 18, 21, 34, 35, 37, 39, 41, 53°

Figure 4.30 XRD patterns for Halide Products

Table 4.6 Halide Solution Concentration vs. XPS Halide to Iron Ratio

Conc. of Halide ion	Solution Halide to Iron Ratio	XPS Halide to Iron Ratio
0.01M Cl^-	0.025:1	0.025:1
0.02M Cl^-	0.050:1	0.031:1
0.03M Cl^-	0.075:1	0.035:1
0.1M Cl^-	0.25:1	0.037:1
0.15M Cl^-	0.38:1	0.029:1
0.2M Cl^-	0.50:1	0.034:1
0.4M Cl^-	1.0:1	0.033:1
0.6M Cl^-	1.5:1	0.057:1
0.8M Cl^-	2.0:1	0.060:1
0.01M Br^-	0.025:1	<0.01:1
0.02M Br^-	0.050:1	<0.01:1
0.03M Br^-	0.075:1	<0.01:1

F. Adsorption of Acids

The adsorption of dicarboxylic acids and EDTA on α-FeOOH was carried out to examine the pH dependence of acid adsorption on α-FeOOH, the effect of acid adsorption on suspension viscosity, and whether the amount of time of adsorption affected the surface concentration of species. The pH of an α-FeOOH suspension which contains no dicarboxylic acid is 3.5. The viscosity of the α-FeOOH-dicarboxylic acid suspensions at approximately pH 2.5 is similar to the viscosity of α-FeOOH without any acid. PAS-IR spectra of the samples from the adsorption of dicarboxylic acids at pH 2.5 show no peaks that can be assigned to adsorbed dicarboxylic acid species. After the suspensions containing dicarboxylic acids were adjusted to pH 5.3, the viscosity of all the suspensions dropped significantly. Examination of the samples from the adjusted pH adsorption experiment by PAS-IR showed peaks from adsorbed dicarboxylic acids on the α-FeOOH crystals. (Figures 4.31 and 4.32) The pK_a values for the dicarboxylic acids are listed in Table 4.7. The IR results indicate that at pH values where the dicarboxylic acids are protonated in solution, strong adsorption of the acids on α-FeOOH does not occur, and the viscosity of the α-FeOOH suspensions is not affected. At higher pH values where the dicarboxylic acids are deprotonated, adsorption of the dicarboxylic acids on α-FeOOH occurs, and produces the change in surface charge of the crystals which drops the suspension viscosity. This experiment showed that the large drops in suspension viscosity were not due to the presence of the dicarboxylic acids in solution. Adsorption of the acids on α-FeOOH was necessary to affect the viscosity. The change in ionic strength did not contribute to the differences in viscosity values with and without dicarboxylic acids. The two hour mixing time used in this set of experiments was sufficient to allow adsorption of the acids on α-FeOOH. The results of the time of addition study showed that addition of malonic acid later in the oxidation reaction led to changes in growth modification behavior. These adsorption experiments indicate that two hours is sufficient time for adsorption of dicarboxylic acids on α-FeOOH in the pH

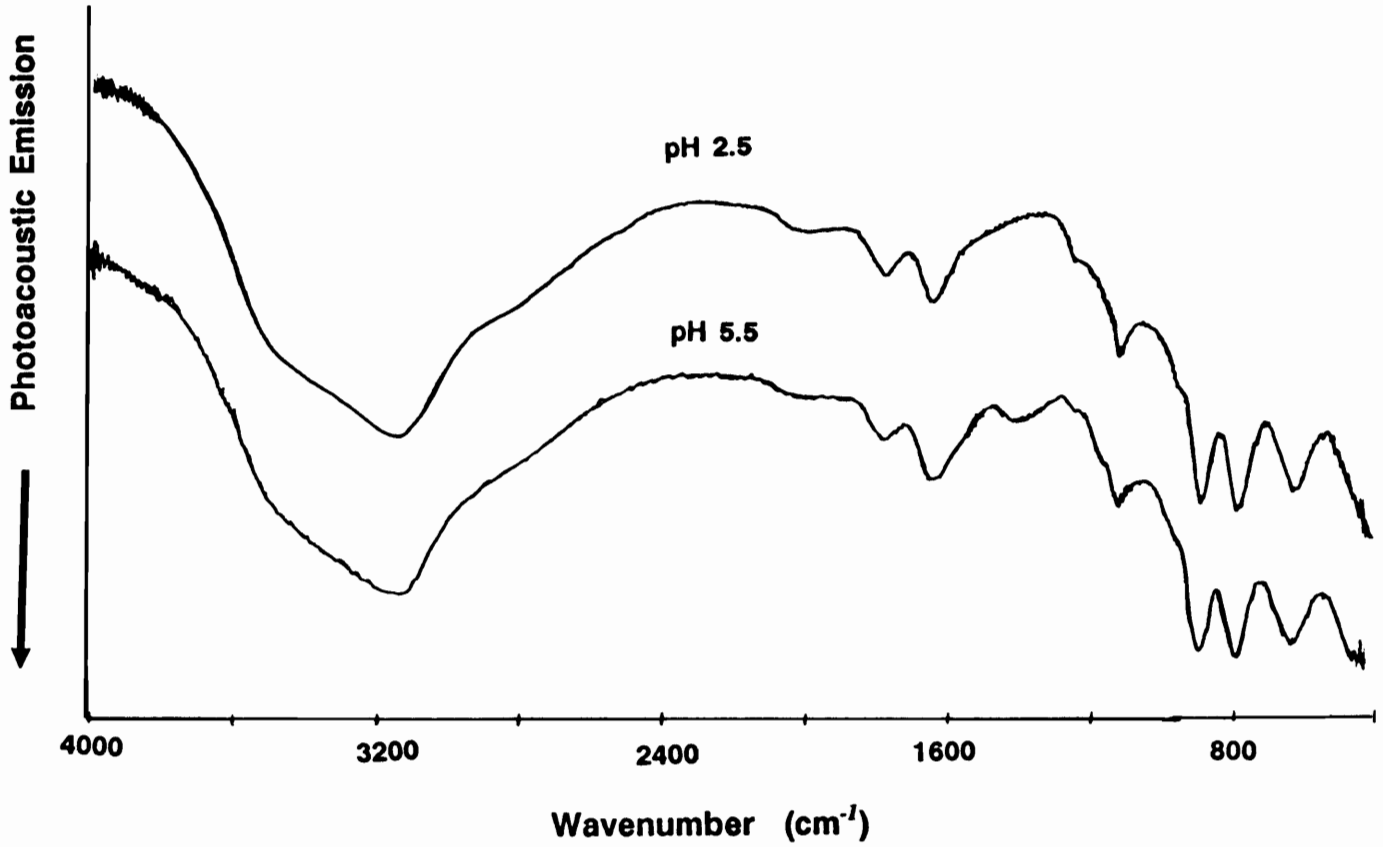

Symmetric carboxyl stretch - 1300 to 1450 cm^{-1}
Asymmetric carboxyl stretch - 1500 to 1700 cm^{-1}

Figure 4.31 PAS-IR Spectra - Adsorption of Malonic Acid on α-FeOOH

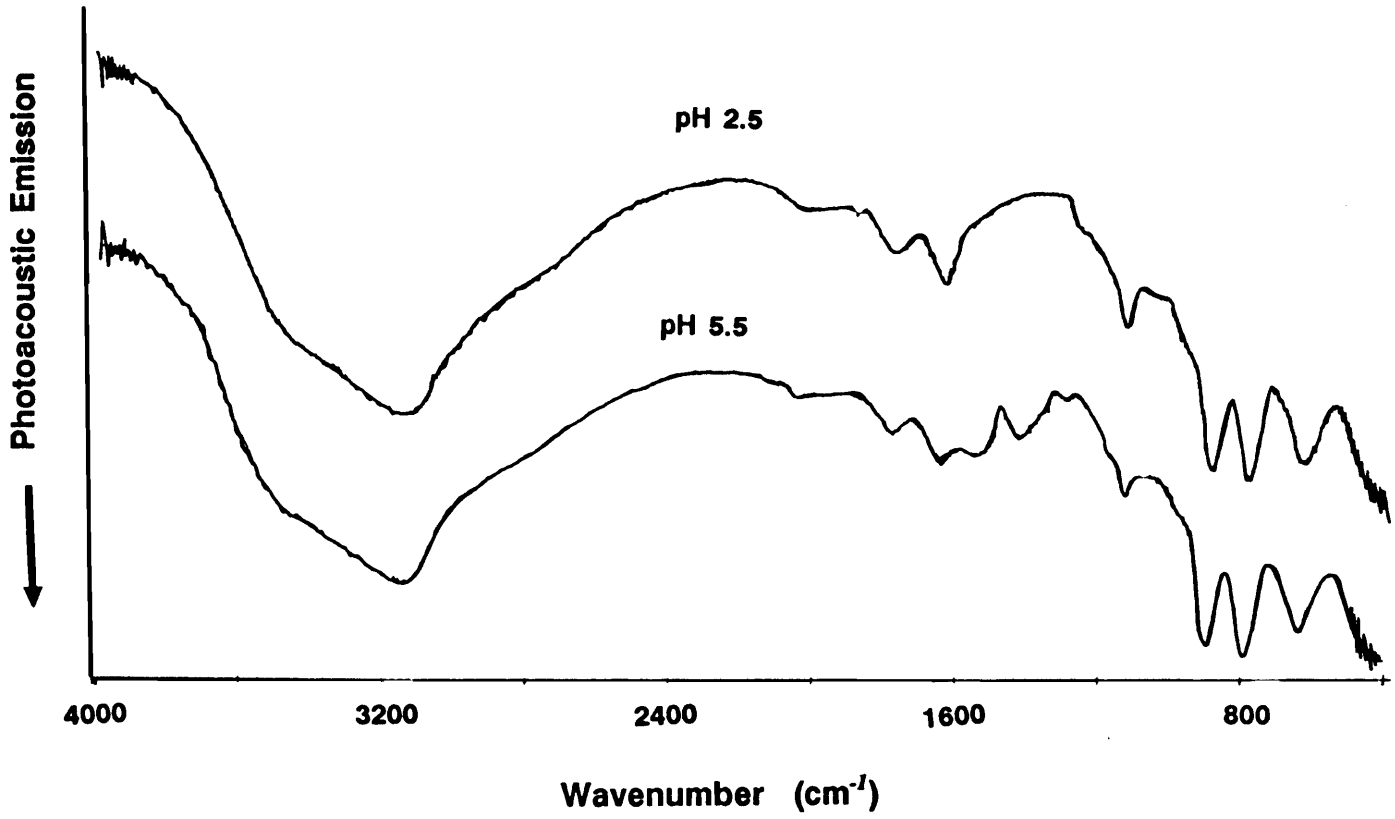

Symmetric carboxyl stretch - 1300 to 1450 cm^{-1}
Asymmetric carboxyl stretch - 1500 to 1700 cm^{-1}

Figure 4.32 PAS-IR Spectra - Adsorption of Succinic Acid on α-FeOOH

Table 4.7 pK_a Values for Dicarboxylic Acids

Dicarboxylic acid	pK_a 1	pK_a 2
oxalic acid	1.23	4.19
malonic acid	2.83	5.69
succinic acid	4.16	5.61
glutaric acid	4.34	5.41
adipic acid	4.41	4.43

*CRC Handbook of Chemistry and Physics; Weast, R., Ed.; CRC Press: West Palm Beach, FL., 1978, p D184

range that exists during oxidation.

The addition of EDTA to an α-FeOOH suspension showed no measurable adsorption of EDTA on the crystals at either pH 2.5 or at pH 5.5. This was surprising, considering the strong coordination between EDTA and metal ions in solution. The strength of the coordination of EDTA to α-FeOOH was confirmed by the desorption experiments using the 100 minute time of addition reaction product. PAS-IR confirmed that EDTA was present in the 100 minute product as was shown in Figure 4.23. Adjustment of the suspension pH down to pH 1.5 with H_2SO_4 did not significantly change the IR spectra of α-FeOOH materials. No evidence for EDTA desorption was found at these pH levels.

G. Intermediate Sampling

Intermediate sampling experiments involved extracting samples from oxidation reactions at different times to determine the identity of any crystalline intermediates that occurred during the formation of FeOOH. The first study compared α-FeOOH growth from $FeSO_4$ and γ-FeOOH grown from $FeCl_2$. The intermediates in these reactions have been examined by Bernal et al. (32). This study allowed a comparison between published data and XRD results obtained from the gelatin suspension method carried out in this investigation. For the reaction containing $FeSO_4$ with no addititves, the 60 minute sample showed strong peaks at 8°, 16°, and 24° 2Θ which correspond to the [00x] reflections of Green Rust II. (Figure 4.33) For a 100 minute sample, the intensity of the same reflections was greatly increased. (Figure 4.34) The intensity of the same three peaks was reduced for a 180 minute sample, and a small peak near the 100% peak of α-FeOOH was evident. This data indicates conversion of the intermediate phase into α-FeOOH crystals. In the XRD peaks for a 300 minute sample, peaks corresponding to Green Rust II were not detected, and only peaks for α-FeOOH remained. The formation of a single intermediate, Green Rust II, was reported by Bernal et al. (32)

In the oxidation reaction of $FeCl_2$, the XRD pattern for the 60 minute sample had peaks at

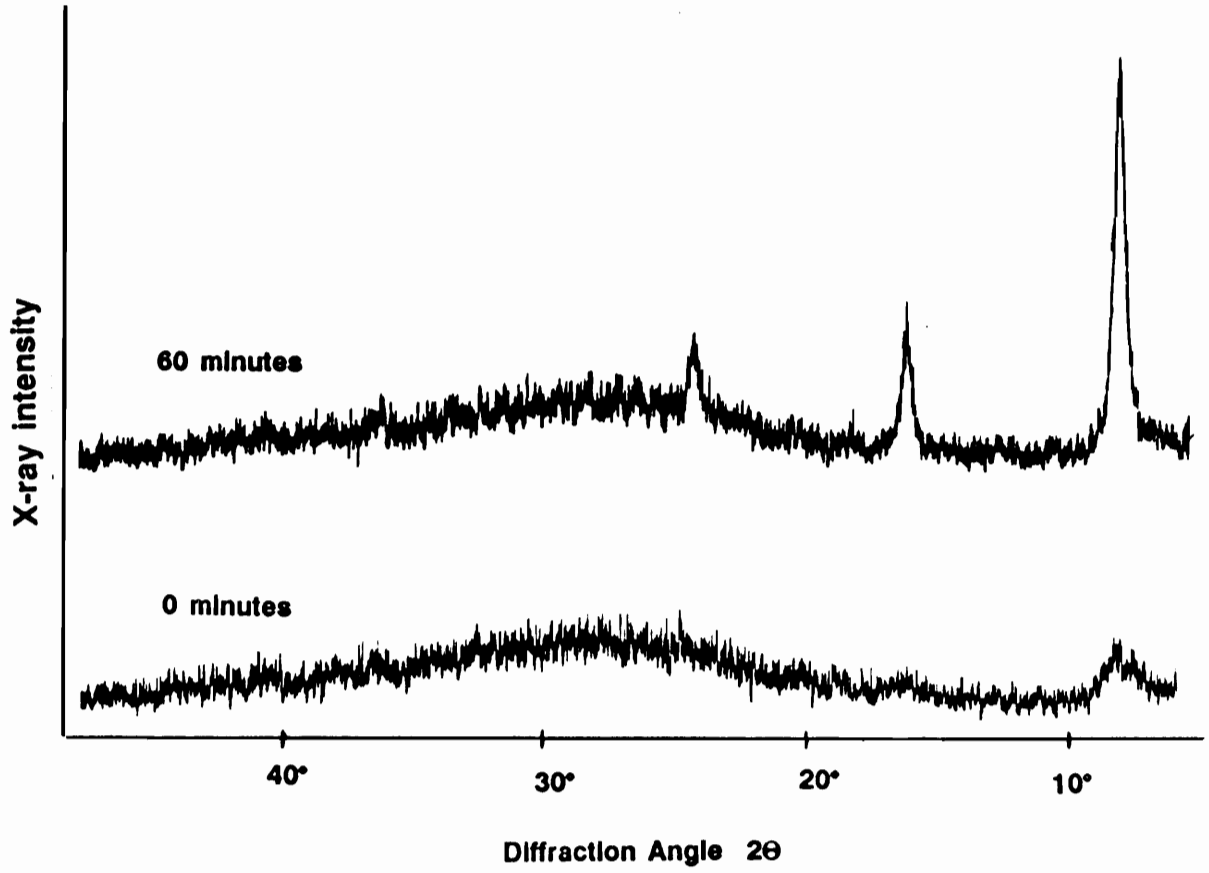

Figure 4.33 XRD Patterns for Intermediate Samples - $FeSO_4$

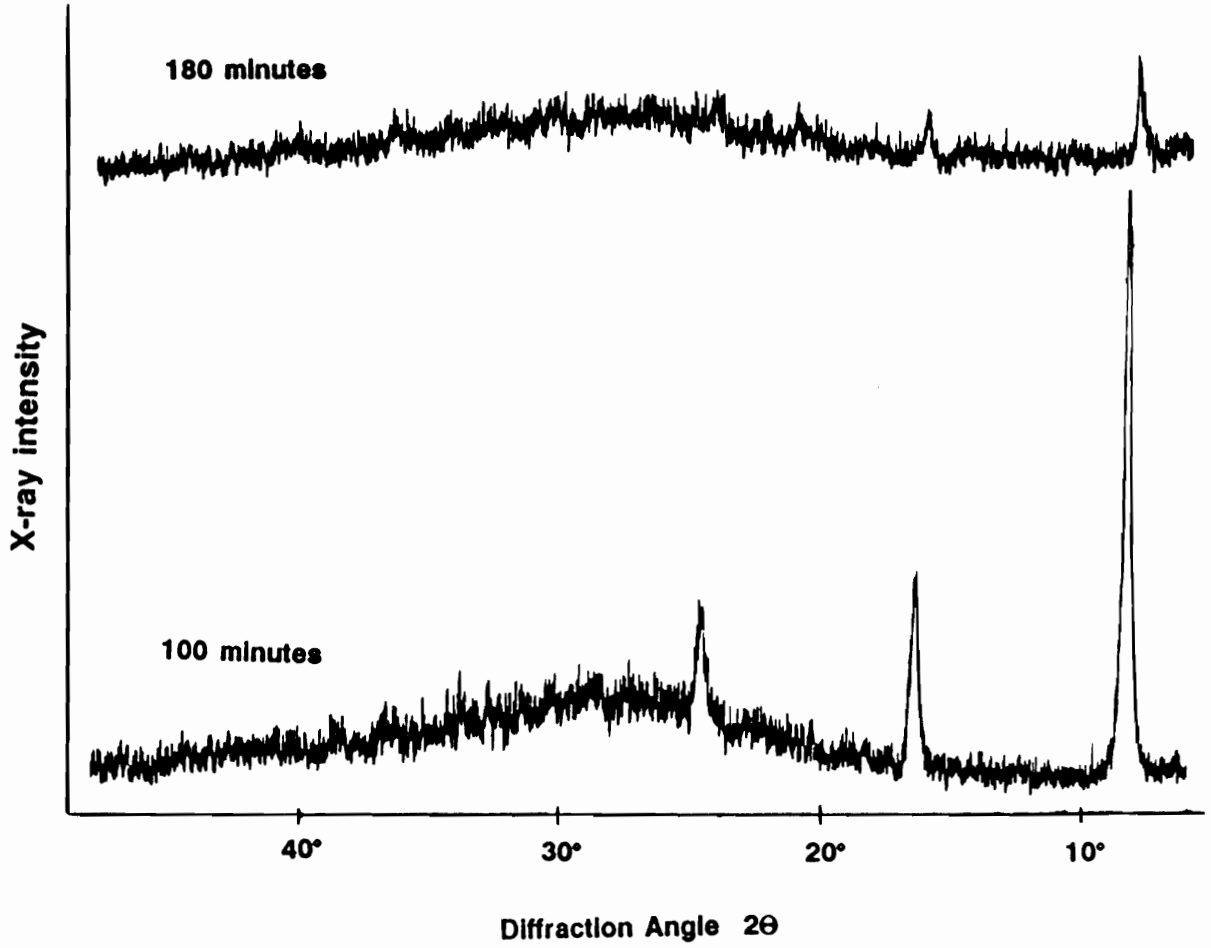

Green Rust II - 8, 16, 24°

Figure 4.34 XRD Patterns for Intermediate Samples - $FeSO_4$

8° and 11.5° indicating a mixture of Green Rust II and Green Rust I in a ratio approximately 1:2. (Figure 4.35) In the 100 minute sample, the ratio of Green Rust II to Green Rust I was approximately 1:1. In the 180 minute sample, no Green Rust I was detected, a small amount of Green Rust II was present, and peaks for γ-FeOOH were evident. This data also agrees with Bernal who found the same two intermediate species during oxidation of $FeCl_2$. His conclusion was that Green Rust I contained mostly Fe^{2+}, and some Fe^{3+}, with hydroxide, water, and chloride ions making up the rest of the composition. As further oxidation occurred, Green Rust I converted to Green Rust II. Green Rust II was thought to be comprised of Fe^{2+} and Fe^{3+}, with a higher Fe^{3+} concentration, and no chloride coordination.

In the oxidation of $FeSO_4$ in the presence of 0.01M EDTA, the XRD pattern for the 60 minute sample showed strong peaks corresponding to the [00x] reflections of Green Rust II, and no evidence of Green Rust I. (Figure 4.36) The XRD pattern for the 100 minute sample contained very strong reflections from the [00x] planes of Green Rust II. Reflections from other planes, either from Green Rust II, or any other intermediate species were not detected. (Figure 4.37) The intensity of the Green Rust II reflections for the 180 minute sample had diminished greatly, and a peak at 14° 2Θ from γ-FeOOH was found. Only reflections from γ-FeOOH were evident in the XRD pattern for the sample collected at 300 minutes. In the XRD patterns containing peaks for Green Rust II in the $FeCl_2$ reaction, and the $FeSO_4$ reactions with and without EDTA, no evidence of any reflections other than the [00x] family were found. In the $FeCl_2$ reaction and the $FeSO_4$ reaction without EDTA, the XRD signal strength may have been insufficient to detect peaks due to other families of reflections. The gelatin support also contributed an amorphous hump to the patterns centered about 30° 2Θ which could hide XRD peaks at higher 2Θ values.

The XRD pattern for the 100 minute sample from the oxidation of $FeSO_4$ containing EDTA was so strong, that the absence of non [00x] family reflections cannot be due to a lack of signal strength. The formation of both γ-FeOOH and α-FeOOH from Green Rust II without any sign of another intermediate phase is at first glance inexplicable. Several mechanisms, however,

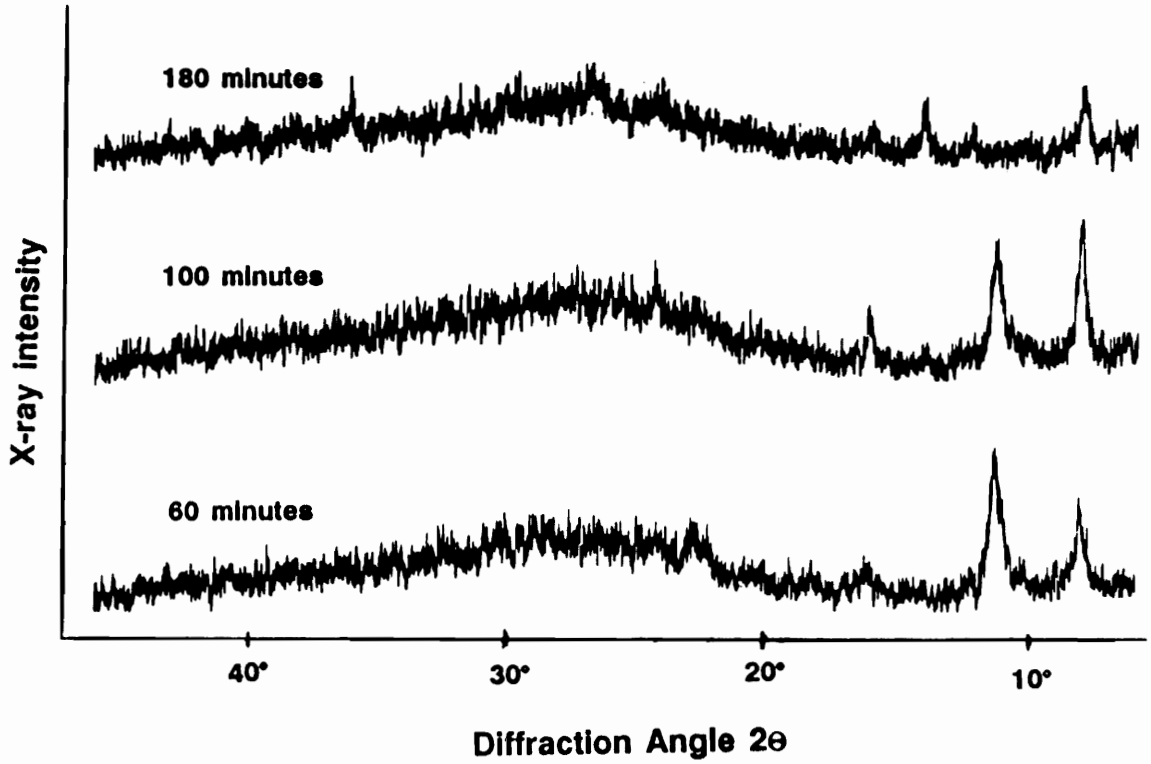

Green Rust I - 11.5°

Green Rust II - 8, 16, 24°

γ-FeOOH - 14, 27, 36°

Figure 4.35 XRD Patterns for Intermediates Samples - $FeCl_2$

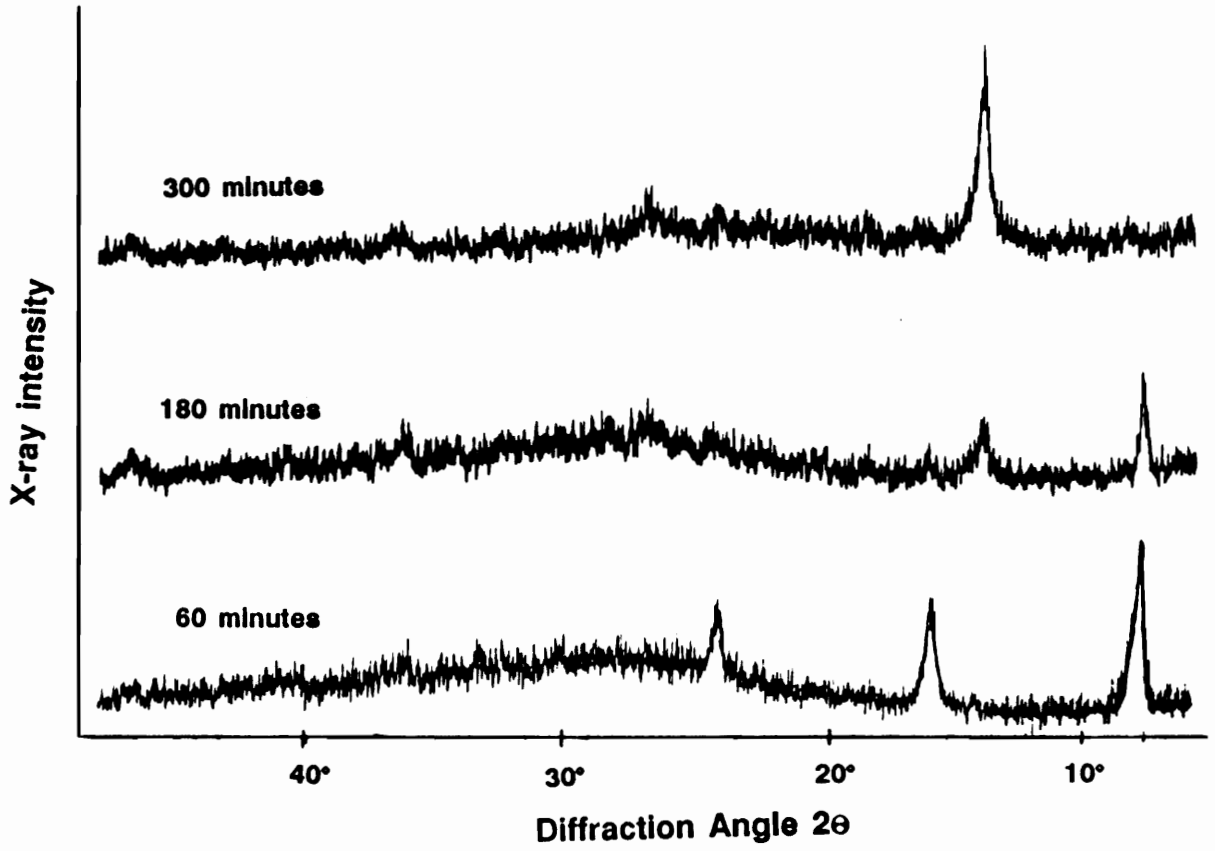

Green Rust II - 8, 16, 24°

γ-FeOOH - 14, 27, 36°

Figure 4.36 XRD Patterns for Intermediates Samples - $FeSO_4$ + EDTA

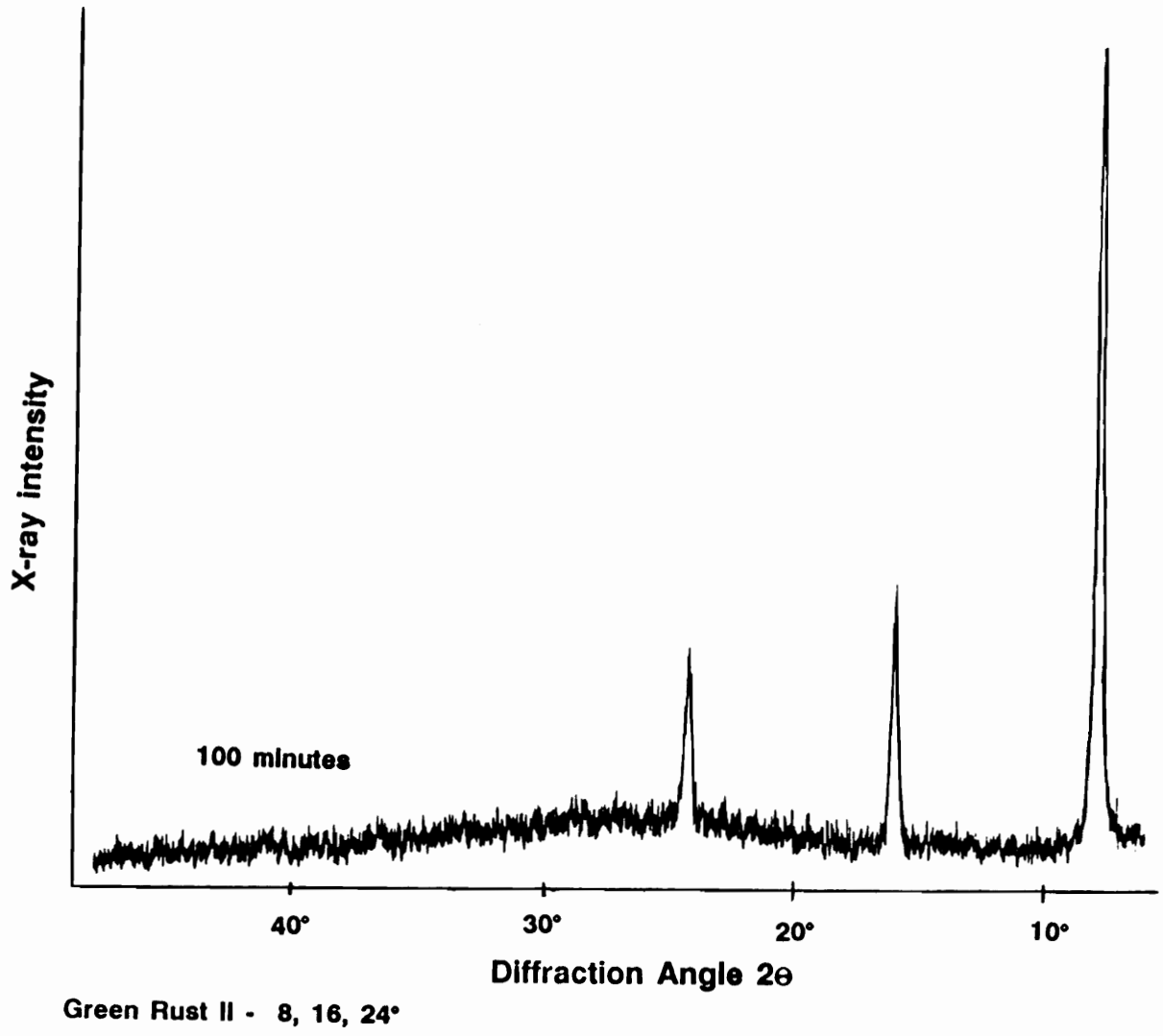

Figure 4.37 XRD Pattern for Intermediate Sample - $FeSO_4$ + EDTA

are possible. Perhaps Green Rust II does not convert directly to FeOOH, but rather passes through an amorphous intermediate that would not be detected by XRD. The amorphous phase would have to be influenced by the presence of EDTA or chloride during the formation of γ-FeOOH or α-FeOOH. Another possibility is that Green Rust II produced during the formation of γ-FeOOH with EDTA and Green Rust II that occurs during the formation of α-FeOOH in the absence of EDTA are not the same phase. γ-FeOOH and α-FeOOH share a common acicular axis. Down to severals hundredths of an angstrom, the organization of the z axis, which corresponds to the [00x] family of planes in Green Rust II, is the same for both γ-FeOOH and α-FeOOH. The absence of [10x] and [01x] type reflections in the intermediates of the Green Rust found in the EDTA reaction may indicate that there is little or no organization of the lattice off the z axis. Differences in the x and y directions due to EDTA adsorption might not be detected if the lattice organization off the z axis is minimal. Therefore it is the conversion of a Green Rust II' containing EDTA that forms γ-FeOOH.

There was no evidence of any FeOOH formation until the intensity of Green Rust II peaks had maximized and begun to diminish. The time dependent behavior of EDTA addition may not be due to nucleation of FeOOH from $Fe(OH)_2$ type species, but rather the conversion of Green Rust II or Green Rust II'. The critical reaction time, after which the addition of EDTA did not lead to γ-FeOOH, may be after Green Rust II was completely formed. If FeOOH formation does not occur until Green Rust II has fully formed and organized, addition of a potential growth modifier before the Green Rust II organization period, could still have an effect on FeOOH morphology, providing the additive reacts with the forming Green Rust II. Addition of the growth modifier after Green Rust II had completely organized might not affect the subsequent conversion of Green Rust to FeOOH. This mechanism would explain why dicarboxylic acids and EDTA act as FeOOH morphology modifiers with time of addition dependence. Placing a dicarboxylic acid into the reaction suspension late in the oxidation does not allow coordination of the acid to the intermediate phase where the morphology modification takes place.

This possible mechanism does not explain how the change in morphology occurs between the intermediate, Green Rust II or Green Rust II', and the additives. The existence of preferential binding sites of dicarboxylic acids may still be the method of action of morphology modification, where the binding sites exist on the intermediate species rather than FeOOH crystals. The size, shape, and position of carboxyl groups of the coordinating molecule might define where the molecule binds to Green Rust, and in binding, inhibit growth of the crystal in certain directions. The presence of EDTA might induce reorganization of iron and oxygen atoms in the intermediate in a way that favors the formation of γ-FeOOH over α-FeOOH.

Another intermediate sampling experiment was carried out with 0.02M phosphate in solution. For samples extracted from this reaction, there was little difference among the XRD patterns for the 60, 100, and 180 minute samples, as shown in Figure 4.38. There were peaks corresponding to Green Rust II, but the peaks were small and broad throughout the oxidation. The product of a 0.02M phosphate reaction was shown to be a combination of tiny amorphous particles and a small number of crystals of γ-FeOOH. The low intensity of the Green Rust II peaks is evidence that the resulting γ-FeOOH crystals grow from Green Rust II, while the amorphous product does not derive from any crystalline intermediate, but is amorphous throughout the oxidation. The mechanism of phosphate's action to produce amorphous material, and induce the growth of γ-FeOOH from $FeSO_4$ is not evident. This may be due to coordination of phosphate to iron species in solution preventing crystal nucleation. The small amount of Green Rust II that is formed is somehow altered by phosphate to form γ-FeOOH.

II. Fe_3O_4

A. $FeSO_4$

The formation of Fe_3O_4 from $FeSO_4$ requires oxidation of two thirds of the starting Fe^{2+} to Fe^{3+}. This part of the Fe_3O_4 study was designed to investigate the oxidation process as it affected the morphology of Fe_3O_4 crystals. The variables investigated were the oxidation source

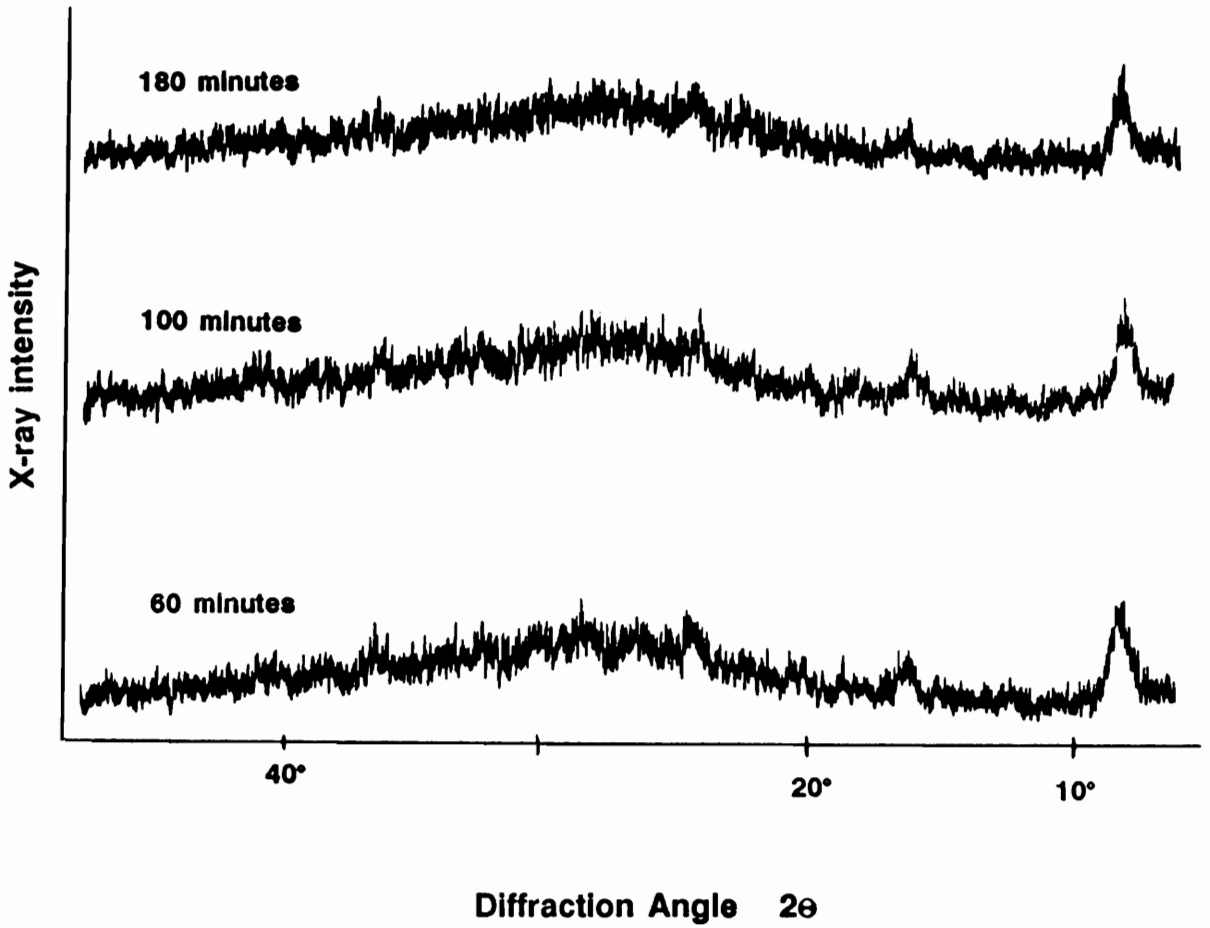

Figure 4.38 XRD patterns for Intermediate Samples - $FeSO_4$ + Phosphate

and rate, hydroxide concentration, and the effect of metal ion other than Fe on the morphology and characteristics of the resulting Fe_3O_4.

The two methods of oxidation were the controlled flow of oxygen into the reaction vessel, and the diffusion of room air through the open reflux condenser. The diffusion method of oxidation was less controlled than the use of pure oxygen through a flow meter, but allowed the study of slower oxidation rates. Under these conditions however, the diffusion of room air through the reflux condensor turned out to be insufficient to carry out the necessary oxidation of Fe^{2+} to allow a 20 hour reaction time with no initial Fe^{3+} concentration. Oxygen bubbling through the reaction did convert the necessary amount of Fe^{2+} to Fe^{3+} when flow rates greater than 0.4 cm^3/sec were used. The efficiency of oxygen uptake was dependent upon hydroxide concentration. Using 1.8 equivalents of NaOH for every equivalent of Fe^{2+}, an oxygen flow rate of 0.2 cm^3/sec was necessary to convert two thirds of the Fe^{2+} to Fe^{3+} in 20 hours. With 4 equivalents of NaOH for every equivalent of Fe^{2+}, a 0.4 cm^3/sec of oxygen flow rate was required to carry out the same oxidation. The lowest oxygen flow rates, estimated at 0.05 cm^3/sec, would have been sufficient to oxidize Fe^{2+} to Fe^{3+} if oxygen use was 100% efficient. The reason for the difference in oxygen use as a function of the hydroxide concentration is not known. The predominant species of iron at different pHs may be one variable in the use of oxygen.

The investigation of hydroxide content on Fe_3O_4 morphology showed that while oxidation occurred faster at hydroxide to Fe^{2+} ratios of approximately 2:1, the size of the particles was quite small, only approximately 0.25 μ in width. (Figure 4.39) This material had a surface area of approximately 9 m^2/g. The Fe_3O_4 crystals were octahedral in shape. At higher hydroxide Fe^{2+} ratios of up to 4:1, the surface area decreased to approximately 3 m^2/g, and the average particle width was 1 μ. The larger particles were also octahedral.

The formation of crystals from a suspension is based on two processes which are in competition, crystal nucleation and crystal growth. With a fixed concentration of iron, production

a) $OH^-:Fe^{2+}$ = 3.5:1

24,000X

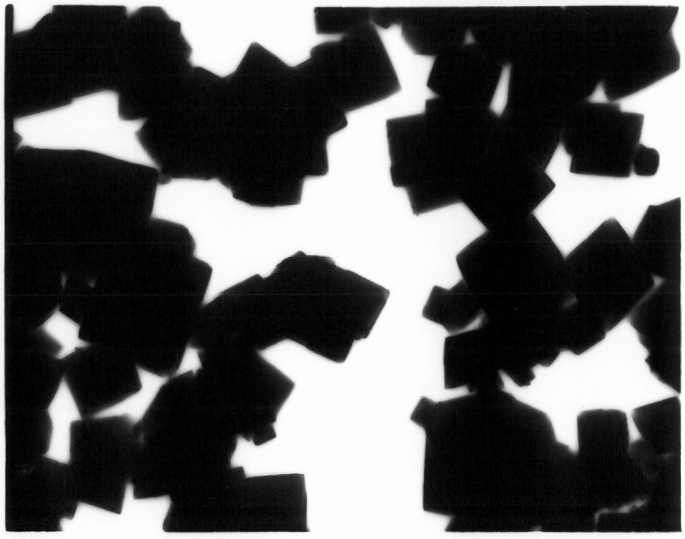

b) $OH^-:Fe^{2+}$ = 2:1

Figure 4.39 TEM Micrographs of Fe_3O_4 with Different $OH^-:Fe^{2+}$ Ratios

of larger crystals at higher hydroxide content must be due either to a reduction in nucleation rate, or an increase in crystal growth rate. Intermediate samples were extracted from a reaction using $FeSO_4$ and 3.5 equivalents of NaOH per equivalent of Fe^{2+}. The XRD pattern for the sample extracted after 60 minutes of oxidation shows only peaks corresponding to crystalline $Fe(OH)_2$. (Figure 4.40) The XRD patterns for the 180 and 300 minute samples show peaks appearing for Fe_3O_4, and the peaks due to $Fe(OH)_2$ diminishing over time. Intermediate samples were also extracted from a reaction containing $FeSO_4$ with 2 equivalents of NaOH per equivalent of Fe^{2+}. The XRD pattern for the 60 minute sample from this reaction shows peaks due to Green Rust II, crystalline $Fe(OH)_2$, Fe_3O_4, and an unidentified phase. (Figure 4.41) The XRD pattern for the 180 minute sample shows peaks due to Fe_3O_4, and a small amount of Green Rust II. The formation of Green Rust II and the unidentified phase indicate that a second mechanism of Fe_3O_4 formation may be occurring at lower hydroxide concentrations. The production of pure crystalline $Fe(OH)_2$ at high hydroxide concentrations led to single crystals of Fe_3O_4 with high uniformity of size and shape. At lower hydroxide concentrations, the presence of multiple iron hydrous oxide species led to secondary nucleation and smaller particles with a broader size distribution.

Evidently the consumption of oxygen by Green Rust II and other species was faster than the consumption of oxygen by crystalline $Fe(OH)_2$. Lower oxygen flow rates were required at lower hydroxide concentration to carry out the total conversion to Fe_3O_4 in 20 hours. Crystalline $Fe(OH)_2$ may be more stable with respect to oxidation than Green Rust II.

The introduction of metal ions other than iron into the ferrite structure was examined to determine how these ions affected particle size and shape. The use of mixed metal ferrites is common for the production of electronic materials such as $BaFe_2O_4$ (78). The surface area results for Fe_3O_4 grown with various amounts of metal additives are listed in Table 4.8. The addition of Zn^{2+} from 20 to 1 mole %, relative to Fe^{2+} in Fe_3O_4, does not produce a recognizable trend in the surface area data. All products containing Zn^{2+} had surface areas

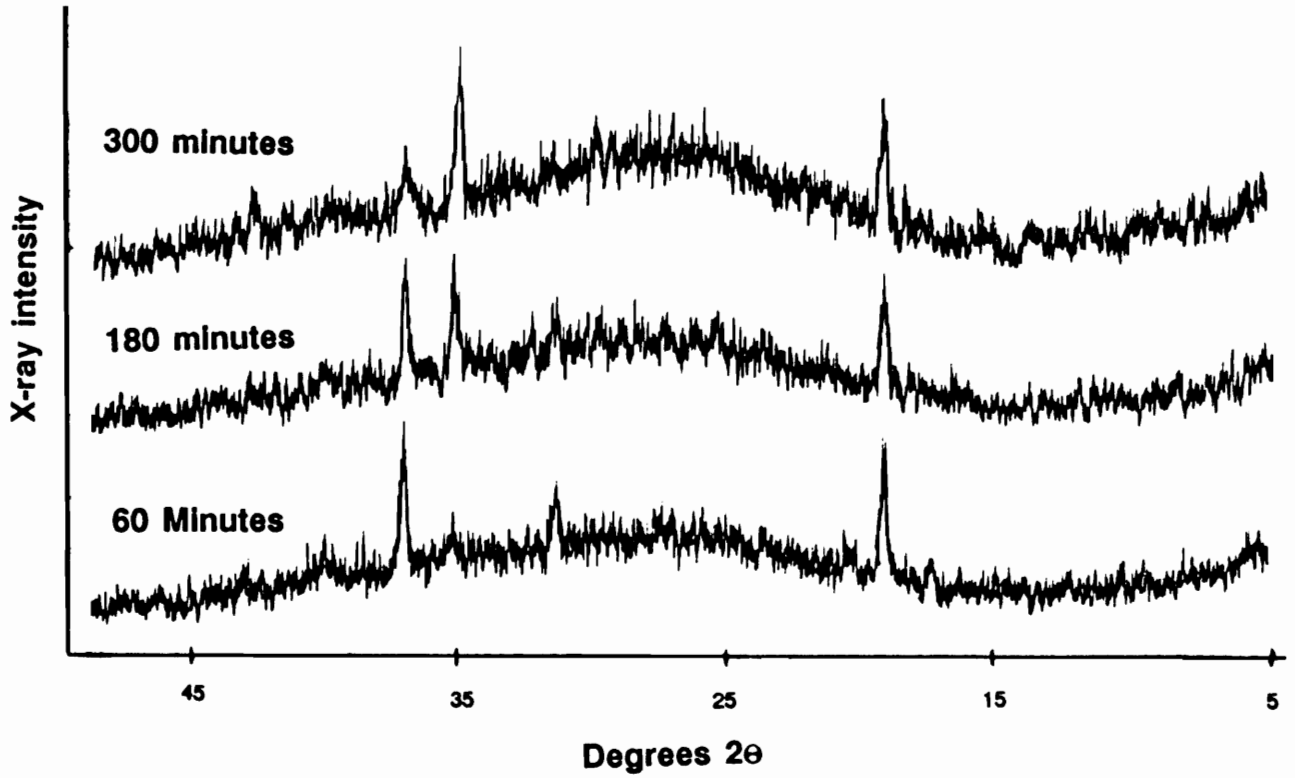

Fe_3O_4 - 35, 30, 43°

$Fe(OH)_2$ - 19.5, 37°

Figure 4.40 XRD Patterns for Intermediates - $FeSO_4$ + 3.5 NaOH

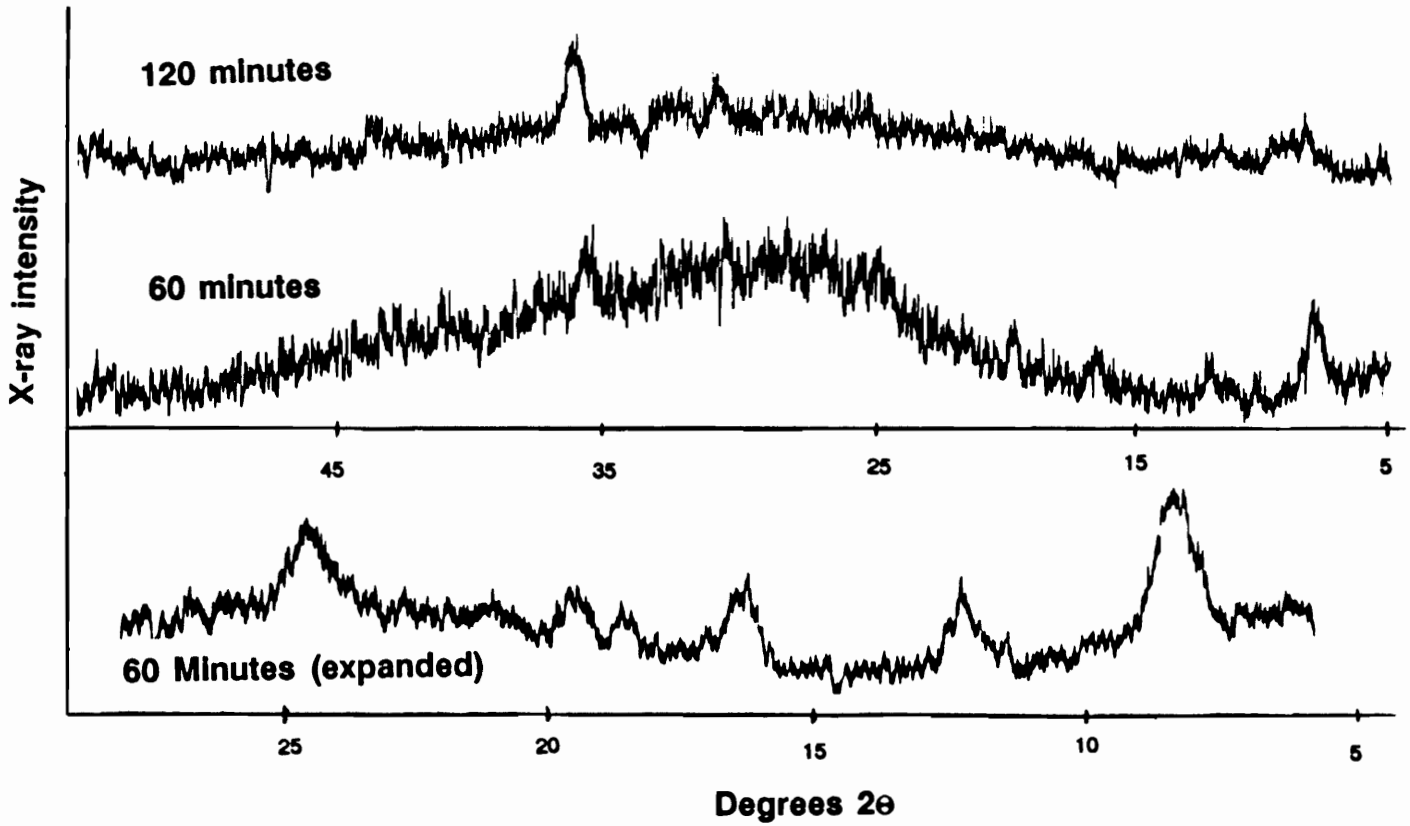

Green Rust II - 8, 24, 16°

Fe_3O_4 - 35, 30, 43°

$Fe(OH)_2$ - 19.5°

Unknown - 12.4, 18.5°

Figure 4.41 XRD Patterns for Intermediates - $FeSO_4$ + 2 NaOH

Table 4.8 Surface Areas for Fe_3O_4 Containing Metal ions

BET values in m^2/g

*	**	Zn^{2+}	Mn^{2+}	Ni^{2+}	Mg^{2+}	Ca^{2+}	Cu^{2+}
20%	6.7%	5.9	4.5	25.8	-	-	19.8
10%	3.3%	4.0	5.1	-	20.3	-	-
5%	1.7%	7.0	6.6	40.2	4.4	7.6	8.1
1%	0.3%	2.8	4.7	-	3.4	-	-

* Metal ion mole % relative to Fe^{2+} in Fe_3O_4 product

** Metal ion mole % relative to Fe^{2+} in initial $FeSO_4$

of 7 m^2/g or less, and were intensely black in color. The Zn^{2+} product suspension settled very quickly over a permanent magnet.

The results for Mn^{2+} were similar to the results for Zn^{2+} with regard to surface area, color and settling behavior. The products containing Ni^{2+} were grayish in color, had poor settling characteristics, and large surface areas. The addition of 10% Mg^{2+} gave a grayish material with a surface area of 20 m^2/g. Addition of 5% and 1% Mg^{2+} gave black magnetic products with low surface areas. The low solubility of Ca^{2+} limited the addition to 5% relative to Fe^{2+}. The 5% Ca^{2+} addition gave a black product which settled well, and had a surface area of 7.6 m^2/g. The 20% Cu^{2+} product was grayish while the 5% product was black; the latter material settled well, and had a surface area of 8.1 m^2/g.

The micrographs of Fe_3O_4 grown with Zn^{2+} show that the surface area values depend on two factors, the average particle size, and the particle size distribution. (Figure 4.42) The 20% Zn^{2+} crystals are octahedral in shape with a high uniformity in size and shape, and a mean particle width of 0.25μ. Addition of 10% Zn^{2+} gave crystals with a particle width of 0.5μ also with a high uniformity. The 5% Zn^{2+} material had a broad particle size distribution with the largest particles approximately 1.0μ in width. Also evident in the 5% Zn^{2+} product were small particles adhering to the surface of the larger crystals. The 1% Zn^{2+} product also showed evidence of smaller particles adhering to larger Fe_3O_4 crystals.

The addition of 10% Mn^{2+} produced crystals up to 1μ in width with some smaller adhering crystals. (Figure 4.43) The 5% Mn^{2+} product may have slightly more adhering crystals than the 10% Mn^{2+}, and the 1% Mn^{2+} product had slightly fewer adhering crystlas. The larger particles for 5% and 10% Mn^{2+} products were approximately 0.75μ in width.

The 5% Mg^{2+} product contained large crystals with a width of 0.5μ, with some adhering crystals. (Figure 4.44) The products of the 5% Ca^{2+} and 5% Cu^{2+} reactions were very similar in that the particles showed high uniformity in size and shape, with little evidence of smaller adhering crystals, and an average particle width of 0.25μ.

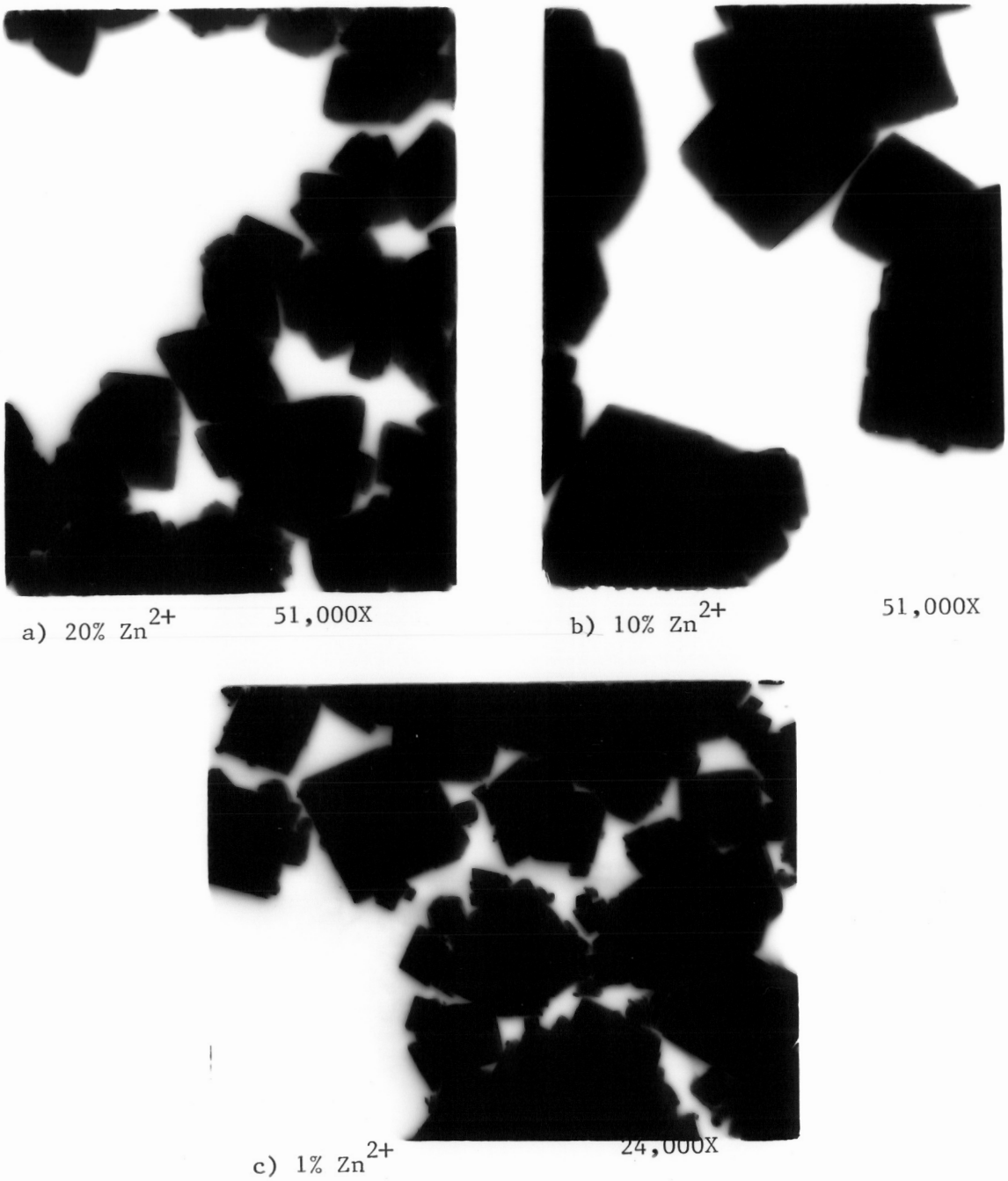

Figure 4.42 TEM Micrographs of Fe_3O_4 Containing Zn^{2+}

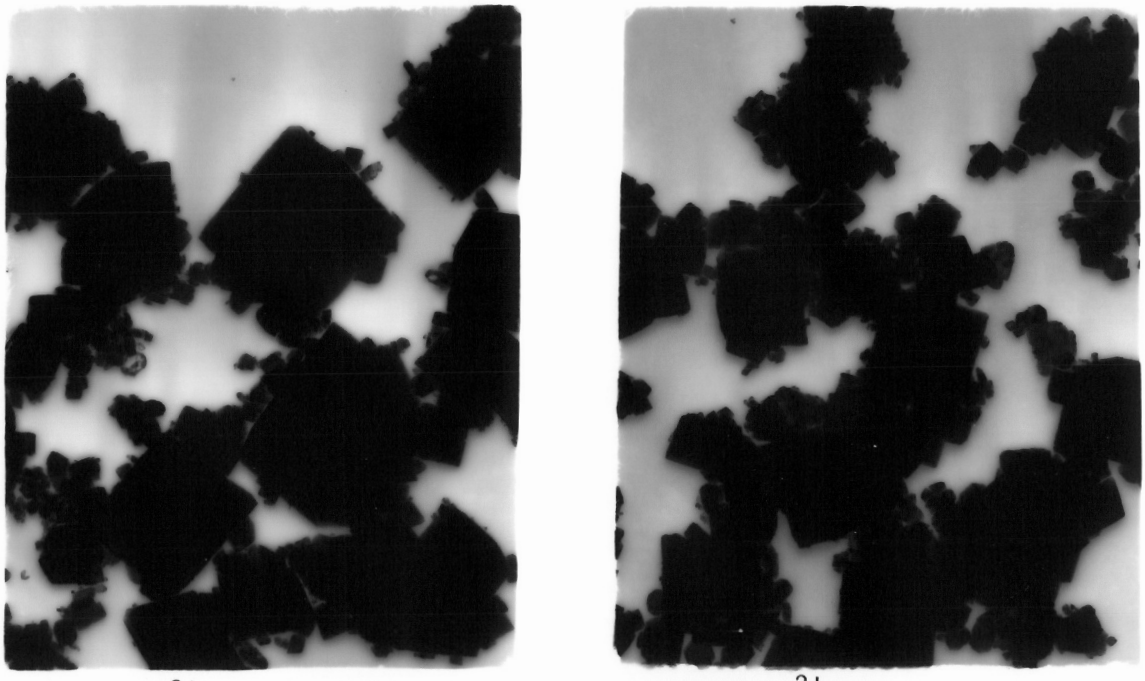

a) 10% Mn^{2+}

b) 5% Mn^{2+}

24,000X

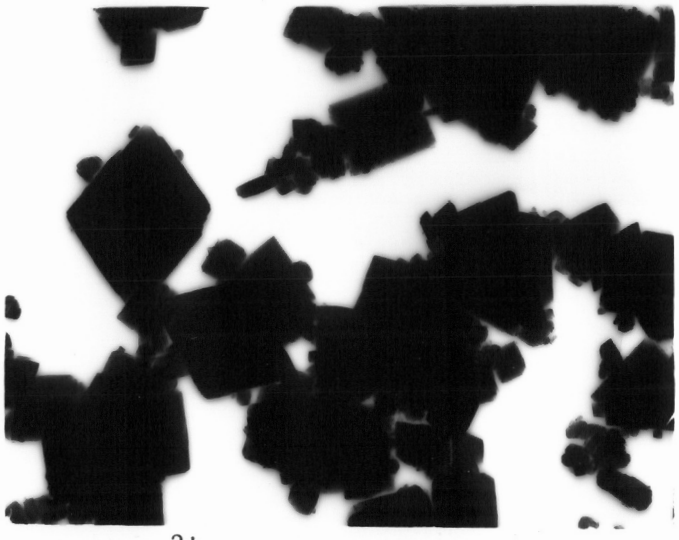

c) 1% Mn^{2+}

Figure 4.43 TEM Micrographs of Fe_3O_4 Containing Mn^{2+}

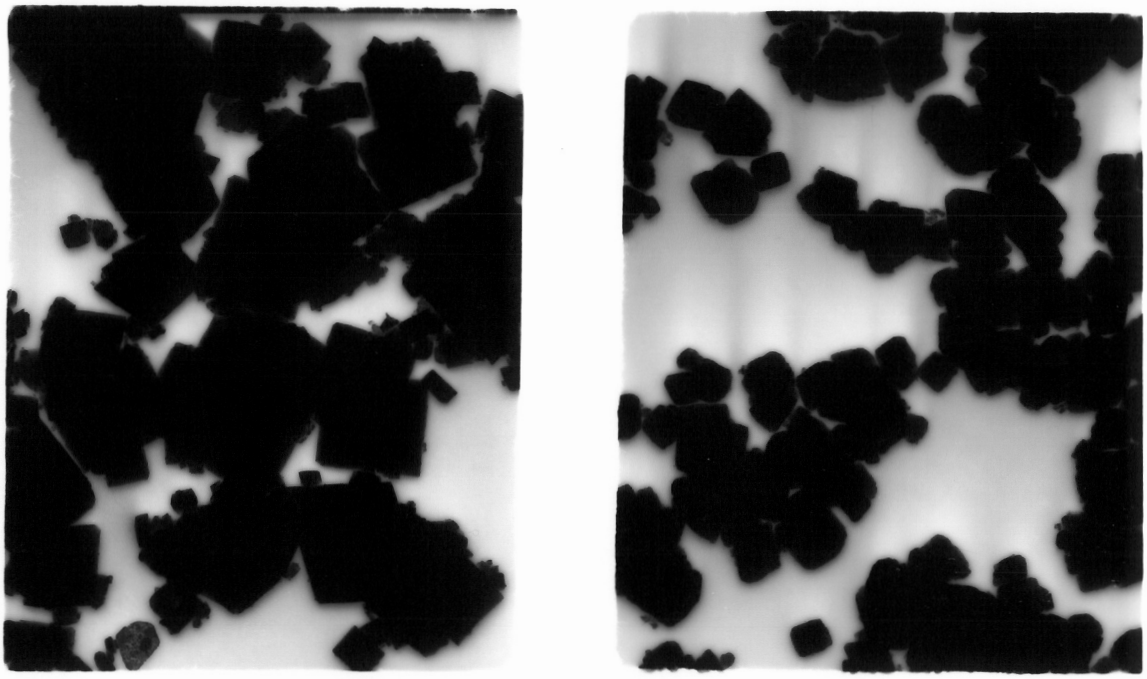

a) 5% Mg^{2+}

b) 5% Ca^{2+}

24,000X

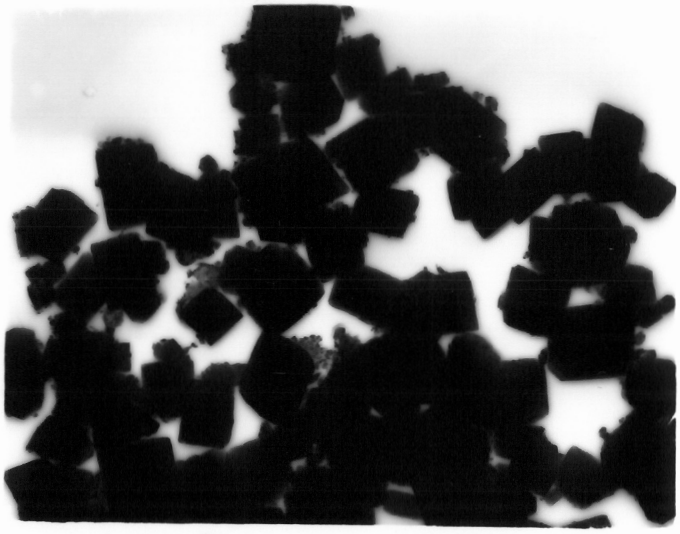

c) 5% Cu^{2+}

Figure 4.44 TEM Micrographs of Fe_3O_4 Containing Mg^{2+},Ca^{2+}, and Cu^{2+}

These TEM and surface area results of the influence of metal ions on Fe_3O_4 particle morphology show that all +2 metal ions do not behave similarly with regard to ferrite formation. Zn^{2+} and Mn^{2+} affect ferrite formation similarly as far as particle size and uniformity are concerned. At up to 20% incorporation of Zn^{2+} and Mn^{2+}, the Fe_3O_4 crystals have quite low surface areas. The formation of smaller adhering crystals during certain additions may be a function of the reaction conditions. A single hydroxide to Fe^{2+} ratio of 3:1 was used for all the metal ion addition reactions. The sensitivity of Fe_3O_4 crystal growth to hydroxide concentration has already been shown. By adding metal ions which potentially could behave differently during nucleation, the hydroxide to metal ion ratio of 3:1 might not be optimal with regard to growing large single crystals for all the different metal additions. The surface area data and the TEM photos indicated that metal ions do not all behave the same in ferrite formation. Ni^{2+} did not form ferrite material well at any concentration, while Mg^{2+} gave large crystals at lower concentrations and smaller crystals at higher concentrations. Some ions may be more efficient in nuclei formation than other metal ions, even Fe^{2+}. Zn^{2+} may combine with Fe^{3+} with Fe^{3+} ions as they are produced, faster than Fe^{2+} ions combine with Fe^{3+}. While no quantitative oxidation rate studies were carried out, visual observations showed that the suspension turned black faster when Zn^{2+} or Mn^{2+} were in the reaction than for an oxidation carried out with only Fe^{2+}. If Zn^{2+} ions are involved with Fe_3O_4 nuclei formation, this would explain the existence of a larger particle size distribution at lower Zn^{2+} concentrations, when nuclei with and without Zn^{2+} may be produced, compared to higher Zn^{2+} concentrations, in which only nuclei containing Zn^{2+} may be formed.

B. α-FeOOH + $FeSO_4$

The use of crystalline Fe^{3+} reagents such as α-FeOOH in the growth of Fe_3O_4 changes the mechanism of crystal growth to one involving recrystallization. α-FeOOH crystals supply nucleation sites, in addition to being a source of Fe^{3+}. Using two equivalents of α-FeOOH as

the source of Fe^{3+}, 1.1 equivalents of $FeSO_4$, and 2 equivalents of NaOH, the Fe_3O_4 crystals had a surface area of 4.3 m^2/g and a diameter of approximately 0.4μ. These particles shown in Figure 4.45 are roughly spherical, rather than the octahedral crystals grown form pure $FeSO_4$. The diameter of the crystals is also roughly equivalent to the long axis of the precursor α-FeOOH. XRD patterns of samples extracted from an α-FeOOH and $FeSO_4$ reaction shows the formation of Green Rust II after NaOH addition. (Figure 4.46) After the reaction mixture was heated to 90°C, the peaks due to Green Rust II increased in size, and the peaks for α-FeOOH were sharper. Since no oxidation had occurred at this point in the reaction, any Fe^{3+} in Green Rust II came from α-FeOOH. Following 120 minutes of oxidation, the XRD pattern of the extracted sample showed strong peaks for Fe_3O_4 and α-FeOOH. No peaks for Green Rust II were detected. Presumably the formation of Fe_3O_4 occurs by the precitation of $Fe(OH)_2$ on the surface of α-FeOOH crystals. Amorphous $Fe(OH)_2$ reacts with the surface of α-FeOOH to form Green Rust II which converts to Fe_3O_4 during the course of the reaction. The increase in α-FeOOH peak sharpness upon heating may be due to some recrystallization that occurs at 90°C.

Reducing the amount of Fe^{3+} in at the start of the reaction so that the initial Fe^{3+} to Fe^{2+} ratio is 1:1 complicates the growth of Fe_3O_4 from a process in which the reagents are just chemically combined, to a growth which involves oxidation of excess Fe^{2+}. In the series of reactions in which all reagents were placed into suspension at the beginning of the reaction, each variable changed during the oxidation process led to different characteristics in Fe_3O_4 crystals. Carrying out the reaction at 97°C produced some red color in the product. This red material was identified as amorphous or tiny crystals of Fe_3O_4. Lowering the reaction temperature to 90°C produced less red color in the product. Using a hydroxide to Fe^{2+} ratio of 2:1 produced Fe_3O_4 with a surface area averaging 15 m^2/g. Reducing the hydroxide to Fe^{2+} ratio to 1.8:1 gave a material which contained no red color if the oxidation was carried out using the diffusion of room air. When 0.12 cm^3/sec O_2 was flowed through the reactor vessel, the product was gelatinous and had significant red color when dried. Increasing the hydroxide

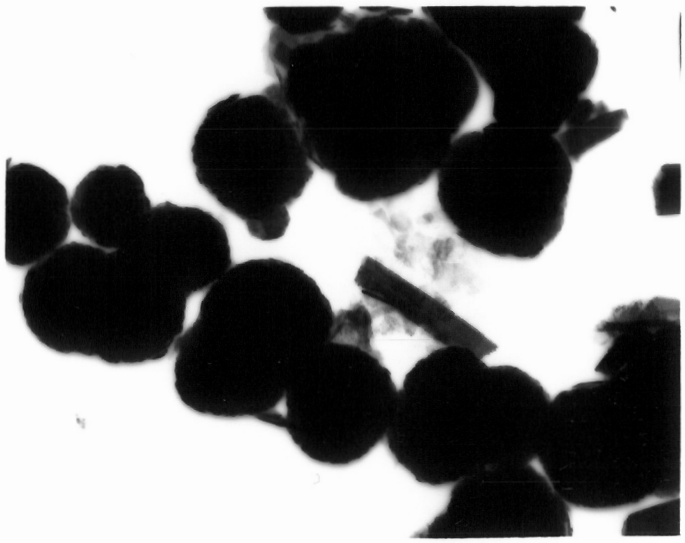

-FeOOH
crystal

51,000X

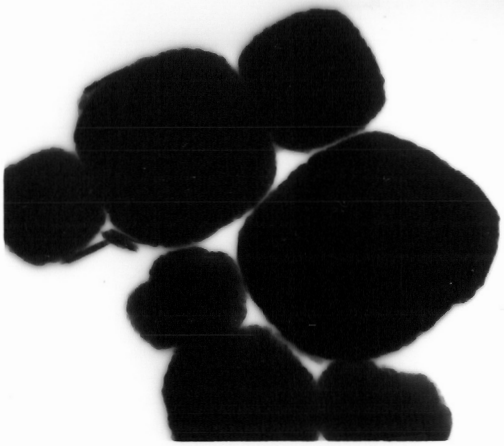

Figure 4.45 TEM Micrograph of Fe_3O_4 from α-FeOOH + $FeSO_4$

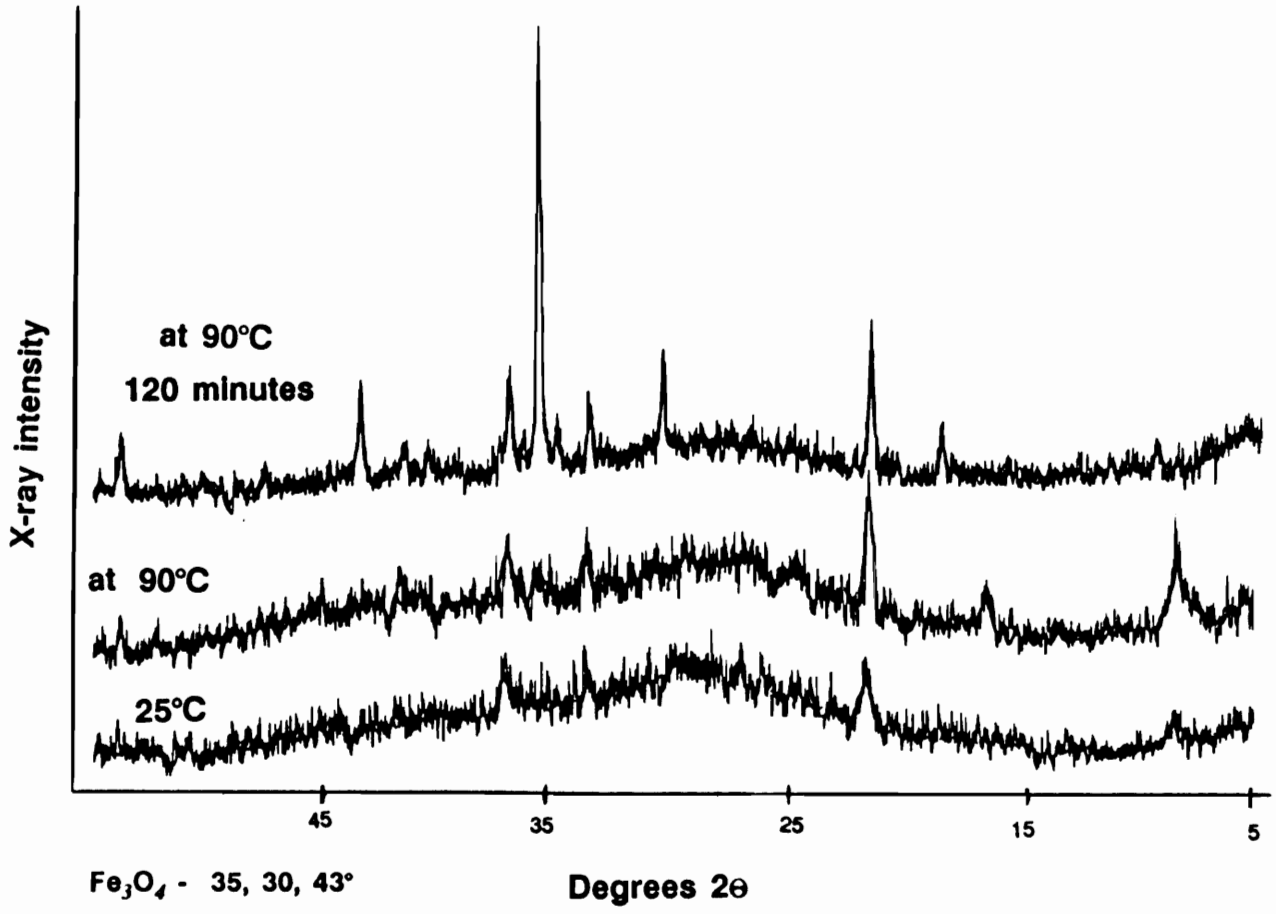

Figure 4.46 XRD Patterns for Intermediates - $FeSO_4$ + α-FeOOH + 2.2 NaOH

to Fe^{2+} ratio to 4 lowered the surface area of the product to 6.0 m^2/g, but there was some yellow color in the material indicating that some α-FeOOH remained unconverted. Reducing the hydroxide to Fe^{2+} ratio to 3, and using slow diffusion of air, the Fe_3O_4 product had a surface area of 5.4 m^2/g, and no sign of red amorphous material or any unconverted α-FeOOH.

The control of nucleation and growth is very complicated using α-FeOOH and $FeSO_4$ as the starting reagents for the preparation of Fe_3O_4. There are some similarities between preparation of Fe_3O_4 from α-FeOOH and $FeSO_4$, and Fe_3O_4 prepared from $FeSO_4$ alone. At lower hydroxide concentrations, the oxidation rate of Fe^{2+} is faster than in reactions containing higher concentration of hydroxide. Reducing the reaction temperature to 90°C appears to slow nucleation. The slow diffusion of room air also favors growth over nucleation when compared to high oxygen flows.

The sensitivity of α-FeOOH conversion to Fe_3O_4 on hydroxide concentration was also evident. At a hydroxide to Fe^{2+} ratio of 4:1, some α-FeOOH remained unconverted to Fe_3O_4 even though there was excess Fe^{2+}. At these high concentrations of hydroxide, crystalline $Fe(OH)_2$ may form new nuclei rather than react with α-FeOOH to form Fe_3O_4. Intermediate sampling during the $FeSO_4$ reactions showed formation of crystalline $Fe(OH)_2$ at high hydroxide concentrations, and Green Rust II at lower hydroxide concentrations. Amorphous $Fe(OH)_2$ reacts to form Green Rust II on the surface of α-FeOOH. It would seem likely that any additional Green Rust II formed would precipitate on α-FeOOH. The high hydroxide concentrations inhibit the formation of Green Rust II, and promote the formation of crystalline $Fe(OH)_2$ which does not react with the α-FeOOH surface.

The experiments termed 'seed and growth' in the experimental chapter used multiple steps in reagent addition. Seed crystals were produced, and then growth of the seeds was attempted. In these reactions the total Fe^{3+} to Fe^{2+} ratio of the starting materials was 1:1. The seeds with the best characteristics were produced using 2 equivalents of α-FeOOH, 1.1 equivalent of $FeSO_4$, and 1.9 equivalents of NaOH. Using less or more NaOH duplicated the

results discussed above with the production of red amorphous material, or unconverted α-FeOOH. Having produced the seeds, additional Fe^{2+} and NaOH were added in the attempt to grow larger crystals. Using a hydroxide to Fe^{2+} ratio of 2:1 during the growth step gave Fe_3O_4 with the lowest surface area, 9.4 m^2/g. This value is significantly higher than the best value obtained (5.4 m^2/g) using the one step growth process; α-FeOOH and $FeSO_4$ at 1:1 Increasing the aging time of the seeds from 5 hours to 24 hours had no effect on the size of Fe_3O_4 crystals. Apparently the 'growth' step did not increase the size of the seed crystals, but rather nucleated addition Fe_3O_4 crystals. The precipitation of $Fe(OH)_2$ onto the surface of Fe_3O_4 may not be favored under these conditions, and the seed crystals do not provide nucleation sites for further growth. The electrostatic attraction between Fe_3O_4 particles and iron hydroxide species may be small if the charge on Fe_3O_4 at high pH is negative, and the iron hydroxides are also negatively charged.

C. Fe^{3+} + $FeSO_4$

When NaOH is added to the solution of $FeSO_4$ and $Fe_2(SO_4)_3$ the mixture immediately turns very dark. The finely divided black precipitate is magnetic, indicating that the formation of some Fe_3O_4 is instantaneous. XRD patterns of intermediate samples extracted from a reaction containing $Fe_2(SO_4)_3$ and $FeSO_4$ show that initially Green Rust II and Fe_3O_4 are precipitated when NaOH is added to the Fe solution at room temperature. (Figure 4.47) After the mixture was heated to 90°C, but before any oxidation had occurred, no peaks due to Green Rust II were detected. The peaks corresponding to Fe_3O_4 had increased in size. Following 120 minutes of oxidation, the peaks due to Fe_3O_4 are sharper. The surface area results shown in Figure 4.48 demonstrate that immediate precipitation of Fe_3O_4 limits the size of the particles. Such a large number of nuclei was formed initially that vey little subsequent growth of the nuclei occurred. It is not clear from the XRD patterns of the intermediate species whether Green Rust II precipitated at room temperature contributes to crystal growth on Fe_3O_4 seeds, or nucleates

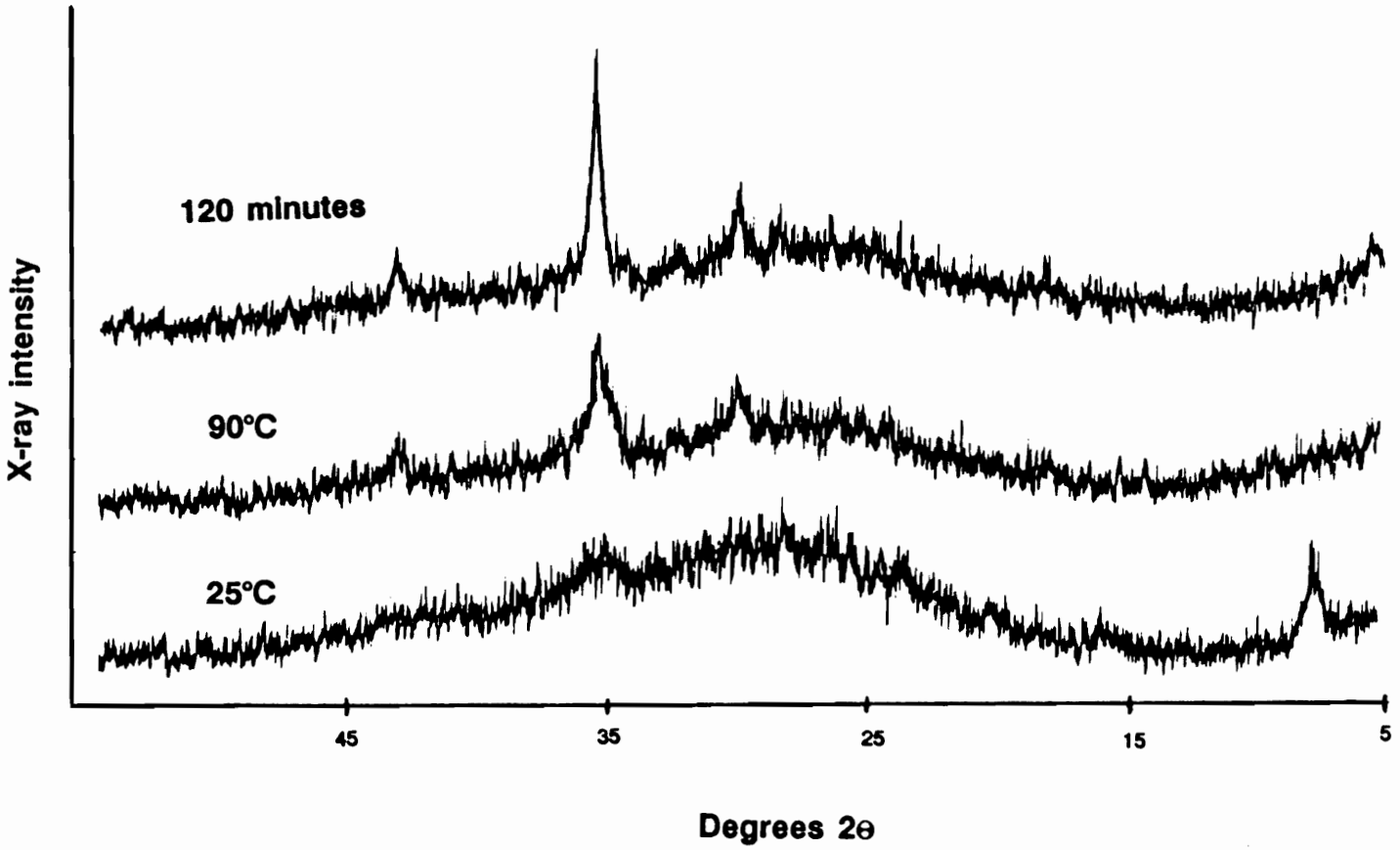

Fe_3O_4 - 35, 30, 43°

Green Rust II - 8, 24, 16°

Figure 4.47 XRD Patterns for Intermediates - $FeSO_4$ + $Fe_2(SO_4)_3$ + 5 NaOH

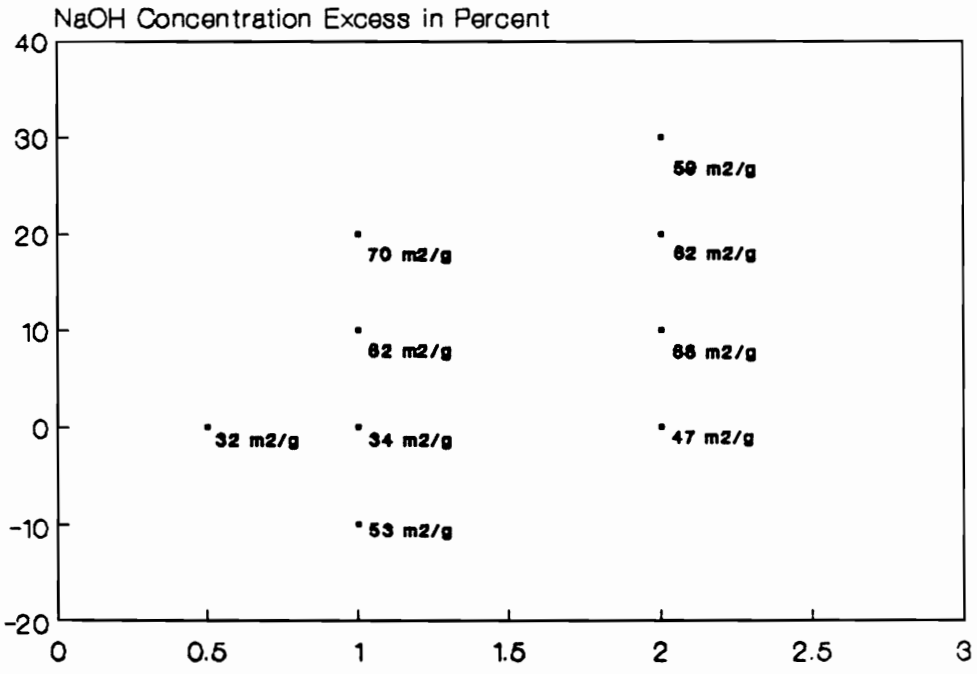

Figure 4.48 Surface Areas of Fe_3O_4 - $Fe_2(SO_4)_3$ + $FeSO_4$

independently to form additional Fe_3O_4 seed crystals upon heating. The results with α-FeOOH and $FeSO_4$ demonstrate that additional growth on Fe_3O_4 seeds does not occur readily.

The lowest surface area values were obtained using stoichiometric amounts of NaOH, regardless of the Fe^{3+} to Fe^{2+} ratio. Increasing or decreasing the NaOH concentration relative to the stoichiometric value increased the surface area of the resulting Fe_3O_4 crystals. The poor settling behavior and color of the higher surface area materials indicated that some amorphous species were formed at higher NaOH concentrations.

$Fe(NO_3)_3$ was used as the source of Fe^{3+} in six reactions, four of which were carried out using an Fe^{3+} to Fe^{2+} ratio of 1:1. In a reaction using 10% excess of NaOH over the stoichiometric amount, a suspension of Fe_3O_4 with a pH greater than 14 was produced, and a distinct smell of ammonia could be detected over the solution. The surface area of the product which smelled like ammonia was 155 m^2/g. Sugimoto and Matijevic (42) reported the use of KNO_3 as an alternate source of oxidation in the conversion of $Fe(OH)_2$ to Fe_3O_4. In this reaction NO_3^- is reduced to ammonia, but the reduction was pH dependent. The ammonia smell occurred only when 10% excess NaOH was used. When the stoichiometric amount of NaOH was used, the product was bright red and non-magnetic with a surface area of 5.5 m^2/g. XRD confirmed that this red material was α-Fe_2O_3. In this case no ammonia was detected at the end of the reaction, and the final pH of the solution was 5.0. While the presence of NO_3^- did change the oxidation process, at this NaOH concentration the reduction of NO_3^- does not go to ammonia. If NO_3^- is reduced, the reduction may be limited to the conversion to NO_2^-, although no analysis for nitrite ion was carried out. The formation of α-Fe_2O_3 from Fe_3O_4 can occur using oxygen as the oxidizing agent, but the reaction is normally carried out at 300°C in air. The mixture of nitrate, oxygen and iron hydroxide cannot be strictly regarded as a catalytic system since all the components may be changed during the course of the reaction. The presence of nitrate ion does appear to change the activation energy for the oxidation of Fe^{2+} under these circumstances.

Using $FeCl_3$ as the source of Fe^{3+}, and an Fe^{3+} to Fe^{2+} ratio of 2, Fe_3O_4 produced using stoichiometric NaOH had a surface area of 62 m^2/g. Using a Fe^{3+} to Fe^{2+} ratio of 1 and stoichiometric NaOH, the surface area of the product was 47 m^2/g. The presence of chloride ion does not affect the formation of Fe_3O_4 in any significant way. The increase in solubility of Fe_3O_4 due to chloride is not sufficient at these concentrations to alter the growth of Fe_3O_4 (74).

The results of the FeOOH study and the Fe_3O_4 study are compared in the Summary and Conclusions chapter.

Chapter 5: Summary and Conclusions

This chapter summarizes the results from the FeOOH study and the Fe_3O_4 study, compares the data from both investigations, and examines the total results with respect to previously published work on the hydrolysis and nucleation of iron oxides. The similarities and differences between the two iron oxide systems are discussed with regard to crystal nucleation and growth.

I. FeOOH

Experimental variables that affect the nucleation and growth of FeOOH phases include temperature, oxidation rate, pH, and the presence of species not in the stoichiometric equation:

$$4Fe(OH)_2 + O_2 \rightarrow 4FeOOH + 2H_2O$$

These added species include anions, such as sulfate and chloride, metal ions, such as sodium and zinc, and organic additives designed to act as growth modifiers. In this dissertation, the effects of the additive species were emphasized, while other important variables were held constant. To this end, the oxidation was carried out using a constant oxygen flow rate and the reaction temperature was kept constant. The temperature was only changed when examining the dependence of the behavior of an additive on temperature. For each experiment, the amounts of $FeSO_4$ and NaOH added were fixed.

The potential growth modifiers fell within four classes of compounds: multifunctional carboxylic acids, sodium halide salts, metal sulfate salts, and inorganic oxides with strong acid/base character. Of the four classes of compounds, each class acted differently in the modification of the nucleation and growth of FeOOH.

Sodium halide salts produced no measurable change in the physical characteristics of FeOOH when the halides were present at relatively low concentrations. Only the addition of NaCl at concentrations approximately equal to the concentration of Fe^{2+} began to affect the phase production of FeOOH. In a reaction containing 0.8M NaCl and 0.4M Fe^{2+}, traces of γ-

FeOOH were evident in the XRD patterns in addition to α-FeOOH. In contrast, in the experiment using $FeCl_2$ as the source of Fe^{2+}, the product was 100% γ-FeOOH. The only difference between the addition of 0.8M NaCl as an additive, and the the use of 0.4M $FeCl_2$ as a starting material, is the presence of Na^+ and SO_4^{2-} ions in solution. The effect of Na^+ ions on iron oxide formation is assumed to be negligible. The effects of sulfate anions are mentioned in the literature, but the effects are not well explained. Sapieszko et al. (58) examined the thermodynamic characteristics of $FeSO_4$ solutions at different pHs. Their conclusion was that the interaction between Fe^{2+} and SO_4^{2-} was weak, especially at higher hydroxide concentrations. Blesa and Matijevic (54) agreed with the conclusion that simple adsorption of sulfate ions was unlikely to affect iron oxide growth due to the weakness of the interaction. They proposed that sulfate ions could act as bridging species during the formation of oxide/hydroxide polymeric species of iron. One difference between sulfate and chloride as counterions, therefore, would be the potential to act as bridging ligands under the experimental conditions that exist during the oxidation reaction. There would be a direct competition between the two ligands for bridging sites when both anions were present. The lack of data on the incorporation of either ligand into the lattice of FeOOH leaves the evidence for the bridging mechanism in doubt. XPS spectra of the chloride reaction products showed surface concentrations of chloride ion less than 1.0 atomic %. Also evident in sulfate reactions was adsorbed sulfate at approximately 1.0 atomic %. No evidence was found by XRD analysis, such as a shift in lattice reflections or additional peaks, that would confirm incorporation of bridging chloride or sulfate into the lattice of FeOOH. The ligand could still bridge in the intermediate phase, but perhaps not be incoporated into the final crystalline phase. How sulfate or chloride, in a bridging situation, would act to nucleate one phase of FeOOH or another is unknown. The distance between Fe atoms in the bridging structure may be different with sulfate and with chloride, leading to a different conformation of Fe in the intermediate phase, Green Rust II. To maintain a topotaxial phase transformation, some of the structure of the intermediate would be

carried into the FeOOH phase. This idea is discussed further later in this chapter.

Phosphate ions can also act as bidentate ligands, and are therefore potential bridging ligands. Phosphate behaved quite differently from sulfate or chloride ion during the formation of FeOOH. While a small percentage of the product from the reaction containing phosphate was crystalline FeOOH, the majority of the material was amorphous iron oxide. The formation of both amorphous and crystalline material under a variety of reaction temperatures in the presence of phosphate is difficult to explain. There are evidently two competing processes involved, one process to produce crystalline FeOOH, while a second process that produces amorphous iron oxide. The inhibition of crystallization of iron species may occur due to the formation of iron hydrous phosphate complexes which do not easily polymerize, leading to the production of amorphous ferric hydrous oxides. The growth of a small number of crystals of FeOOH may occur due to a similar process proposed for sulfate and chloride, with phosphate acting as a bridging ligand. The other inorganic oxide compounds chosen to model phosphate produced little change in the growth of FeOOH. The substituted phosphates acted like phosphate in the production of amorphous material and α-FeOOH, but did not form γ-FeOOH under any conditions.

The use of 3 wt % Zn^{2+} as an additive in the preparation of α-FeOOH reduced the size of the α-FeOOH crystals, and increased the viscosity of the reaction suspension. The viscosity of the suspension was dependent upon the surface charge of the α-FeOOH crystals. It is suggested that the change in crystal size due to the presence of Zn^{2+} is due to changes in the lattice free energy in growing α-FeOOH crystals, due to substitution of Zn^{2+} on Fe^{3+} sites. Mg^{2+} did not produce any measurable change in the physical properties of α-FeOOH. There was no XPS evidence for adsorption or incorporation of Mg^{2+} into the α-FeOOH lattice.

The multifunctional carboxylic acids were found, as a class, to act as morphology modifiers

for FeOOH. There were significant differences among the multifunctional carboxylic acids as to the type of morphology change induced in FeOOH, extending to phase modification of FeOOH produced by EDTA and DACHTA.

The series of linear dicarboxylic acids, oxalic to malonic acid adsorb on α-FeOOH during the course of the growth reaction. Additional adsorption experiements showed that the dicarboxylic acids adsorbed on α-FeOOH when in solution at a pH above their pK_a values. The suggestion is that the acids became deprotonated in solution, and then adsorbed as anions on α-FeOOH. The adsorption of dicarboxylic acids increases the isoelectric point of α-FeOOH crystals, and leads to a decrease in suspension viscosity. The extent of the decrease in α-FeOOH suspension viscosity is a function of the concentration of dicarboxylic acid.

Surface area analysis and transmission electron microscopy showed that the presence of dicarboxylic acids in solution led to changes in the size and shape of α-FeOOH crystals. The α-FeOOH crystals were significantly shorter and wider when grown in the presence of malonic, succinic, and glutaric acids, the three, four, and five carbon dicarboxylic acids.

In experiments where two dicarboxylic acids were put into reactions, malonic proved to be the most effective α-FeOOH morphology modifier, producing α-FeOOH crystals with characteristics similar to those found for the products of reactions containing malonic acid alone. Succinic acid seemed to be more effective at modifying α-FeOOH than sodium carbonate or adipic acid, but less effective than malonic acid. The observation from the these experiments, and the experiments with the series of linear dicarboxylic acids, was that certain size dicarboxylic acid molecules are effective as growth modifiers of α-FeOOH. The position of the carboxylic acid groups on the organic molecules was such that the growth of α-FeOOH was affected. It is proposed that the dicarboxylic acids fit like a piece to a puzzle into the intermediate phase, Green Rust II. Incorporated as bridging molecules in Green Rust II, the dicarboxylic acid molecules altered the conversion and growth of Green Rust II to α-FeOOH.

The importance of Green Rust II was confirmed by time of addition experiments with malonic

acid, and intermediate sampling during the course of the reaction. These experiments demonstrated that addition of a dicarboxylic acid, after the point in the reaction where Green Rust II had begun to convert to α-FeOOH, had less effect than if the dicarboxylic acid were added before Green Rust II was completely formed.

The effect of EDTA in FeOOH synthesis was to produce γ-FeOOH. The reaction temperature was important in phase determination. At higher temperatures, more EDTA was required to produce 100% γ-FeOOH. This temperature dependence is postulated to be a measure of the relative stability of EDTA coordination to the reaction intermediate, Green Rust II. Intermediate samples extracted from an EDTA reaction were found to be the same intermediate phase as in the preparation of α-FeOOH without EDTA. However, the peaks in the XRD pattern were detected only for the [00z] family of planes in Green Rust II. The absence of reflections due to off-axis planes ([x0z] and [xyz] family planes) is evidence of the lack of organization in the in the x and y directions of the Green Rust II lattice. The conclusion drawn from the XRD results is that EDTA and other multifunctional carboxylic acids coordinated to Green Rust II alter the growth of FeOOH to produce crystals of varying morphology. The extent of morphology alteration is dependent upon the concentration and structure of the multifunctional carboxylic acid. Coordination of the compounds in the non-[00z] planes of Green Rust II changes particle morphology, while coordination in the z axis, postulated to occur in the case with phosphate, prevents FeOOH crystal formation and leads to formation of amorphous ferric hydrous oxides.

A mechanism, consistent with the evidence found in this research, by which EDTA and dicarboxylic acids alter the morphology of FeOOH, is shown in Figure 5.1. The z axis backbone of Green Rust II first develops as a long chain of iron and oxygen atoms. This highly developed backbone gives the strong [00z] reflections evident in the XRD patterns of intermediate samples. EDTA and dicarboxylic acid molecules coordinate to this iron-oxygen chain, blocking sites on faces in the x and y directions of Green Rust II. The coordinated acid molecules then act to change the growth of Green Rust II. The difference in behavior between

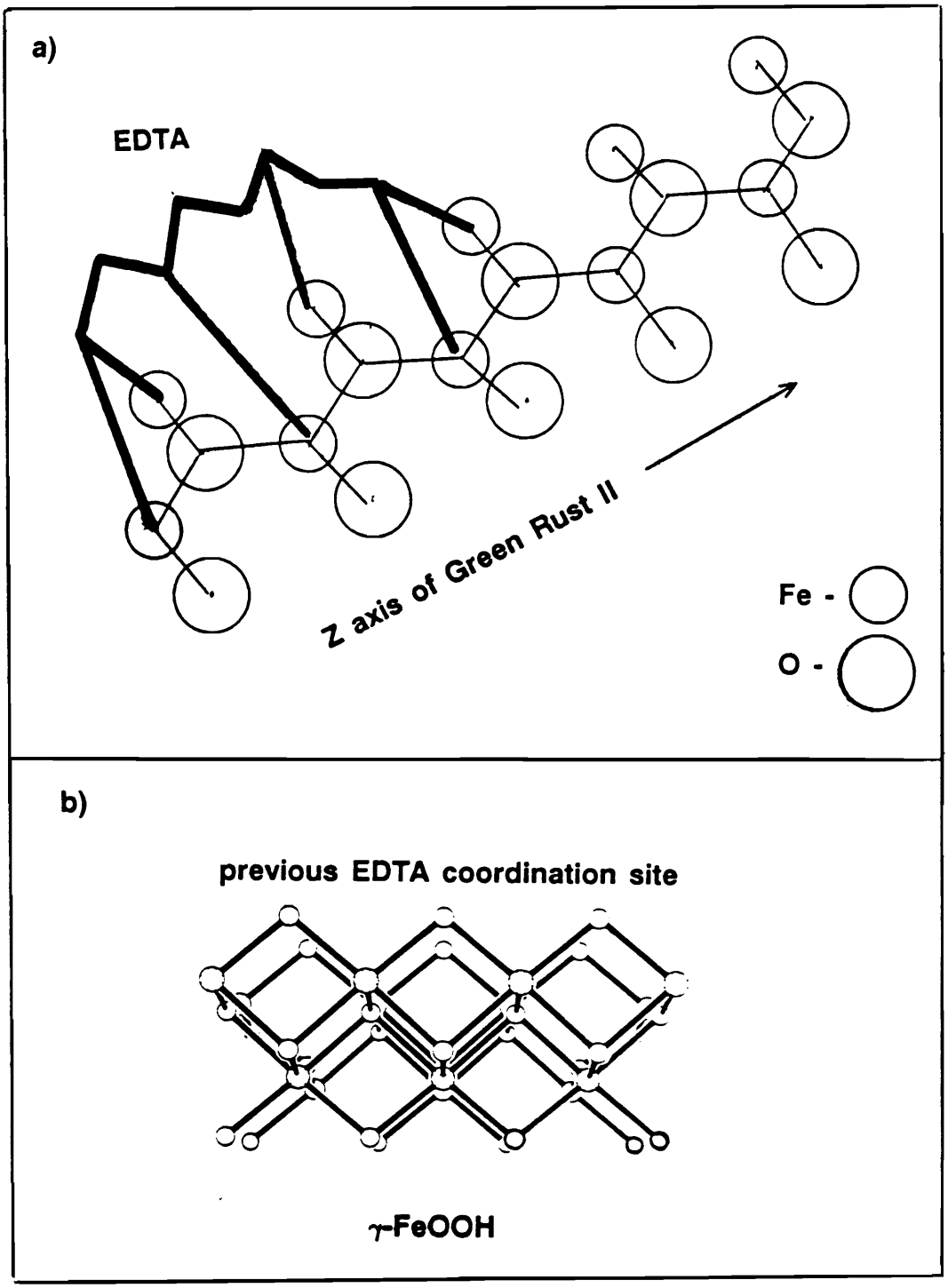

Figure 5.1 Mechanism of Green Rust II Alteration by EDTA

EDTA and dicarboxylic acids in altering growth of FeOOH may be in both the strength of their coordination and the size of the molecules. γ-FeOOH has a layered structure. (Figure 2.1) The sixfold coordination of EDTA limits the site of adsorption to a side of the Green Rust II chain, which prevents growth of that face of the crystal. After Green Rust II has stopped growing, the transformation to γ-FeOOH occurs in which EDTA has formed the outside surface of the layered structure of γ-FeOOH. The coordination of dicarboxylic acids is only bidentate, and is less limited to sites of adsorption. Coordination of dicarboxylic acid molecules to Green Rust II inhibits growth of Green Rust II based on the size of the dicarboxylic acid molecules, and the possible sites of adsorption. This idea of site specific adsorption based on the location of ligand size and shape is addressed in Chapter 2 and in references 89-91. The type of coordination of dicarboxylic acids to Green Rust II may be similar to the structure of adsorption of organic acids on the (100) face of α-FeOOH. (Figure 5.2)

II. Fe_3O_4

The two most important variables in the formation of Fe_3O_4 were the Fe reagents, and the hydroxide concentration. The formation of Fe_3O_4 by the oxidation of $FeSO_4$ occurred by two processes based on the hydroxide concentration. At high hydroxide concentration, crystalline $Fe(OH)_2$ was oxidized to form large octahedral crystals of Fe_3O_4. At lower hydroxide concentration, some Green Rust II was produced, and the conversion of a mixture of Green Rust II and crystalline $Fe(OH)_2$ led to higher surface area particles of Fe_3O_4. Fast oxygen consumption by the mixture of Green Rust II and $Fe(OH)_2$ produced a mixture of Fe_3O_4 and amorphous material. Slower oxidation rates reduced the amount of amorphous material. This was probably due to different oxidation rates for Green Rust II and crystalline $Fe(OH)_2$. Oxygen consumption by Green Rust II was faster than for $Fe(OH)_2$. At high oxygen flow rates, Green Rust II was converted to amorphous oxide. The establishment of more equilibrium-like conditions ie, lower temperature and slower oxidation rate, led to formation of crystalline Fe_3O_4.

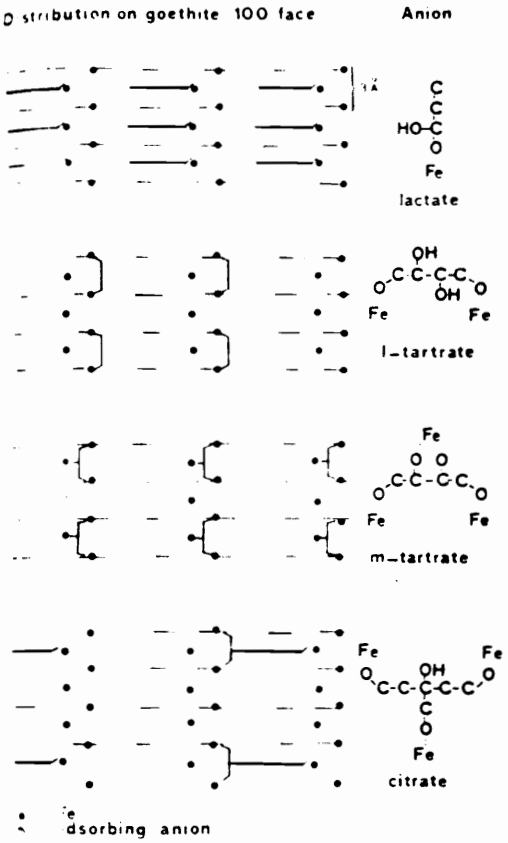

Fig. 2 Schematic arrangement of organic acids on the (100) face of goethite (= α-FeOOH)

Cornell, R.; Schindler, P. *Colloid Polymer Sci.*, **1980**, 258, 1175.

Figure 5.2 Site Specific Adsorption of Organic Acids to α-FeOOH

The addition of ferrite forming metal ions such as Zn^{2+} and Mn^{2+} produced low surface area octahedral crystals with highly uniform size and shape. Addition of other metal ions such as Cu^{2+} and Ni^{2+} produced high surface area materials. The ferrite forming metals increased the rate of oxygen consumption in the reaction. This presumably occurred by the fast formation of nuclei containing the +2 metal additives and Fe^{3+} ions as they were oxidized from Fe^{2+}.

$$Zn(OH)_2 + 2Fe(OH)_3 \text{ ---- } ZnFe_2O_4 + 4H_2O$$

The conversion of α-FeOOH and $FeSO_4$ to Fe_3O_4 was carried out by precipitating amorphous Fe^{2+} hydroxide species on the surface of α-FeOOH. A layer of Green Rust II grew at the interface of the α-FeOOH crystals. The formation of Fe_3O_4 occurred by the incorporation of Fe^{2+} into the α-FeOOH lattice. At high hydroxide concentrations, formation of crystalline $Fe(OH)_2$ led to secondary nuclei which formed Fe_3O_4 independently of α-FeOOH. Spherical particles produced under stoichiometric NaOH conditions appeared as agglomerates of smaller particles. Sugimoto and Matijevic reported that agglomeration occurred at pH 6.5, approximately the isoelectric point for Fe_3O_4 (42). Changing the reaction pH from neutral conditions was not conducive to agglomerate formation, and higher surface area materials were produced. Thus, hydroxide concentration had effects on both the intermediates formed during the reaction, and the manner in which Fe_3O_4 crystals combined.

The addition of NaOH to a solution of Fe^{3+} and Fe^{2+} led to initial precipitation of Fe_3O_4 and Green Rust II at room temperature. Upon heating to 90°C, Green Rust II was converted to Fe_3O_4. The large number of initial nuclei formed led to very small Fe_3O_4 crystals with high surface areas. The presence of different counterions such as sulfate, chloride, and nitrate did not affect the surface area of the Fe_3O_4 crystals. Nitrate ion acted as a secondary oxidation source at stoichiometric NaOH concentrations. α-Fe_2O_3 was formed as Fe_3O_4 continued to oxidize. The mechanism of reduction of nitrate to lower oxidation states is described by Sugimoto and Matijevic (42). The reduction of nitrate ion to ammonia was evident at higher pH, but no α-Fe_2O_3 was produced.

III. Morphology of Iron Oxide Crystals

A diagram in Figure 5.3 shows the growth schemes investigated for FeOOH and Fe_3O_4 with various reaction conditions and additives. The reaction intermediates that were identified and the products of the reactions are indicated.

The control of nucleation and morphology of iron oxides is best described as control of the formation of intermediate phases. In both FeOOH preparation and Fe_3O_4 formation, chemical factors which affect the intermediate iron species affect the morphology of the iron oxide crystals. While the phase of iron oxide produced is most dependent upon reaction temperature and hydroxide concentration, compounds which interact strongly with the intermediate phases can alter the size and shape of the resulting oxide crystals over a wide range. Multifunctional carboxylic acids interact strongly with Green Rust II, the intermediate in FeOOH production. The morphology of FeOOH is dependent upon the structure of Green Rust II due to topotaxial phase transformation. Modifications of Green Rust II induced by incorporation of carboxylic acids are carried into the final FeOOH phase. Compounds which are regarded as non-reagents, such as sulfate and chloride counterions, also can change crystal morphology, presumably by coordination to reaction intermediates.

The acid base behavior of the surface of the growing crystals has a great deal to do with the interaction of secondary species in solution. The ability to grow larger iron oxide crystals under nonhydrothermal reaction conditions is dependent on the interaction between the surface of the seed crystals, and iron hydroxide species. For both Fe_3O_4 production and FeOOH formation, a strong attraction between the α-FeOOH crystals and iron hydroxide leads to crystal growth, while a poor attraction leads to secondary nucleation and broad particle size distributions. The attraction of potential growth modifiers is also dependent on the charge of the solution species and the isoelectric point of the iron oxide crystals.

The major difference in Fe_3O_4 and FeOOH growth is the relative lack of activity of Fe_3O_4 after seed crystals have been produced. FeOOH crystals can be grown larger, or converted into

other iron oxides with relative ease, while the growth or conversion of Fe_3O_4 requires hydrothermal processing in most cases (46,51). The low solubility of Fe_3O_4 relative to FeOOH is evidence for inertness of Fe_3O_4 (74). The high temperature (90 -95°C) required for the formation of Fe_3O_4 under most conditions reduces the importance of adsorbates as growth modifiers due to the adsorbate-crystal stability under these more rigorous conditions (76).

In conclusion, the morphology of iron oxides can be controlled by chemical modification of the crystal surfaces during nucleation and growth. Species which act as strong adsorbates on iron oxide can act as potential growth modifiers. Changes in the phase and shape of iron oxide were made, and intermediates in the growth processes were identified.

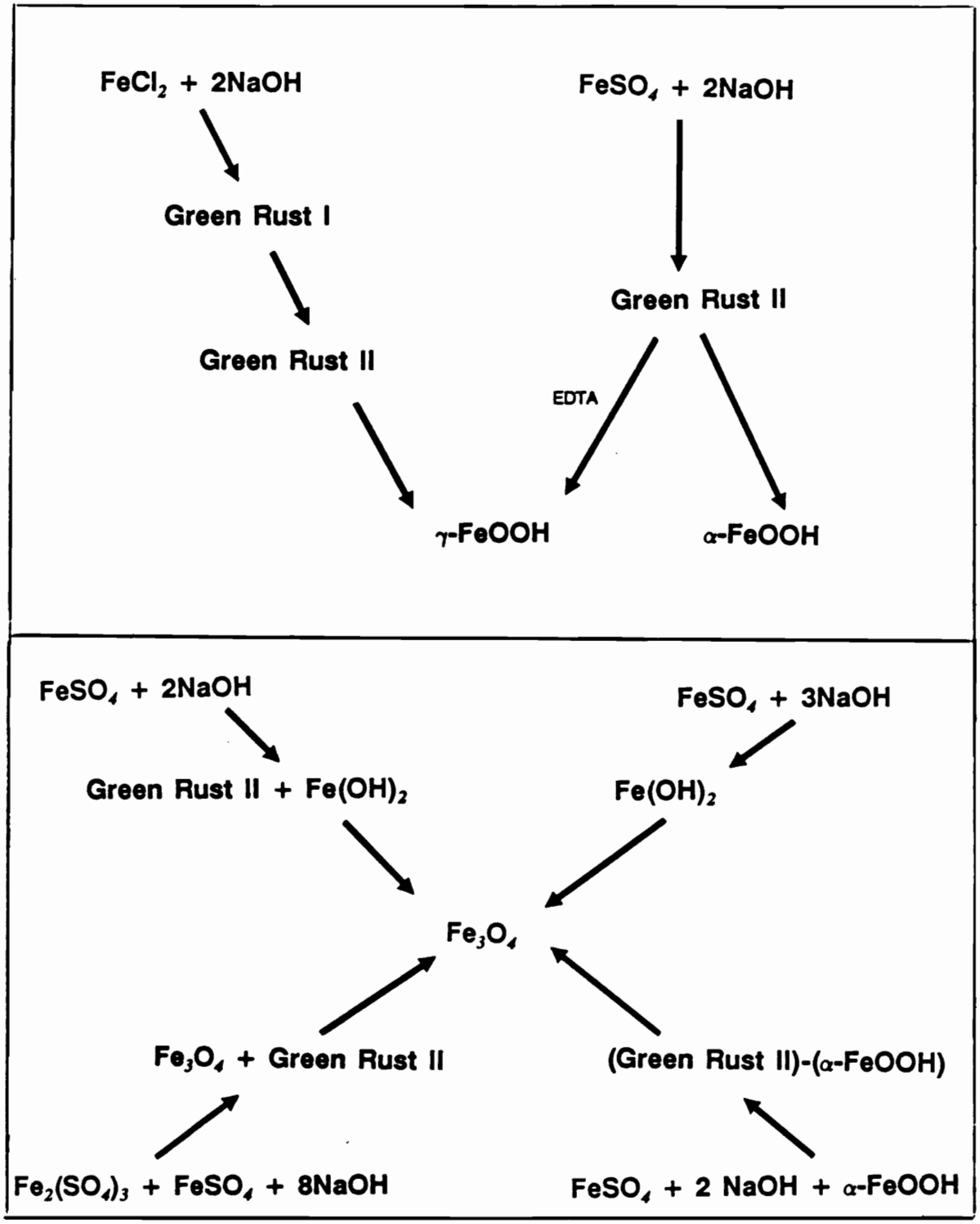

Figure 5.3 Flow Chart of FeOOH and Fe_3O_4 Reactions

References

1. Theophrastus Περι λιθων; 325 B.C.
2. Wulffing, C., Ger. Patent 183,118 **1906.**
3. Neighbors, C., U.S. Patent 2,365,720 **1944.**
4. Szegari, A., U.S. Patent 2,719,009 **1955.**
5. Sutheim, G.; Southcomb, H., U.S. Patent 3,029,157 **1962.**
6. Isurugi, M.; Saito, K., Japan Patent 61,258,259 **1986.**
7. Kline, G. *Modern Plastics* **1945**, *23*, 152.
8. Ozaki, M.; Matijevic, E. *J. Colloid Interface Sci.* **1988**, *107*, 199.
9. Morrish, A. "Crystals: Growth, Properties, and Applications;" Pergammon Press: Oxford, 1980; p 171.
10. Corradi, A. *IEEE Trans. Mag.* **1978**, *MAG-14*, 655.
11. Nobouka, S.; Ando, T.; Hayama, F., U.S. Patent 3,081,264 **1963.**
12. Sharrock, M.; Bodnar, R. *J. Appl. Phys.* **1985**, *57*, 3919.
13. Koster, E. *IEEE Trans. Mag.* **1972**, *MAG-8*, 428.
14. Umeki, S.; Saitah, S.; Imaoka, Y. *IEEE Trans. Mag.* **1974**, *MAG-10*, 655.
15. Fukumoto H.; Yamaji, M., Japan Patent 62,009,357 **1987.**
16. Isurugi, M.; Saita, K., Japan Patent 61,258,260 **1986.**
17. Ishikawa, T.; Matijevic, E. *Langmuir* **1988**, *4*, 26.
18. Smith, H., Ger. Patent 968,935 **1958.**
19. Matsumoto, S.; Koga, T.; Fukui, K.; Nakatani, S., U.S. Patent 4,202,871 **1980.**
20. Francombe, M.; Rooksby, H. *Clay Miner. Bull.* **1959**, *4*, 1.
21. Welo, L.; Baudisch, O. *Phil. Mag.* **1934**, *17*, 753.

22. Bernal, J.; Dasgupta, D.; Mackay, A. *Nature* **1957**, *180*, 645.

23. Sosman, R.; Posnjak, E. *J. Wash. Acad. Sci.* **1925**, *15*, 329.

24. Herroun, E.; Wilson, E. *Proc. Phys. Soc.* **1928**, *41*, 100.

25. Pliny "Historis Naturalis;" 25 A.D.

26. Haidlinger, W. "Handbuch der Bestimmenden Mineralogie;" Weih, 1845 p 551.

27. Becher, J. "Mineralogishe Beschreibung Oraniennassauischen Lander;" Marburg, 1789; p 40.

28. Lenz, D. "Tabellen des Gesammten Mineralreich;" Jena, 1806; p 46.

29. Ullmann, J. "Systematisch - Tabellarische Uebersichte der Mineralogisch Enfachen Fossilien;" Cassel, 1814; p 299.

30. Scheele, C. "Chemische Abhandlung von der Luft und dem Feuer;" Upssala, 1777.

31. Mellor, J. "A Comprehensive Treatise on Inorganic and Theoretical Chemistry;" Volume XIII, Longmans, Green, and Co.: London, 1934; pp 701-724.

32. Bernal, J.; Dasgupta, D.; Mackay, A. *Clay Miner. Bull.* **1959**, *4*, 15.

33. Misawa, T.; Hashimoto, K.; Suetaka, W.; Shimodaira, S. *J. Inorg. Nucl. Chem.* **1973**, *35*, 4159.

34. Misawa, T.; Hashimoto, K.; Shimodaira, S. *J. Inorg. Nucl. Chem.* **1973**, *35*, 4167.

35. Misawa, T.; Hashimoto, K.; Shimodaira, S. *Corrosion Sci.* **1974**, *14*, 331.

36. Hsu, P. *J. Soil Sci.* **1972**, *23*, 409.

37. van der Woude, J.; de Bruyn, P. *Colloids Surfaces* **1983**, *8*, 55.

38. Knight, R.; Silva, J. *J. Inorg. Nucl. Chem.* **1974**, *36*, 59.

39. Dousma, J.; de Bruyn, P. *J. Colloid Interface Sci.* **1976**, *56*, 527.

40. Atkinson, R.; Posner, A.; Quirk, J. *Clays Clay Miner.* **1977**, *25*, 49.

41. Kiyama, M. *Bull. Chem. Soc. Jpn* **1974**, *47*, 1646.

42. Sugimoto, T.; Matijevic, E. *J. Colloid Interface Sci.* **1980**, *71*, 227.

43. Kanzaki, T.; Katsura, T. *J. Chem. Soc., Dalton Trans.* **1986**, 1243.

44. Tamaura, Y.; Saturno, M.; Yamada, K.; Katsura, T. *Bull. Chem. Soc. Jpn* **1984**, *57*, 2417.

45. Biernat, R.; Robins, R. *Electrochim Acta* **1972**, *17*, 1261.

46. Solcova, A.; Subrt, J.; Hanousek, F.; Bechine, K.; Zapetal, V.; Zoiotovskii, B.; Krivoruchko, O.; Buyanov, R.; Lipka, J. *Z. Anorg. Allg. Chem.* **1985**, *526*, 191.

47. Baes, C.; Mesmer, R. "The Hydrolysis of Cations"; Wiley-Interscience: New York, NY, 1976; pp 226-235.

48. Ricci, J. *J. Am. Chem. Soc.* **1948**, *70*, 109.

49. Lewis, D.; Schwertmann, U.; *J. Colloid Interface Sci.* **1980**, *78*, 543.

50. Leskela, T.; Leskela, M. *Thermochim Acta* **1984**, *77*, 177.

51. Bohm, J. *Z. Anorg. Allg. Chem.* **1925**, *149*, 203.

52. Miyamoto, S. *Bull. Chem. Soc. Jpn* **1927**, *5*, 41.

53. Miyamoto, S. *Bull. Chem. Soc. Jpn* **1928**, *6*, 137.

54. Blesa, M.; Matijevic, E. *Adv. Colloid Interface Sci.* **1989**, *29*, 173.

55. Glemser, O.; Gwinner, E. *Z Anorg. Allg. Chem.* **1939**, *240*, 163.

56. von Hauer, K. *Miner. Mag. J. Miner. Soc.* **1876**, *1*, 243.

57. Evans, U.; Taylor, C. *Corrosion Sci.* **1972**, *12*, 227.

58. Sapieszko, R.; Patel, R.; Matijevic, E. *J. Phys. Chem.* **1977**, *81*, 1061.

59. Strahm, U.; Patel, R.; Matijevic, E. *J. Phys. Chem.* **1979**, *83*, 1639.

60. Murphy, P.; Posner, A.; Quirk, J. *J. Colloid Interface Sci.* **1976**, *56*, 284.

61. Hamada, S.; Kuma, K. *Bull. Chem. Soc. Jpn* **1976**, *49*, 3295.

62. Kiyama, M.; Akita, T.; Shimizu, S.; Okuda, Y.; Taksda, T. *Bull. Chem. Soc. Jpn* **1972**, *45*, 3422.

63. Murphy, P.; Posner, A.; Quirk, J. *J. Colloid Interface Sci.* **1976**, *56*, 298.

64. Liepina, L.; Vaivads, A. *Latvijas PSR Zinatu Akad. Vestis* **1956**, *3*, 115.

65. Hand, F., Bel. Patent 649,659 **1964**

66. Kuhnel, R.; Roorda, H.; Steensma, J. *Clays Clay Miner.* **1975**, *23*, 349.

67. Mann, S.; Cornell, R.; Schwertmann, U. *Clay Minerals* **1985**, *20*, 225.

68. Schwertmann, U. *Clay Minerals* **1984**, *19*, 9.

69. Hamada, S.; Matijevic, E. *J. Colloid Interface Sci.* **1981**, *84*, 274.

70. Schwertmann, U. *Geoderma* **1969**, *3*, 207.

71. Cornell, R.; Schwertmann, U. *Clays Clay Miner.* **1979**, *27*, 402.

72. Waite, T.; Morel, F. *J. Colloid Interface Sci.* **1984**, *102*, 121.

73. van der Woude, J.; Rijubout, J.; de Bruyn, P. *Colloids Surfaces* **1986**, *18*, 313.

74. Bohnsack, G. "The Solubility of Magnetite in Water and in Aqueous Solutions of Acid and Alkali;" Harper and Row: Washington DC, 1987; pp 106-114.

75. Sapieszko, R.; Matijevic, E. *J. Colloid Interface Sci.* **1980**, *74*, 405.

76. Jones, R.; Bloom, M. *Naval Research Lab. Report* **1966**, 6442.

77. Ito, K.; Tamaura, Y.; Katsura, T. *Bull. Chem. Soc. Jpn* **1984**, *57*, 2820.

78. Takada, T.; Kiyama, M. *Ferrites: Proc. Int. Conf.* **1970**, *1*, 69.

79. Freundlich, V.; Greensfelder, B. *Kolloid Zeit.* **1929**, *48*, 318.

80. Paterson, R.; Rahman, H. *J. Colloid Interface Sci.* **1984**, *98*, 494.

81. Paterson, R.; Rahman, H. *J. Colloid Interface Sci.* **1983**, *94*, 60.

82. Goncalves, M.; Sigg, L.; Stumm, W. *Envir. Sci. Tech.* **1985**, *19*, 141.

83. Dzombak, D.; Morel, F. *J. Colloid Interface Sci.* **1986**, *112*, 588.

84. Farley, K.; Dzombak, D.; Morel, F. *J. Colloid Interface Sci.* **1985**, *106*, 226.

85. Theis, T.; West, M. *Envir. Tech. Letters* **1986**, *7*, 309.

86. Zeltner, W.; Anderson, M. *Langmuir* **1988**, *4*, 469.

87. Buckland, A.; Rochester, C.; Topham, S. *J. Chem. Soc., Faraday Trans. 1* **1980**, *76*, 302.

88. Hughes, R. *Corrosion Sci.* **1969**, *9*, 535.

89. Cornell, R.; Schlindler, P. *Colloid Polymer Sci.* **1980**, *258*, 1171.

90. Torres, R.; Kallay, N.; Matijevic, E. *Langmuir* **1988**, *4*, 706.

91. Rueda, E.; Grassi, R.; Blesa, M. *J. Colloid Interface Sci.* **1985**, *106*, 246.

92. Szklarska-Smialowska, Z.; Zakroczymski, T.; Fan, C. *J. Electrochem. Soc.* **1985**, *132*, 2543.

93. Motekaitis, R.; Martell, A.; Hayes, D.; Frenier, W. *Can. J. Chem.* **1980**, *58*, 1999.

94. Haber, J.; Stoch, J.; Ungier, L. *J. Electronspec. Rel. Phenom.* **1976**, *9*, 459.

95. Oku, M.; Hirokawa, H. *J. Electronspec. Rel. Phenom.* **1976**, *8*, 475.

96. Mitchell, D.; Sproule, G.; Graham, M. *Appl. Surface Sci.* **1985**, *21*, 199.

97. Micale, F.; Kiernan, D.; Zettlemoyer, A. *J. Colloid Interface Sci.* **1985**, *105*, 570.

98. Matijevic, E.; Scheiner, P. *J. Colloid Interface Sci* **1978**, *63*, 509.

99. Gasca, R.; Cornejo, J.; Arambarri, P. *Anales de Edafol. Agrobio.* **1977**, 662.

100. Heller, W. *J. Colloid Interface Sci.* **1982**, *89*, 61.

101. Maeda, Y.; Hirono, S. *Jpn J. Appl. Phys.* **1981**, *20*, 1991.

102. Cornell, R.; Mann. S.; Skarnulis, A. *J. Chem. Soc., Faraday Trans. 1* **1983**, *79*, 2679.

103. Mackenzie, R.; Paterson, E.; Swaffield, R. *J. Thermal Anal.* **1981**, *22*, 269.

104. Williams, R.; Thewlis, J. *Trans. Faraday Soc.* **1931**, *27*, 767.

105. Rochester, C.; Topham, S. *J. Chem. Soc., Faraday Trans. 1* **1979**, *75*, 591.

106. Tejedor-Tejedor, M.; Anderson, M. *Langmuir* **1986**, *2*, 203.

107. Dziobkowski, C.; Wrobleski, J.; Brown, D. *Inorg. Chem.* **1981**, *20*, 671.

108. Music, S.; Vertes, A.; Simmons, G.; Czako-Nagy, I.; Leidheiser, H. *J. Colloid Interface Sci.* **1982**, *85*, 256.

109. Christensen, A.; Lehmann, M.; Wright, A. *Acta Chem. Scand.* **1983**, *37*, 63.

110. Christensen, A.; Lehmann, M.; Convert, P. *Acta Chem. Scand.* **1982**, *36*, 303.

111. Seah, M. *Surface Interface Anal.* **1989**, *14*, 488.

112. "CRC Handbook of Chemistry and Physics;" Weast, R., Ed.; CRC Press: West Palm Beach FL, 1978, p D184.

113. McClelland, J. *Anal. Chem.* **1983**, *55*, 89A.

Appendix A : X-ray Powder Diffraction Standards

8-98 MAJOR CORRECTION

d	4.26	3.29	2.47	4.24	FeO(OH)	1/2($Fe_2O_3.H_2O$)
I/I_1	100	90	90	100	IRON OXIDE HYDROXIDE	LEPIDOCROCITE

Rad. CoKα λ 1.7902 Filter Fe Dia. 19CM
Cut off I/I_1 VISUAL
Ref. ROOKSBY "X-RAY IDENTIFICATION AND CRYSTAL STRUCTURES OF CLAY MINERALS" LONDON, 1951,FACING P. 264

Sys. ORTHORHOMBIC S.G. AMAM (63)
a_o 3.89 b_o 12.54 c_o 3.07 A 0.309 C 0.245
α β γ Z 4 Dx 3.95
Ref. IBID.

nα 1.94 nwβ 2.20 nγ 2.51 Sign -
2V 49° D 3.854 mp 450°C Color RED TO RED BROWN
Ref. POSNJAK AND MERWIN, AM.J.SCI. 47 311 (1919)

PEACOCK, TRANS. ROY. SOC. CANADA 36 IV, 117 (1942)
SAMPLE FROM SIEGEN, BESTPHALIA, GERMANY, GIVES Aa3.87, bw2.58, c=3.07, D_x=3.97.
QM (BESTPHALIA)
FIRED VALUES BY ROOKSBY ONLY

d Å	I/I_1	hkl	d Å	I/I_1	hkl
4.26	100	021	1.196	20	112,131
3.29	90	120	1.189	20	1.10.0
2.79	10R	011	1.10	8	
2.47	90	002	1.09	40	INDICES
2.46	20	111			BY PEACOCK
2.09	20	1.040			
1.93	70	061,200			
1.849	20	220			
1.736	40	151			
1.564	20	240			
1.535	20	202			
1.524	10	241			
1.496	10R	202			
1.449	10	190			
1.433	20	171			
1.418	10	260			
1.389	10	112			
1.367	10	251			
1.261	10	042,260			
1.210	10	240			

17-536

d	4.18	2.69	2.45	4.98	αFeO(OH)	$Fe_2O_3.H_2O$
I/I_1	100	30	25	10	Iron Oxide Hydroxide	Goethite

Rad. Co λ Filter Fe Dia. 19cm.
Cut off I/I_1
Ref. G. Brown, X-ray Ident. and Cryst. Struct. Clay Minerals, p. 386 London 1961 *

Sys. Orthorhombic S.G. Pbnm (62)
a_o 4.596 b_o 9.957 c_o 3.021 A 0.462 C 0.303
α β γ Z 4 Dx 4.264
Ref. Peacock, Trans. Roy. Soc. Canada 36 IV, 116 (1942)

nα 2.260 nwβ 2.393 nγ 2.398(Na) Sign
2V D 4.26 mp Color Black
Ref Posnjak and Merwin, Am. J. Sci. 47 311 (1919)

Peacock records a weak line at 2.09, 5, 220.
* Cited by Harrison and Peterson, Am. Min. 50 704-712 (1965)

d Å	I/I_1	hkl	d Å	I/I_1	hkl
4.98	10	020	1.467	4	320
4.18	100	110	1.453	10	061
3.38	10	120	1.418	2	112
2.69	30	130	1.392	8	330
2.58	8	021	1.357	8	311
2.520	4	101	1.317	8	321
2.490	16	040	1.264	2	331
2.452	25	111	1.241	2	142
2.252	10	121	1.198	2	341
2.192	20	140			
2.009	2	131			
1.920	6	041			
1.799	8	211			
1.770	2	141			
1.721	20	221			
1.694	10	240			
1.661	4	060			
1.606	6	231			
1.564	16	151,160			
1.509	10	250,002			

13-92 MAJOR CORRECTION

d	10.9	5.48	3.65	10.9	$Fe_2O_3 \cdot H_2O$?
I/I_1	100	80	80	100	IRON OXIDE HYDROXIDE ? (GREEN RUST II)

Rad. CoKα? λ Filter Dia.
Cut off I/I, VISUAL
Ref. BERNAL, DASGUPTA AND MACKAY, CLAY MINERALS BULL. 4 15 (1959)

Sys. HEXAGONAL S.G.
a_o 3.17 b_o c_o 10.9 A C 3.44
α β γ Z D_x
Ref. IBID.

nωε ε γ Sign
2V D mp Color DARK GREEN
Ref. IBID.

PREPARED FROM FERROUS SULFATE AND SODIUM HYDROXIDE MIXED IN 1:1 PROPORTIONS, AND OXIDATION OF THE PRECIPITATE.
O ASSIGNED BECAUSE COMPOSITION IS DOUBTFUL. (ED.)

d Å	I/I₁	hkl	d Å	I/I₁	hkl
10.9	100	001			
5.48	80	002			
3.65	80	003			
2.747	40	004,100			
2.660	60	101			
2.459	40	102			
2.195	40	005,103			
1.938	40	104			
1.712	20	105			
1.587	20	110			
1.570	20	111			
1.525	20	112			

Green Rust I

hkl	d in Å	I
003	8.02	vs
006	4.01	s
10-2	2.701	m
10-5	2.408	m
10-8	2.037	w
10-1	1.805	vw
110	1.598	mw
113	1.567	mw
116	1.487	w
20-4	1.040	vvw

Bernal, Dasgupta, and Mackay, Clay Minerals Bull. **1959**, *4*, p 24

19-629

d	2.53	1.49	2.97	4.85	Fe_3O_4 ★
I I$_1$	100	40	30	8	Iron Oxide (Magnetite)

Rad. CuKα$_1$ λ 1.5405 Filter Ni Dia.
Cut off I I$_1$ Diffractometer
Ref. National Bureau of Standards, Monograph 25, Sec. 5, 31 (1967)

Sys. Cubic S.G. Fd3m (227)
a$_0$ 8.396 b$_0$ c$_0$ A C
α β γ Z 8 Dx 5.197
Ref. Ibid.

ε ω β ε γ Sign
2V D mp Color Black
Ref. Ibid.

Sample obtained from the Columbian Carbon Co., New York 17, New York.
Spectrographic analysis showed the following major impurities: 0.01 to 0.1% Co, 0.001 to 0.01% Ag, Al, Mg, Mn, Mo, Ni, Si, Ti and Zn.
Pattern taken at 25°C.

d Å	I I$_1$	hkl	d Å	I I$_1$	hkl
4.85	8	111	.8952	2	664
2.967	30	220	.8802	6	931
2.532	100	311	.8569	8	844
2.424	8	222	.8233	4	1020
2.099	20	400	.8117	6	$\overline{9}51$
1.715	10	422	.8080	4	$10\underline{22}$
1.616	30	511			
1.485	40	440			
1.419	2	531			
1.328	4	620			
1.281	10	533			
1.266	4	622			
1.212	2	444			
1.122	4	642			
1.093	12	731			
1.050	6	800			
0.9896	2	822			
.9695	6	751			
.9632	4	662			
.9388	4	840			

$Fe(OH)_2$

hkl	d in Å	I
001	4.597	vs
100	2.817	s
101	2.403	vs
102	1.782	s
110	1.629	s
111,003	1.535	m
200	1.411	vw
103,201	1.349	m
202	1.203	vw
004	1.148	vw
113	1.115	vw
104,210	1.067	w
203,211	1.040	m

Bernal, Dasgupta, and Mackay, Clay Minerals Bull. **1959**, *4*, p 19

Vita

The author was born in 1961 as, happily, the last of six children to George and Helen Barton. He was raised in Morrisville, Vermont where he attended public school. He graduated high school from Peoples Academy in 1979. He entered Purdue University in the fall of 1979, and after a long and trying period, graduated in the spring of 1986. In the interim, the author co-oped at IBM for three semesters, one semester in Charlotte NC, and two semesters in Boca Raton, FL. He began at Virginia Tech in the summer of 1986 in the lab of John Dillard. After four fun and rewarding years, he finished the requirements for his degree in the spring of 1990. Following graduation, the author set off for two years in the lab of R. P. Cooney at the University of Auckland, New Zealand for further study and fun.